Chapter I.3

Transverse beam dynamics

Bernhard Holzer
CERN, Geneva, Switzerland

The transverse beam dynamics of charged particles in an accelerator describes the movement of single particles under the influence of external transverse bending and focusing fields with main focus on synchrotrons or storage rings. Starting from the basic principles of how to design the geometry of the ring we develop the transverse motion of the particles under the influence of external fields, motivate the equation of motion and show the solutions for typical storage ring elements. In a second step the concept of emittance of the particle ensemble is introduced as well as the beta function, which reflects the overall focusing properties of the ring. The adiabatic shrinking due to Liouville's theorem is discussed and—in linear approximation—the effects arising from a non-vanishing momentum spread of the beam, like dispersion and chromaticity.

The transverse beam dynamics in the sense we use it in this book describes the movement of charged particles in an accelerator under the influence of electromagnetic fields. It is based on the detailed arrangement of magnets and other devices in the accelerator, i.e. their positions in the machine and their strength and it allows us to obtain well-defined, predictable parameters of the single particle trajectories as well as the parameters of the beam as an ensemble of many particles. In the context of these lectures, we will restrict the description to the so-called linear approximation, where we refer to small amplitudes of the particles' oscillations, and to external fields that are either constant or linear dependent on the particle's amplitude. In other words, we will use dipole or quadrupole fields for bending and focusing of the particles. The advantage of this approach is that the equations that we will obtain can be solved analytically—which usually means that we can understand the physics behind! Non-linear effects will be introduced later as a kind of distortion of the linear approach. Still, our approximations have to be good enough and the accuracy of our calculations as well as that of our technical engineering has to be on the highest possible level in order to keep the particles stored for many hours. Figure I.3.1 shows a typical collider run of the LHC, where the counter rotating beams are stored for more than 12 hours, a time span which corresponds to the travel of the particles across the complete solar system.

The basis of transverse beam dynamics as we use it nowadays in the treatment of modern accelerators, and the magnet lattice which will be the result of an optimised accelerator design, was laid in 1952, when Courant, Livingston and Snyder developed the theory of strong focusing [1] and in this book we will follow rather closely the approach and also the nomenclature. Starting on a very fundamental level, we make the statement, that from all interactions that we know in physics, strong, weak, gravitational and electromagnetic, (and if you prefer we could even include the Higgs field) it is only the electromagnetic

This chapter should be cited as: Transverse beam dynamics, B. Holzer, DOI: 10.23730/CYRSP-2024-003.73, in: Proceedings of the Joint Universities Accelerator School (JUAS): Courses and exercises, E. Métral (ed.),
CERN Yellow Reports: School Proceedings, CERN-2024-003, DOI: 10.23730/CYRSP-2024-003, p. 73.

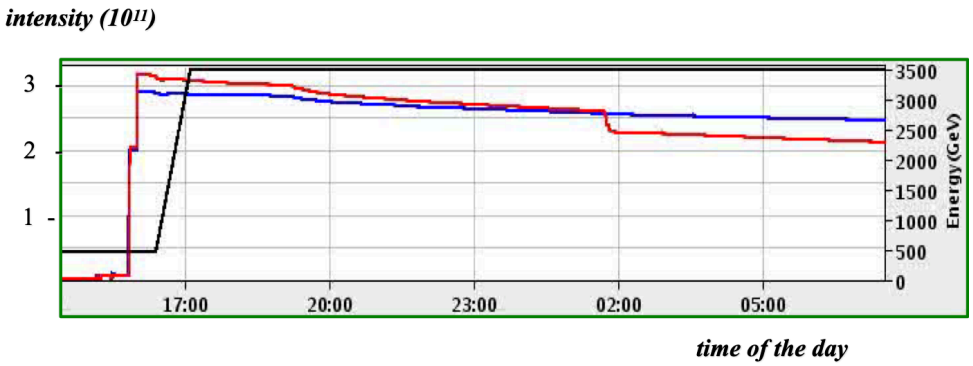

Fig. I.3.1: Typical operation of a particle collider: The red and blue curves show the number of protons stored in the two beams of the LHC during a collider run. The black curve indicates the storage ring energy (right scale). While the beams are stored for many hours to provide proton collisions to the four detectors, the intensity of the beams is decaying slowly until the luminosity is too small and the beams will be replaced, injecting a fresh train of bunches for the next run.

force that can technically be used and applied in physics and engineering. And thus, as a consequence the only force available for us is the Lorentz-force. In general form we can write it as

$$\vec{F} = q \cdot (\vec{E} + \vec{v} \times \vec{B}) \quad , \tag{I.3.1}$$

where the electric field and magnetic induction are written in vector form, $\vec{E}, \vec{B}$ and q and $\vec{v}$ correspond to the particle's charge and velocity.

Talking about high energy physics means talking about particle velocities close to the speed of light, c, and given that $v \approx c$, we realise that the magnetic $\vec{B}$ field in Eq. I.3.1 has a nice amplification factor, that does not exist for the electric field. As an example assume a magnetic field of

$$B = 1\mathrm{T} \quad .$$

The corresponding Lorentz-force acting on a particle of charge $q = 1e$, with e being the elementary charge, is

$$F \approx e \cdot 3 \cdot 10^8 \frac{\mathrm{m}}{\mathrm{s}} \cdot 1 \frac{\mathrm{Vs}}{\mathrm{m}^2} = e \cdot 300 \frac{\mathrm{MV}}{\mathrm{m}} \quad .$$

In other words, a magnetic field of 1 T - something that you can do with a piece of copper wire and magnetic steel in your handicraft workshop - is equivalent to an electric field that is far beyond the usual technical limit of $E \approx 1\,\mathrm{MV/m}$. For the time being, therefore, we will ignore electrical forces and restrict our treatment to the magnetic part of Eq. I.3.1. Nevertheless we have to to mention, that in case we have to design an accelerator for very low energetic particles, where $v \approx 0$, we better use electric fields as the magnetic force is basically zero. The equations of motion and the conclusions that we draw here are nevertheless easily adapted to that case, by replacing $\vec{B}$ by $\vec{E}$, see for example Ref. [2].

1 Magnetic guide field and beam rigidity

In a perfect situation, a charged particle moving in a homogeneous magnetic B-field will follow an ideal circle that depends only on the charge and the momentum of the particle. Schematically the situation is shown in Fig. I.3.2.

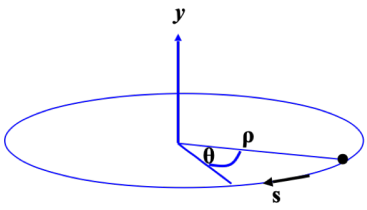

Fig. I.3.2: The movement of a charged particle in a perfect homogeneous magnetic field will describe an ideal circle with bending radius ρ. The coordinate that follows the particle along the ring is called azimuthal coordinate s, the corresponding azimuthal angle is θ and we introduced already the vertical coordinate y which will be used to describe eventual orbit fluctuations in the vertical plane.

The condition for this ideal circle is that the Lorentz-force will counteract the centrifugal force of the circular movement

$$F_{\text{Lorentz}} = evB$$
$$F_{\text{centrifugal}} = \frac{\gamma m_0 v^2}{\rho} \quad .$$

And with

$$\frac{\gamma m_0 v^2}{\rho} = evB \quad ,$$

we obtain

$$\frac{p}{e} = B \cdot \rho \quad , \tag{I.3.2}$$

where we have used the relativistic correct expression for the particle's momentum, $p = \gamma m_0 v$, and $\gamma = \frac{1}{\sqrt{1-v^2/c^2}}$ clearly stands for the Lorentz-factor. Implicitly we have assumed that the magnetic field lines are perpendicular to the movement of the particle and so we could replace the cross product by a normal multiplication. The expression $B \cdot \rho$ in Eq. (I.3.2) is called beam rigidity. It defines the (maximum) momentum that can be carried in our ring for a particle of charge e in a magnetic field B. ρ describes the bending radius of the particle's movement and thus in the end the size of the machine. In case of heavy ions with particles that carry higher charges, we clearly have to modify the equation accordingly, replacing e by q. All in all, we are not too much surprised that we need strong magnetic fields and a large ring to store high energy particle beams.

During acceleration, our magnetic fields will have to follow the energy (or better momentum) of the beam. Therefore it is more convenient to work with normalised values. Dividing the dipole field by the beam rigidity provides us with a parameter that is independent of the particle momentum. And so we have to solve one single equation of motion (what we will do in the next paragraph) instead of doing the

tedious job all along the energy ramp of the machine.

$$\frac{B}{p/q} = \frac{B}{B \cdot \rho} = \frac{1}{\rho} \quad .$$

The inverse of the bending radius of the dipole magnets is indeed the parameter that describes the normalised bending strength of the magnet. In ultra relativistic approximation we can express this normalised bending strength in convenient units: following Eq. I.3.2 we can write

$$\frac{1}{\rho[\mathrm{m}]} \approx 0.3 \cdot \frac{B[\mathrm{T}]}{p[\mathrm{GeV}/c]} \quad .$$

Later, when introducing quadrupole magnets for the focusing of the particle beam, we will come back to this concept and refer to normalised field gradients.
In a typical synchrotron or storage ring, there is clearly no single magnet providing the required bending strength, as implied in Fig. I.3.2. Instead, we replace this ideal scenario by a number of dipoles, doing the job. Still, in each and every dipole magnet, the particle trajectory will follow a part of a circle.
Figure I.3.3 shows an example of a typical storage ring magnet. The two flat pole shoes create a homogeneous field of a certain strength and we only have to power them correctly in order to get a path that closes upon itself. A so-called storage ring therefore is never really a "*ring*" but rather a polygon, where *"poly"* stands for the number of dipole magnets that are positioned along the circumference of the machine. The bending angle that is created by a single dipole magnet is given by the ratio of the orbit

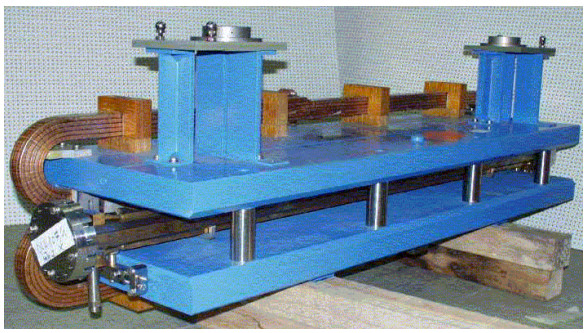

Fig. I.3.3: Example of a normal conducting storage ring dipole magnet that will bend the beam by a well defined angle and so defines the design orbit.

length, which is in an ideal situation the fraction of a circle, and the bending radius ρ

$$\alpha = \frac{ds}{\rho} = \frac{B \cdot ds}{B \cdot \rho} = \frac{B \cdot ds}{p/q} \quad .$$

Schematically the situation is shown in Fig. I.3.4 which shows the measured field map of a storage ring dipole magnet. In practice we have to determine the integrated field strength along the actual particle

trajectory for each dipole magnet in order to determine the corresponding bending angle,

$$\alpha = \frac{\int Bds}{B\rho} \quad .$$

Finally the bending angle of all dipole magnets around the ring has to add up to a full circle, so we have to require

$$\Sigma\left(\alpha_{\text{dipoles}}\right) = \frac{\oint Bds}{p/q} = 2\pi \quad .$$

where we are integrating over the dipole fields around the complete ring. In practice, it turns out that

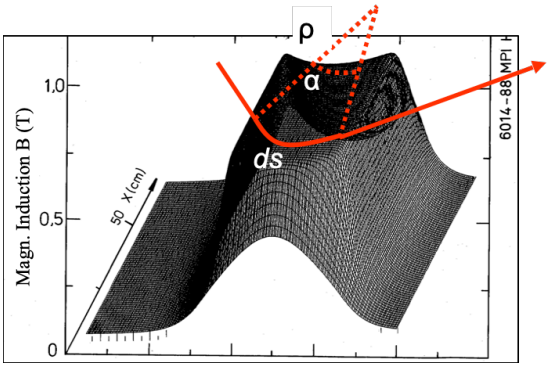

Fig. I.3.4: Field map of a storage ring dipole magnet. Schematically the ideal orbit of a charged particle is included with the path length *ds* and the bending radius ρ.

working with integrated fields is not always an easy story and for practical reasons therefore, the so-called *effective magnetic length* is defined. Assume we integrate in Fig. I.3.4 the *B*-field along the path *ds*. We will get a plot that looks more or less like the one in Fig. I.3.5. It shows a constant field in the centre of the dipole magnet and fringe fields, on both sides. Now, to be more convenient in our calculations and, even more, to have something in hand that we can put into our simulation codes, we replace the area described by the measured field, by a constant magnet field in the centre of the magnet, B_0, and an effective length, as represented by the rectangular shape in the plot, that is defined by

$$B_0 \cdot l_{\text{eff}} := \int_0^{l_{\text{dipole}}} Bds \quad . \tag{I.3.3}$$

This effective length clearly is not the same as the iron length of the magnet yoke. And so, when talking about magnet length in our calculations, we usually refer to the definition given in Eq. (I.3.3).

1.0.1 Example LHC

Figure I.3.6 shows a picture of the two super conducting (s.c.) dipole magnets of the LHC, built out of NbTi filaments, which are operated at a temperature $T = 1.9\,\text{K}$. Unlike particle-antiparticle colliders, where both beams can be guided and stored in the same magnet lattice, two counter rotating proton beams are accelerated and stored in the machine. Therefore, independent apertures have to be provided with the dipole field lines pointing in opposite directions to bend the beams. In this sense, the LHC is a true double ring collider.

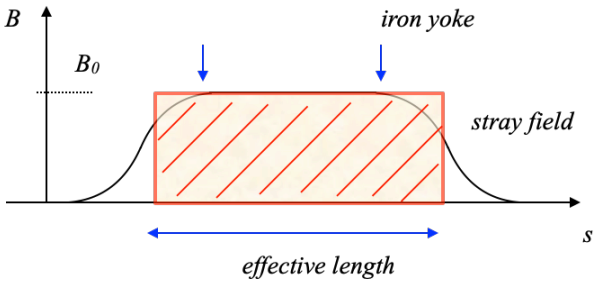

Fig. I.3.5: Effective length of a storage ring magnet replacing the integrated field along the orbit by a simple product of $B_0 \cdot l_{\text{eff}}$.

Fig. I.3.6: Super Conducting LHC dipole magnet. The two dipoles, acting on the counter rotating beams are housed in one common return yoke and cryostat.

1.0.2 Exercise I

The Large Hadron Collider, LHC, provides the highest energy protons available for particle physics experiments. The super conducting dipole magnets create a field of $B = 8.33\,\mathrm{T}$ *and the momentum of the protons is* $p = 7000\,\mathrm{GeV}/c$. *A few main parameters are listed in the table below.*

Table I.3.1: Magnet parameters of the LHC storage ring

circumference	C_0	26 658.9 m	
particle momentum	p	7 TeV/c	
dipole field	B	8.392 T	l_B = 14.2 m
quadrupole gradient	g	235 T/m	l_q = 5.5 m

Calculate the magnetic rigidity of the design beam, the bending radius of the main dipole magnets in the arc and determine the number of dipoles that is needed in the machine.

1.0.3 Exercise II

Question . . . for the fun of it:
Let's build a really cheap storage ring. Just put it to the North Pole and use the magnetic field of the earth

whose field lines are perpendicular to the surface at that nice place. Forget about focusing, . . . that's for nitpickers. What will be the size of the ring for a 10 keV electron beam if the earth magnetic field is about 0.5 Gauß? (1 Gauß $= 10^{-4}$ *Tesla). And in the end, in which direction do you have to circulate the electrons to get stored beam?*

2 Focusing fields: quadrupole magnets

In addition to the main bending magnets that guide the beam onto a closed orbit, focusing fields are needed to keep the particles close together. In modern storage rings and light sources, we have to keep more than 10^{12} particles in the machine, distributed over a number of bunches, and these particles have to be focused to keep their trajectories close to the design orbit. Furthermore, these particles are stored in the machine for many hours, and a carefully designed focusing structure is needed to maintain the necessary beam size at different locations in the ring and guarantee stability of the transverse motion. In other words, on our way through the solar system, we have to keep a very large number of particle trajectories together and we do so, by applying the trick of linear restoring forces.

Following classical mechanics, linear restoring forces lead to harmonic oscillations

$$F = m \cdot a = -const \cdot x = -k \cdot x \qquad ,$$

that's just good old Newton, where a is the acceleration, x refers to the amplitude with respect to the rest position and the constant k describes the strength of the restoring force. Harmonic oscillations have several characteristics that are most adequate for a storage ring: they are stable, have a well defined amplitude and frequency, and most of all, they can be calculated analytically; an advantage that should not be underestimated.

In the case of a storage ring or particle accelerator in general, quadrupole magnets provide the corresponding field property: they create a magnetic field that depends linearly on the amplitude of the particle, i.e., the distance of the particle from the design orbit

$$B_x = -g \cdot y, \qquad B_y = -g \cdot x \qquad .$$

The constant g is called the gradient of the magnetic field and characterizes the focusing strength of the quadrupole lens in both transverse planes. The minus sign refers to the field pattern in the magnet which means that in both planes a larger gradient actually refers to "a more negative field" (see Fig. I.3.8). For convenience, it is normalized (like the dipole field) with respect to the particle momentum. This normalized gradient is usually denoted by k and defined as

$$k = \frac{g}{B \cdot \rho} = \frac{g}{p/q} \qquad .$$

In Chapter II.3 on magnet technology, the design of such a quadrupole will be explained. Here we only state, that they can be built, basically by arranging four pole shoes in a symmetric way giving them a hyperbolic pole shoe form (. . . , which corresponds to an equi-potential surface). The technical realisation of such a quadrupole is depicted in Fig. I.3.7 and the field lines are sketched in Fig. I.3.8. As for the dipoles, in the case of the LHC, quadrupole magnets were built using superconducting technology

to provide highest possible gradients.
It turns out that the gradient g of the quadrupole describes the effect in both transverse dimensions, the horizontal and the vertical plane. Following Maxwell's fourth equation,

$$\vec{\nabla} \times \vec{B} = \mu_0 \vec{j} + \frac{1}{c^2} \frac{\partial \vec{E}}{\partial t}$$

we get at the position of the beam (where there is vacuum and no explicit time varying electric field),

$$\vec{\nabla} \times \vec{B} = 0$$

and so we conclude that

$$g := -\frac{\partial B_x}{\partial y} = -\frac{\partial B_y}{\partial x} \quad .$$

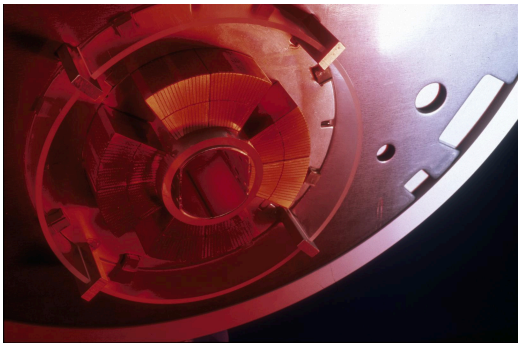

Fig. I.3.7: Super Conducting LHC quadrupole magnet. The main quadrupoles in the arc are powered in series with the dipole magnets and define the basic focusing structure of the machine.

2.0.1 Exercise III

Referring to the magnet parameter list in Table I.3.1 calculate the k-strength of the LHC quadrupole magnets.

In Fig. I.3.8 the direction of the Lorentz-force is included that follows from the usual "right-hand-rule", and there is a slight feeling of discomfort. It seems that the Lorentz-force in the given example has a focusing effect in the horizontal (x-) plane, while in the vertical (y-) plane it will push the particle further away from the magnet centre. We will come back to this defocusing effect in a moment. For the time being we just state that it makes our life not easier.

Now that we have defined the two basic building blocks of a storage ring, we need to arrange them in a so-called magnet lattice and optimize the field strengths in such a way as to obtain the required beam parameters. An example of how such a magnet lattice looks like is given in Fig. I.3.9. This photograph shows the dipole (orange) and quadrupole (red) magnets in the TSR storage ring in Heidelberg [3]. Eight dipoles are used to bend the beam into a "circle", and the quadrupole lenses between them provide the focusing to keep the particles within the aperture limits of the vacuum chamber. A general design principle of modern synchrotrons and storage rings should be pointed out here. In general, these machines

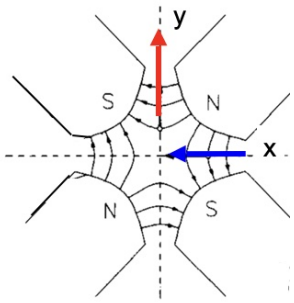

Fig. I.3.8: Field lines in a quadrupole magnet: a focusing effect in the horizontal plane goes along with an inevitable defocusing effect in the vertical plane . . . et vice versa.

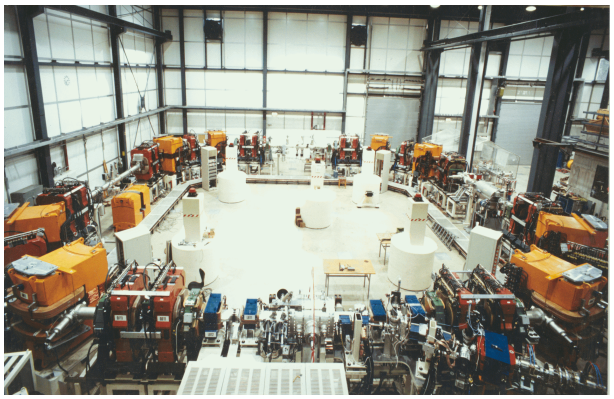

Fig. I.3.9: The TSR storage ring, Heidelberg, as a typical example of a separate-function strong-focusing storage ring (Courtesy: M. Grieser, MPI).

are built following a so-called *separate function* scheme: every magnet is designed and optimized for a certain task, such as bending, focusing, or chromatic correction. We separate the magnets in the design according to the job they are supposed to do; only in rare cases a combined-function scheme is chosen nowadays, where different magnet properties are combined in one piece of hardware. To express this principle mathematically, we use the general Taylor expansion of the normalized magnetic field,

$$\frac{B(x)}{p/e} = \frac{1}{\rho} + k \cdot x + \frac{1}{2!} m \cdot x^2 + \frac{1}{3!} n \cdot x^3 \qquad . \tag{I.3.4}$$

Schematically the field pattern of the individual contributions are shown in Fig. I.3.10. In the context of the linear approximation, we will refer to the two main building blocks, dipoles and quadrupoles, that form the basic lattice of our storage ring.

Higher-order fields will be treated later for correction of optical errors or as (hopefully) small perturbations.

3 Equation of motion

Under these assumptions, we can derive — in a linear approximation — the equation of motion of the transverse particle movement. We start with a general expression for the radial acceleration as known

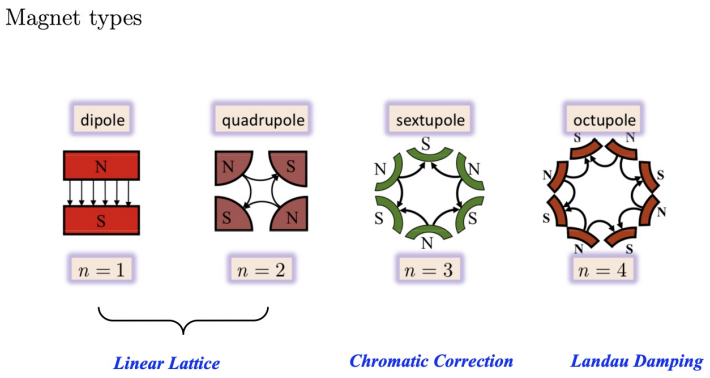

Fig. I.3.10: Field pattern of different magnet types used in accelerators.

from classical mechanics (see, e.g. Ref. [4])

$$a_{\mathrm{r}} = \frac{d^2\rho}{dt^2} - \rho\left(\frac{d\theta}{dt}\right)^2 \quad .$$

There are two terms that contribute to the radial acceleration: An explicit change of the radius with time and the well-known centrifugal force. Assume we rotate a lasso with a fixed length of the rope. In this ideal case the first term is zero, $d\rho/dt = 0$, and we remain with the usual centrifugal force

$$F_{\mathrm{centrifugal}} = m \cdot |a_{\mathrm{r}}| = m \cdot \rho(\frac{d\theta}{dt})^2 = m \cdot \rho\,\omega^2 = mv^2/\rho \quad ,$$

where ω is the angular frequency and v the tangential velocity.

Figure I.3.11, which is basically a copy-paste of I.3.2 describes this situation. On top of the ideal circle that we introduced, we plot schematically a particle trajectory, that is described by the coordinates x, y for the horizontal and vertical amplitude of the particle, at a given location s in the ring. For convenience we use this "Frenet-Serret" ortho-normal basis, $\vec{x}, \vec{y}, \vec{s}$ where the point s, representing the azimuth position of the particle, is travelling with the particle around the ring.

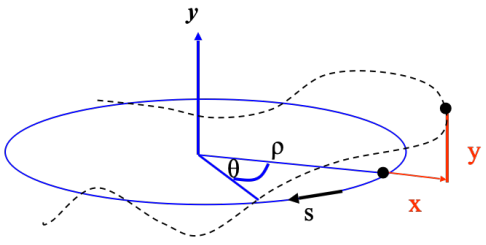

Fig. I.3.11: Coordinate system used in particle beam dynamics; the longitudinal coordinate s moves around the ring with the particle considered. Horizontal and vertical coordinates, x and y refer to the distance to the ideal design orbit.

Referring to our coordinate system, and replacing the ideal radius ρ by $\rho + x$ for the general case, we require a balance between the radial force and the counter-acting Lorentz force, which is the condition

for a circle:

$$F_{\text{centrifugal}} + F_{\text{Lorentz}} = 0$$

or

$$m \cdot \frac{d^2}{dt^2}(x+\rho) - \frac{mv^2}{x+\rho} = -eB_{\text{y}}v \qquad ,$$

where we assume an ideal bending field, with vertical field lines only. The negative sign in front of the *B*-field tells us that indeed the Lorentz-force will point towards the centre of the ring, thus compensating the centrifugal force.
As we consider a constant bending radius ρ that describes the ideal particle, the first term simplifies

$$\frac{d^2}{dt^2}(x+\rho) = \frac{d^2}{dt^2}x$$

and we develop the second term for small amplitudes, in the sense that usually *(i.e. hopefully)* x is of the order of *mm*, while the size of the accelerator is quite macroscopic,

$$\frac{1}{x+\rho} \approx \frac{1}{\rho}(1-\frac{x}{\rho}) \qquad .$$

Indeed, in the case of the very high energy colliders, the dimensions of a typical storage ring are in the order of *meter* or even *kilometer*, while the typical oscillation amplitudes are small: we have to require that the beam trajectories remain well within the vacuum chamber or at least in the accelerator tunnel.
So we get for the balance between centrifugal and centripetal force

$$m\frac{d^2x}{dt^2} - \frac{mv^2}{\rho}(1-\frac{x}{\rho}) = -eB_{\text{y}}v \qquad .$$

Now, in a next step of approximation, we refer to linear (or constant) magnetic fields. However, we would like to emphasize, that this is quite a bit more than *"for convenience"*. By referring to linear fields, we will get finally an equation of motion that can be solved analytically ... and as important as that, ... it leads to stable particle trajectories. We will show later that on the other side, strong non-linear forces can cause orbit distortions of increasing amplitudes and the particles might get lost.

So, for good reasons we make the approximation

$$B_y \approx B_0 + x \cdot \frac{\delta B_{\text{y}}}{\delta x} \qquad .$$

Here the first term refers to the constant dipole field (we will drop the subscript "0" in the future) and the second term describes the bending force of a particle with amplitude x in a quadrupole magnet. All other higher order terms are neglected. But don't worry, we will come back to non-linear fields as higher order corrections in Chapter I.9 or as causes of trouble. For the time being we get

$$m\frac{d^2x}{dt^2} - \frac{mv^2}{\rho}(1-\frac{x}{\rho}) = -ev \cdot (B_0 + x\frac{\partial B_{\text{y}}}{\partial x})$$

and dividing by the mass m we obtain

$$\frac{d^2x}{dt^2} - \frac{v^2}{\rho}(1 - \frac{x}{\rho}) = -\frac{ev \cdot B_0}{m} + x\frac{evg}{m} \quad . \tag{I.3.5}$$

Here we make a little rest to contemplate about the situation. It is convenient in most problems of mechanics to use the time t as independent variable. However, in an accelerator I do not care about *when*. The particles are running at the speed of light anyway (or quite close to it). What we really want to know in accelerators, as soon as it comes to describe particle trajectories, is the *where*. And so we will change from the independent variable *time* to the coordinate s.

$$t \rightarrow s$$

$$\frac{dx}{dt} = \frac{dx}{ds} \cdot \frac{ds}{dt}$$

$$\frac{d^2x}{dt^2} = \frac{d}{dt}(\frac{dx}{ds} \cdot \frac{ds}{dt}) = \frac{d}{ds}(\frac{dx}{ds} \cdot \frac{ds}{dt}) \cdot \frac{ds}{dt}$$

$$\frac{d^2x}{dt^2} = x''v^2 + \frac{dx}{ds} \cdot \frac{dv}{ds}v \quad ,$$

where we have introduced the common notation

$$x' = \frac{dx}{ds}, \qquad x'' = \frac{d^2x}{ds^2}$$

for the angle x' of the trajectory and its rate of change x''. As we can assume that the speed v is constant (at least in the time interval of typical transverse oscillations) the second term of the last equation is zero. And Eq. I.3.5 becomes

$$x''v^2 - \frac{v^2}{\rho}(1 - \frac{x}{\rho}) = -\frac{evB_0}{m} + \frac{e \cdot v \cdot x \cdot g}{m} \quad . \tag{I.3.6}$$

The transformation from time to coordinate s might sound a bit strange or at least abstract. However it is the right thing to do. Figure I.3.12, visualises schematically the story: In order to understand the trajectory we need the particle's amplitude and angle, *x* and *x'*. And we do not have to point out that the same holds for the vertical plane, where traditionally we use *y* and *y'*.

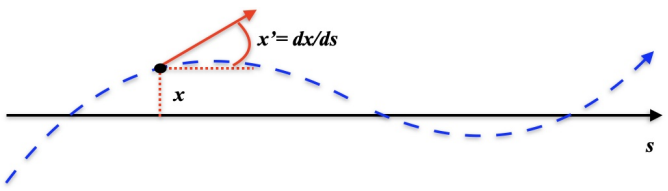

Fig. I.3.12: Schematic particle trajectory with horizontal amplitude *x* and angle *x'*.

Dividing in Eq. I.3.6 both sides by v^2 and remembering that $p = m \cdot v$, we get

$$x'' - \frac{1}{\rho} + \frac{x}{\rho^2} = -\frac{B_0}{p/e} + \frac{xg}{p/e} \quad . \tag{I.3.7}$$

The second term on the left hand side is just the bending strength, $1/\rho$, which cancels with the first term on the right. And so we finally get (with $k = \frac{g}{p/e}$)

$$x'' + x(\frac{1}{\rho^2} - k) = 0 \quad . \tag{I.3.8}$$

3.1 A few remarks

– Looking at the differential Eq. I.3.8, there seems to be a focusing force, even in the absence of any quadrupole field. Indeed, for $k = 0$ we obtain

$$x'' + \frac{1}{\rho^2}x = 0$$

and the restoring force is given by the bending strength of the dipoles. The effect is called "weak focusing" and plays an essential role for small accelerators, where bending radii are small, i.e. more in the range of meters. For large rings with kilometer radii, the effect is usually negligible. Still, to be exact, it will be taken into account, even in the case of the LHC. And—it goes without saying—the weak focusing only contributes in the plane of bending, which is usually the horizontal plane.

– According to this equation, and following the logic of the field line pattern in a quadrupole, the sign convention used in this school refers to negative numerical values for the normalised gradient $k = -|\partial B_y/\partial x| \cdot e/p$ in (horizontally) focusing quadrupole fields and we will find this convention in the very same manner in basically all text books on beam dynamics.

– We would like to emphasize once more that for the derivation of Eq. I.3.8 we referred to linear approximation which means small amplitudes in x and linear terms for the magnetic field.

– Finally, a more serious remark: the Lorentz force points to the centre of the magnet, and we call it a focusing lens. Due to the geometry of the field lines in a quadrupole, schematically shown already in Fig. I.3.8, the very same magnet will have the opposite effect for particles that pass with a vertical amplitude, y. Mathematically expressed, the equation of motion does not have the weak focusing term, as long as we can assume that the machine is built in the horizontal plane. The thrilling fact, however, is that we get a sign change in front of the normalised focusing strength

$$y'' + k \cdot y = 0 \quad .$$

Due to the principal problem arising from the different directions of the Lorentz force in the two transverse planes of a quadrupole field, we have to explicitly introduce quadrupole lenses that focus the beam in the horizontal and vertical directions in some alternating order, and it is the task of the machine designer to find an adequate solution to this problem and to define a magnet pattern that will provide an overall focusing effect in both transverse planes.

4 Solution of trajectory equations

We will start with the focusing case, which is the more comfortable situation, and—following the convention of most textbooks—we combine the weak and strong focusing term in Eq. I.3.8: $K = 1/\rho^2 - k$. The general solution of this differential equation (which is in full beauty the equation of a harmonic oscillator) is the combination of the two fundamental solutions of sin- and cos-type

$$x(s) = a_1 \cdot \cos(\nu\ s) + a_2 \cdot \sin(\nu\ s) \qquad ,$$

where a_1 and a_2 are determined by the initial conditions of amplitude and angle of the particle trajectory and the oscillation frequency ν clearly is determined by the strength of the restoring force.

For simplicity, we refer to the horizontal plane for a moment; a "focusing" magnet is therefore focusing in this horizontal plane and at the same time defocusing in the vertical plane. Starting with the initial conditions for the particle amplitude x_0 and angle x_0' in front of the magnet element, where we set $s = 0$, we obtain the following initial values

$$a_1 = x_0\ , \quad a_2 = \frac{x_0'}{\sqrt{K}}$$

and we can express the general solution for the amplitude of the particle trajectory as

$$x(s) = x_0 \cdot \cos(\sqrt{|K|}\ s) + x_0' \cdot \frac{1}{\sqrt{K}} \sin(\sqrt{|K|}\ s) \qquad . \tag{I.3.9}$$

Differentiating Eq. I.3.9 with respect to the coordinate s we get the angle,

$$x'(s) = -x_0 \cdot \sqrt{|K|} \cdot \sin(\sqrt{|K|}\ s) + x_0' \cdot \cos(\sqrt{|K|}\ s) \qquad . \tag{I.3.10}$$

For convenience we like to combine these two equations in a more compact matrix form, by combining amplitude x and angle x' of the trajectory in form of a vector. The transformation from the position in front of the magnet, point s_0, to a position after the magnet, point s_1, schematically shown in Fig. I.3.13, can then be expressed by a simple matrix multiplication

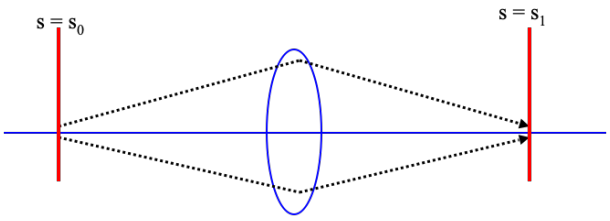

Fig. I.3.13: Schematic drawing of amplitude x and angle x' transferred through a focusing quadrupole magnet.

$$\begin{pmatrix} x \\ x' \end{pmatrix}_{s1} = M_{\text{foc}} \cdot \begin{pmatrix} x \\ x' \end{pmatrix}_{s0} \tag{I.3.11}$$

with the matrix M_{foc}

$$M_{\mathrm{foc}} = \begin{pmatrix} \cos(\sqrt{|K|}\cdot l_{\mathrm{q}}) & \frac{1}{\sqrt{|K|}}\sin(\sqrt{|K|}\cdot l_{\mathrm{q}}) \\ -\sqrt{|K|}\cdot\sin(\sqrt{|K|}\cdot l_{\mathrm{q}}) & \cos(\sqrt{|K|}\cdot l_{\mathrm{q}}) \end{pmatrix} \tag{I.3.12}$$

where via $|K|$ and l_{q} the matrix "knows everything" about the magnet. Namely its focusing strength and effective magnetic length, as defined above. This last statement deserves quite a bit of attention. On our way through the solar system, up to Pluto, we have to be very precise to be successful. In other words: while Eq I.3.11 looks pretty simple and straight forward, a high level of accuracy has to be put on the exact measurement of the magnet parameters in order to condense e.g. the properties of a 14 m long super conducting LHC dipole into two parameters, effective length and normalised gradient.

In the case of a defocusing lens, schematically shown in Fig. I.3.14, we proceed in principle in a equivalent manner. Except one fact: due to the field line pattern, shown above in Fig. I.3.8, the equation of motion now is

$$y'' + k\cdot y = 0$$

and the general solution is based on the *hyperbolic* trigonometrical functions

$$y(s) = y_0\cdot\cosh(\sqrt{|K|}\,l_{\mathrm{q}}) + y_0'\cdot\frac{1}{\sqrt{K}}\sinh(\sqrt{|K|}\,l_{\mathrm{q}})$$

or taken into account again the derivative and expressed again in matrix form

$$\begin{pmatrix} y \\ y' \end{pmatrix}_{s1} = M_{\mathrm{defoc}}\cdot\begin{pmatrix} y \\ y' \end{pmatrix}_{s0} \tag{I.3.13}$$

with

$$M_{\mathrm{defoc}} = \begin{pmatrix} \cosh(\sqrt{|K|}\cdot l_{\mathrm{q}}) & \frac{1}{\sqrt{|K|}}\sinh(\sqrt{|K|}\cdot l_{\mathrm{q}}) \\ \sqrt{|K|}\cdot\sinh(\sqrt{|K|}\cdot l_{\mathrm{q}}) & \cosh(\sqrt{|K|}\cdot l_{\mathrm{q}}) \end{pmatrix} \quad . \tag{I.3.14}$$

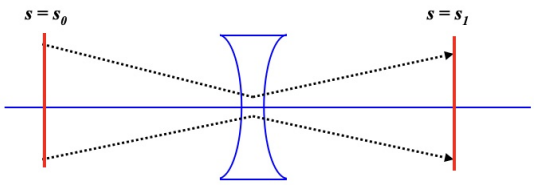

Fig. I.3.14: Schematic drawing of amplitude x and angle x' transferred through a defocusing quadrupole magnet.

We do not have to emphasize that the situation flips if a vertical focusing quadrupole lens is considered.

Now, while Eq. I.3.14 looks pretty similar to Eq. I.3.12 there is a fundamental difference coming from the little h, which is present: the true trigonometrical functions, *sin* and *cos* are limited to values of ± 1; the hyperbolic functions are not. And so, introducing the—unavoidable—defocusing effect, causes a certain

level of trouble. Figure I.3.15 visualises the situation.

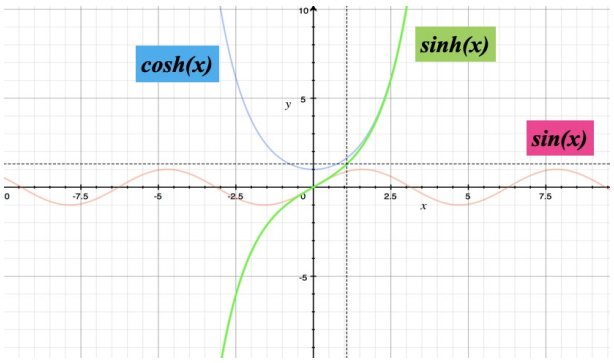

Fig. I.3.15: The fundamental solutions in case of focusing or defocusing magnets.

As a consequence we have to be very careful in combining magnets that are focusing in one plane, while defocusing in the other, and at the same time vice versa. Solutions exist, however it is all too easy to create a magnet lattice that does *not* work.

As last basic element in our storage ring lattice we introduce the drift. Namely everything that has no (or negligible) focusing effect on our trajectories will be treated as bare drift space, and the matrix, describing this is

$$M_{\text{drift}} = \begin{pmatrix} 1 & l_{\text{d}} \\ 0 & 1 \end{pmatrix} \quad ,$$

which means that the particle will follow a straight line, defined by the initial amplitude and angle, going straight until the next focusing element will arrive, see Fig. I.3.16.

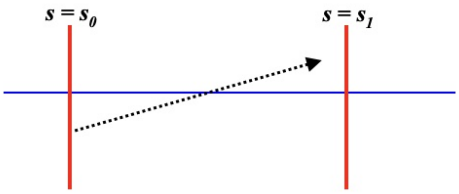

Fig. I.3.16: Schematic drawing of amplitude x and angle x' while propagating in a drift. As no focusing nor defocusing fields are present in this trivial case, the trajectory is a straight line.

Now, clear enough, we can multiply the initial amplitude and angle, x, x' using the matrix for each and every lattice element to find our way through the magnet structure. Or—which is mathematically fully equivalent—we can transform the x, x' though a complete lattice structure by transforming it through the product matrix of the single magnet elements involved

$$\begin{pmatrix} x \\ x' \end{pmatrix}_{\text{s1}} = M_{\text{product}} \cdot \begin{pmatrix} x \\ x' \end{pmatrix}_{\text{s0}} \quad . \tag{I.3.15}$$

One word for Math lovers:

We talk about a differential equation of second order, which has two independent solutions

$$x'' + Kx = 0$$

that can be combined to give the general solution. E.g.

$$x(s) \quad = x_0 \cdot \underbrace{\cos(\sqrt{|K|}\, s)}_{C} + \quad x_0' \cdot \underbrace{\frac{1}{\sqrt{K}} \cdot \sin(\sqrt{|K|}\, s)}_{S} \tag{I.3.16}$$

with its derivative

$$x'(s) \quad = x_0 \cdot \underbrace{[-\sqrt{|K|} \cdot \sin(\sqrt{|K|}\, s)]}_{C'} + \quad x_0' \cdot \underbrace{\cos(\sqrt{|K|}\, s)}_{S'} \quad . \tag{I.3.17}$$

To save some ink we introduced C and S for the trigonometrical terms. Now, Wronski tells us that the two solutions are independent of each other if the *Wronski* determinant *W* is different from zero, with

$$W = \begin{vmatrix} C & S \\ C' & S' \end{vmatrix} \quad .$$

Now, it is easy to show that in our case the derivative of W is zero,

$$\frac{d}{ds}W = CS'' - SC'' = -K(CS - SC) = 0$$

and so $W = \text{const}$, which means we just have to determine the value of *W* at one location and we choose $s = 0$ for convenience. For $s = 0$ we get

$$C_0 = 1, \quad S_0 = 0 \tag{I.3.18}$$

$$C_0' = 0, \quad S_0' = 1 \tag{I.3.19}$$

and so

$$W = 1$$

which is true for all locations s, which is true for all accelerator lattice elements and which is true for any combination of lattice elements, as these are combined by simple matrix multiplications. And this is in the end a quite useful fact.

As example we show in Fig. I.3.17 a simple toy-storage ring out of dipole and quadrupole magnets. The arrangement is a regular sequence of bending and focusing magnets, which is called a "FoDo" structure and we will study it in more detail in a later section. The particle trajectory will circulate around this little ring, while in the two transverse planes it will perform the transverse oscillations that we described above. Mathematically the vector (x, x') will be transferred from one element to the next via a matrix multiplication. However we can combine the effect of several lattice elements by simply

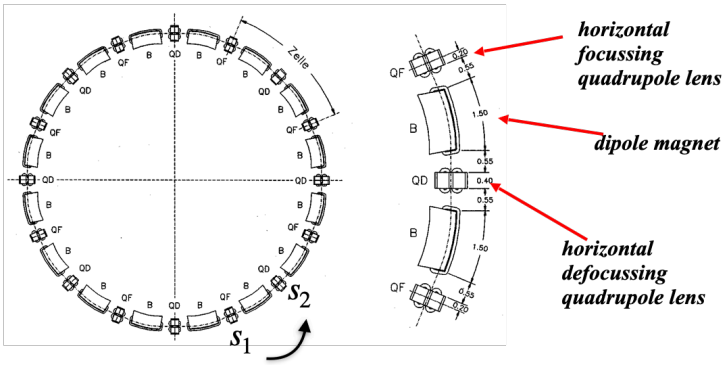

Fig. I.3.17: Toy-storage ring consisting out of dipole and focusing and defocusing quadrupole magnets (Courtesy of K. Wille [5]).

multiplying the different single element matrices together. Form point s_1 to point s_2 as marked in the figure, we get for example:

$$M_{\text{total}} = M_{\text{foc}} \cdot M_{\text{drift}} \cdot M_{\text{bend}} \cdot M_{\text{drift}} \cdot M_{\text{defoc}} \cdot M_{\text{drift}} \ldots$$

which makes it very convenient.
In this little example we have chosen a few *reasonable* values for the basic parameters of the lattice modules, in order to describe what's happening:

- quadrupole length: $l_q = 0.5\,\text{m}$,
- drift length : $l_{\text{d}} = 2.5\,\text{m}$,
- normalised focusing strength: $K = \pm 0.541\,\text{m}^{-2}$.

We can use this values to determine the single element matrix for each module and then—starting from a given value for amplitude x and angle x'—determine step by step the horizontal trajectory while the particle is circulating around the ring. Figure I.3.18 shows the result. Under the influence of the external magnetic fields we observe a kind of zig-zag curve of the transverse motion. Starting from

$$\begin{pmatrix} x \\ x' \end{pmatrix} = \begin{pmatrix} 70\,\text{mm} \\ 0\,\text{mrad} \end{pmatrix}$$

in front of the first focusing quadrupole, the particle is focused towards the middle of the vacuum chamber, drifting with constant angle for a while until it is defocused - but not too strong - in the QD magnet etc. Several facts have to be emphasized here:

- At any moment the trajectory of the particles is a part of a well defined oscillation, in the focusing magnets a *harmonic* oscillation.
- And at every moment we calculate exactly the amplitude and the angle, that depend on the initial conditions and the focusing properties of the magnets.
- There is an overall quasi-harmonic oscillation once around the ring with a well-defined number of oscillations per turn (or per time, which is equivalent). This overall oscillation frequency depends

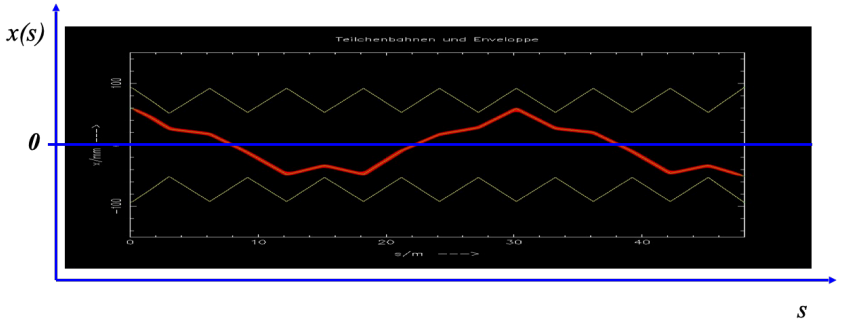

Fig. I.3.18: Particle trajectory in the storage ring of Fig. I.3.17. The particle performs 1.4 transverse oscillations per turn—which is expressed in oscillations per revolution time the eigenfrequency of the particle.

only on the common overall focusing properties of the magnet lattice and is called "tune". Like the tune in music it describes the *"Eigenfrequency"* of the system and is most important. And for obvious reasons it's called *tune* as well.

In the ideal world that we are describing here, each and every particle, independent of its amplitude, will feel the same restoring forces and so will oscillate with the same tune, which is in the example of Fig. I.3.18 approximately 1.4 oscillations per turn.
For those who do not like too many calculations . . . a storage ring of $C_0 = 300\,\mathrm{m}$ with electrons circulating at the speed of light (as they nearly always do) corresponds to a revolution time of $1\,\mu\mathrm{s}$. So in the example chosen, with $C_0 = 50\,\mathrm{m}$ the time for one revolution is $\frac{1}{6}\,\mu\mathrm{s}$ and the frequency of the transverse oscillations is

$$f_0 \approx 8.4\,\mathrm{MHz}.$$

Coming closer to a real, existing machine, we show in Fig. I.3.19 an orbit measured during one of the first injections into the LHC storage ring. The horizontal oscillations are plotted in the upper half of the figure and the vertical oscillations in the lower half, on a scale of ±10 mm. Each histogram bar indicates the value recorded by a beam position monitor at a certain location in the ring, and it is easy going to combine these histogram bars to a quasi-harmonic oscillation. By counting (or, better, fitting) the number of oscillations in both transverse planes, we obtain values of the tunes: $Q_x = 64.3$ and $Q_y = 59.3$.

A last comment on this topic . . . for the time being:
As the tune characterizes the particle oscillations under the influence of all external fields, it is one of the most important parameters of a storage ring and has a far-reaching importance. It is a global machine parameter, that describes the overall focusing properties of the system. Therefore, it is usually measured, displayed and controlled at any moment in a storage ring. Figure I.3.20 shows such measurement. The (non-integer) parts of the horizontal (green) and vertical (red) tunes of the HERA collider are measured and analysed and the Fourier spectrum is displayed in the control room. The peaks indicate the two transverse tunes of the machine, and in a sufficiently linear machine and quasi mono-energetic beams a fairly narrow spectrum is obtained.

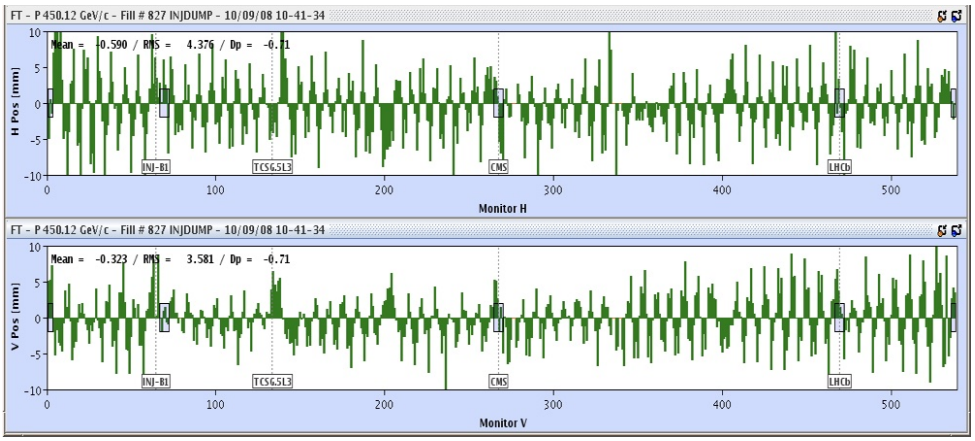

Fig. I.3.19: Particle trajectory in real life: the closed orbit of the LHC storage ring during early commissioning. Each bar corresponds to the measured position in the horizontal (upper part) and vertical (lower part) plane, as measured by a beam position monitor. Given the total length of the machine and the strong focusing, the particles perform many transverse oscillations per turn adding up to a horizontal & vertical tunes of $Q_x = 64.3$ and $Q_y = 59.3$.

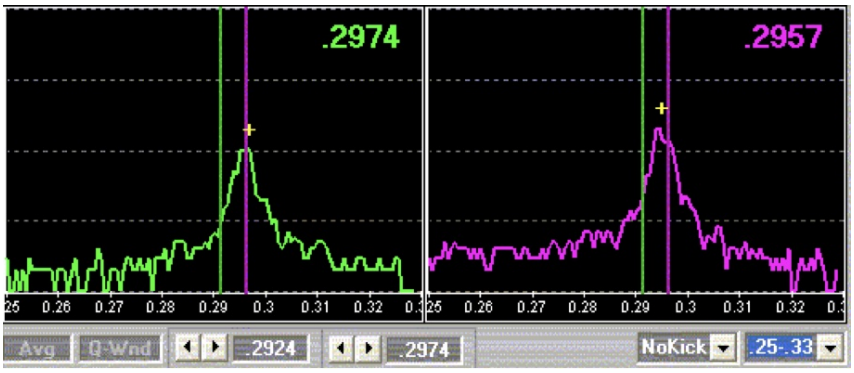

Fig. I.3.20: Tune measurement as usually displayed in the storage ring control room: displayed are Fourrier spectra of the non-integer values of the measured hor & vert. tunes $Q_x = 0.2974$, $Q_y = 0.2957$.

4.1 Thin lens approximation

The matrix formalism, described above is very useful and we can easily transfer the amplitude and angle, *x,x'* at a given position to any other place in the ring . . . provided that we are strong in calculating trigonometrical functions, $\cos$ & $\sin$ and, even more, their hyperbolic colleagues, $\cosh$ & $\sinh$. However we can make our life a bit easier, at least if it comes to a first approximation and we indeed usually do so, before we ask our large computer codes to do the job.
So, in case the focal length f of the quadrupole lens is considerably larger than the actual length of the magnet, we can approximate e.g. in the case of a focusing quadrupole the matrix,

$$M_{\text{foc}} = \begin{pmatrix} \cos(\sqrt{|K|} \cdot l_q) & \frac{1}{\sqrt{|K|}} \sin(\sqrt{|K|} \cdot l_q) \\ -\sqrt{|K|} \cdot \sin(\sqrt{|K|} \cdot l_q) & \cos(\sqrt{|K|} \cdot l_q) \end{pmatrix}$$

by reducing the magnet length to zero, while keeping its focusing properties constant

$$l_q \to 0, \qquad f = \frac{1}{K \cdot l_q} = \text{const.}$$

Using this approximation the matrix simplifies considerably and we obtain in the case of a focusing magnet

$$M_{\text{foc}} = \begin{pmatrix} 1 & 0 \\ \frac{-1}{f} & 1 \end{pmatrix} \quad .$$

For the case of a defocusing lens we only have to change the sign of f

$$M_{\text{defoc}} = \begin{pmatrix} 1 & 0 \\ \frac{1}{f} & 1 \end{pmatrix} \quad .$$

These expressions are very useful for fast (and in large machines still quite accurate) "back on the envelope calculations" . . . and for the guided studies shown in this chapter.

The quantity f that we introduced in this context is called focal length and its meaning corresponds—as schematically shown in Fig. I.3.21—to the equivalent parameter in lenses of the classical light optics. A particle trajectory with amplitude x_0, parallel to *"s"*, so $x_0' = 0$, will be focused to

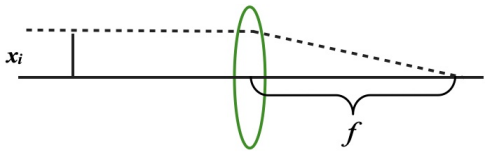

Fig. I.3.21: Definition of the focal length of a quadrupole magnet

$x = 0$ within the length f, i. e.

$$x_i - x_f' \cdot f = 0$$

where x_f' is the angle of the trajectory after passing the magnet, and it is given by

$$x_f' = \frac{l}{\rho} = \frac{B \cdot l}{B\,\rho} \quad . \tag{I.3.20}$$

From the previous equation we have

$$x_f' = \frac{x_i\, g\, l_q}{B\,\rho} = x_i K l_q \tag{I.3.21}$$

and so we can write

$$x_i - x_i \cdot K l_q \cdot f = 0$$

and finally

$$f = \frac{1}{K \cdot l_q} \quad .$$

4.2 Exercise IV

We refer to Exercise III, where we calculated the k-strength of the LHC quadrupoles. The question now is, can this magnet be treated mathematically as a thin lens?

- *How does the matrix for such a (focusing) magnet look like?*
- *How would you establish a description of this magnet in thin lens approximation? Compare the matrix elements.*

Veni vidi vici, as someone said, [6]:

- we can calculate the trajectory of a single particle, inside a storage ring magnet (lattice element);
- for arbitrary initial conditions x_0, x_0';
- and we can combine these trajectory parts (also mathematically) to get the complete transverse trajectory around the storage ring.

Now, it is a matter of fact that we consider a storage ring or a synchrotron and we face the problem that we are dealing with a periodic situation. So, in case we did not make too many mistakes and the particle will survive the first turn in the ring, the question is what will happen now? In other words, referring to Fig. I.3.18, the question is: how will the trajectory of the particle look like on the second turn, or the third, or after an arbitrary number of turns. Now, as we have a circular machine, the amplitude and angle *x* and *x'* at the end of the first turn will be the initial conditions for the second turn, and so on. This provides a level of complication that our colleagues from the linear particle colliders do not have, (which does not mean that these accelerator types are easier). Anyway the trajectory coordinates, *x,x'* and *y,y'* after the first turn will by nature of the problem (called circular machine) be the starting condition of the second turn. And the end coordinates after this second turn will be the start values of turn number three and so on. Schematically we get a situation like in Fig. I.3.22 with an increasing number of turns, overlapping somehow turn by turn. Here we must emphasize an important issue: as the particle will see - turn by turn - the very same external focusing forces, the overall number of oscillations per turn, - called the *tune* - is the same for each and every turn. We will change this nice property in a while, but for the moment everything is perfect.

Now, after many turns, the overlapping trajectories will begin to form a pattern, more or less such as that in Fig. I.3.23, which indeed looks like something that we would call a beam that here and there has a larger and a smaller size but still remains well defined in its amplitude by the external focusing forces. And it makes no difference whether we follow one particle turn-by-turn, or whether we inject a number of particles with different initial conditions that will perform one turn (or hopefully many).

As explained above, repeating the calculations that lead to the orbit of the first turn will—repeated for many turns—result in a large number of matrix multiplications and the single-particle trajectories will overlap in some way and form the beam envelope. Clearly, as soon as we are talking about many turns or many particles, the use of the single-trajectory approach is quite limited and we need a description of the beam as an ensemble of many particles. To make it very clear: if I want to know how warm it is in the audimax of the university, I do not want to get the answer that the Maxwell distribution of a

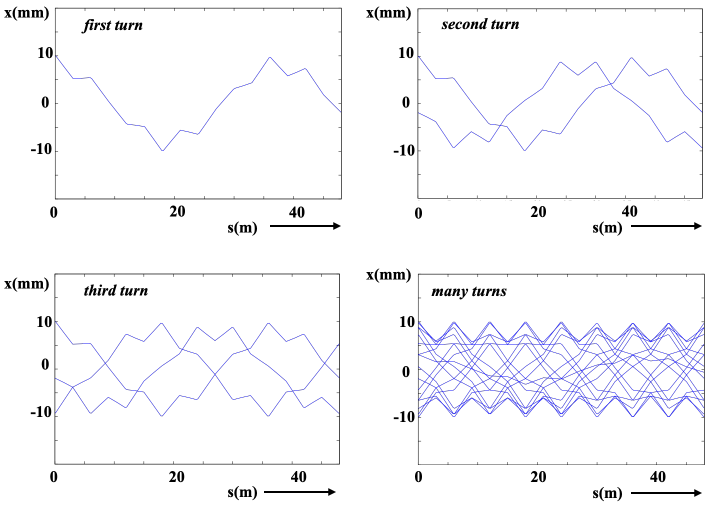

Fig. I.3.22: Particle trajectories in a circular accelerator. The amplitude and angle at the end of turn 1 will be the starting values of turn 2, and so on, turn by turn.

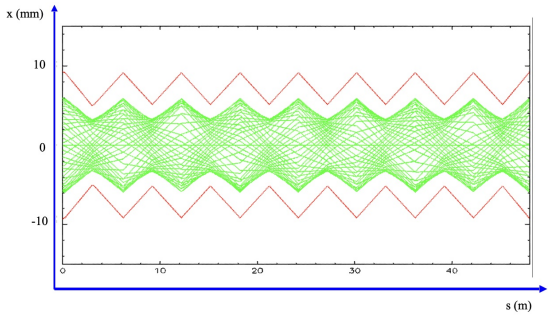

Fig. I.3.23: Over many turns the overlapping tracks of a particle trajectory will form a pattern, that looks indeed like something called “beam”, with a certain envelope surrounding all trajectories, indicated as red curve in the plot.

given idealised gas will be etc. etc. and so we will have a certain kinetic energy for each and every gas molecule. What we want to know is one parameter that describes the situation, which in this case clearly will be the *temperature*. And fortunately such a single parameter also exists in particle beams.

4.3 Solution of Hill’s equation: the beta-function

Fortunately, in the case of periodic conditions in the accelerator, there is another way to describe the particle trajectories and, in many cases, it is more convenient than the above-mentioned formalism. It is important to note that, in a circular accelerator, the focusing elements are necessarily periodic in the orbit coordinate “*s*” after one revolution. Furthermore, storage ring lattices have often an internal periodicity: in most cases they are constructed, at least partly, from sequences in which identical magnetic structures, the lattice cells, are repeated several times in the ring and lead to periodically re-curring focusing properties. In this case, the equation of motion can now be written in a slightly different form.

In order to understand, I am afraid, we have to go back to the year *1886*. An astronomer and bril-

liant mathematician named G.W. Hill, studied the problem of understanding the movement of the moon around the earth. And while we can discuss why any diligent human being would choose such a problem to spend his free time (instead of playing golf e.g.) the problem is not as easy as it looks on the first side. If it were a two-body situation the result is known and we all learned about ellipses that are the solution. However here we encounter the periodic (!) external influence of the sun: while the moon is circulating once around the earth within one month the perpetuate gravitational pull of the sun cannot be neglected. Lucky enough, Mr. Hill found a solution, see Fig. I.3.24 which for a mathematician means he could formulate the differential equation to the problem, that we cite here: The equation of motion, derived in

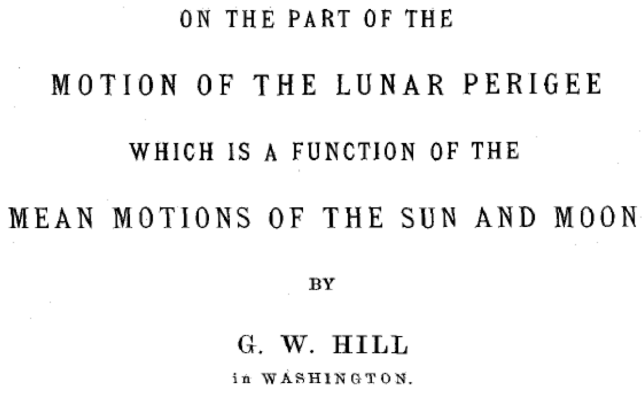
ON THE PART OF THE

MOTION OF THE LUNAR PERIGEE

WHICH IS A FUNCTION OF THE

MEAN MOTIONS OF THE SUN AND MOON

BY

G. W. HILL

in WASHINGTON.

Fig. I.3.24: Original paper of G.W. Hill, which defines the basis of modern storage ring beam dynamics [7].

the above mentioned paper and expressed in a form that is convenient for us is

$$x''(s) + k(s) \cdot x(s) = 0 \tag{I.3.22}$$

where the parameter $k(s)$ describes the external force that can in principle be anything, as long as it is periodic. And by chance this is exactly the situation that we encounter and so Eq. I.3.22 is what we need. The difference to our previous approach with single elements matrices is that here the parameter of the restoring force is not constant, as we have assumed until now inside a magnet. It is a function of the beam coordinate s. However it has to be periodic—at least turn by turn.

We would like to emphasize this fact a bit: in order to describe 21^{st} century accelerators, which are one of the most powerful tools in modern particle physics, we go back by 150 years to the mathematics of planetary motion. Sorry, I find that great.

While the differential equation of motion has been developed for us by our colleague Hill, the solution is another story and is found under the name *"Floquet's Theorem"*. For those who love mathematics, it is explained in detail e.g. in Ref. [8]. Here we refer to the simple statement, that the Ansatz to solve Eq. I.3.22 is

$$x(s) = A \cdot u(s) \cdot \cos[\psi(s) + \phi] \quad .$$

We are not surprised to find a cos-like oscillation, with a phase advance $\psi(s)$ and an initial phase ϕ. We are also not too much surprised that there is a certain constant in front of the oscillation amplitude. Both, ϕ and A are in the end integration constants. The real interesting story is an s dependent amplitude u(s). Well, as our restoring forces are s dependent that also makes somehow sense. So, using the Ansatz, as well as its first and second derivative

$$x'(s) = A \cdot u'(s) \cdot \cos(\psi + \phi) - A \cdot u \cdot \sin(\psi + \phi) \cdot \psi' \tag{I.3.23}$$

$$\begin{aligned} x''(s) &= A \cdot u''(s) \cdot \cos(\psi + \phi) - Au' \cdot \sin(\psi + \phi) \cdot \psi' \\ &\qquad - Au' \cdot \sin(\psi + \phi) \cdot \psi' - Au \cdot (\sin(\psi + \phi) \cdot \psi')' \\ &= A \cdot u''\cos(\psi + \phi) - 2Au'\sin(\psi + \phi) \cdot \psi' - Au\sin(\psi + \phi)\psi'' - Au\psi'^2\cos(\psi + \phi) \\ &= \cos(\psi + \phi) \cdot \{Au'' - Au\psi'^2\} - \sin(\psi + \phi)\{2Au'\psi' + Au\psi''\} \end{aligned}$$

and inserting these expressions into the differential Eq. I.3.22 we obtain

$$\cos(\psi + \phi) \cdot \{Au'' - Au\psi'^2\} - \sin(\psi + \phi) \cdot A\{2u'\psi' + u\psi''\} - kAu \cdot \cos(\psi + \phi) = 0$$

$$\cos(\psi + \phi) \cdot \{Au'' - Au\psi'^2 + kAu^2\} - \sin(\psi + \phi)A \cdot \{2u'\psi' + u\psi''\} = 0 \quad . \tag{I.3.24}$$

In order to fulfill this condition the terms in front of the cos and sin function have to be both zero. And so we get the two conditions

$$\begin{aligned} (i) \quad & u'' - u\psi''^2 - ku = 0 \\ (ii) \quad & 2u'\psi' + u\psi'' = 0 \qquad . \end{aligned}$$

From (ii) we get

$$2\frac{u'}{u} + \frac{\psi''}{\psi'} = 0$$

which we can integrate to get the expression for the phase advance of the oscillation

$$\psi(s) = \int_0^s \frac{d\tilde{s}}{u^2(\tilde{s})} \qquad . \tag{I.3.25}$$

This result is already worth a comment. Unlike to the usual harmonic oscillations that we find basically everywhere in nature, here the phase-advance of the oscillation depends on the amplitude, $u(s)$. The physics behind is quite clear: if the external restoring force is increased while travelling through the storage ring, e.g. in case we encounter a stronger quadrupole, the amplitude of the oscillation is reduced, and at the same time the oscillation frequency becomes larger, which is just another way to say the phase

advance is increased. So, indeed we have a quasi harmonic oscillation with changing external conditions and the particles will react at any moment in frequency, amplitude and phase according to that.
It's more or less the same story as tuning a race car for formula one, or the sound of a well tuned piano. - I prefer the piano, by the way.
The expression obtained in Eq. I.3.25 can be put into (i) to determine the amplitude, $u(s)$

$$u'' - u \cdot \frac{1}{u^4} - k(s)\, u = 0$$

and finally

$$u'' - \frac{1}{u^3} - k(s)\, u = 0 \qquad . \tag{I.3.26}$$

This expression defines the amplitude function of our oscillation, which - we will remember - has to be periodic, i.e. $u(s+L) = u(s)$, where L is either the circumference of the accelerator or, in case an inner periodicity is found, the length of the structure which repeats itself around the ring periodically. There is just a tiny little problem when talking about Eq. I.3.26. It cannot be solved analytically. Which is indeed an uncomfortable situation. However it can be solved numerically (which is done by our computer codes) and even more important, there is an indirect way to determine the amplitude function via equivalence of the lattice matrices ... as we will show in the section on lattice design.
Now - as last step and before discussing Eq. I.3.26 in detail - we follow a certain tradition concerning the nomenclature in literature and set $A = \sqrt{\varepsilon}$ and define the so-called *"beta-function"*

$$\beta(s) := u^2(s) \quad .$$

There is not much behind that definitions, except mathematical beauty of the equations. Especially the introduction of ε instead of the constant A has no other sense than making the physics picture a bit more clear and elegant, as we will see in the next section. There is nothing more than this definition, and we could go on using $u^2(s)$, but this is not what you will find in the textbooks. So re-writing a few expressions that we encountered before we state that

- the β-function defines the amplitude of the particle oscillation,
- depends on the position s,
- must be periodic $\beta(s+L) = \beta(s)$,
- the phase advance through a certain part of the magnet structure – say from $s = 0$ to s – depends on the inverse of the amplitude

$$\psi(s) = \int_0^s \frac{1}{\beta(s)} \quad ,$$

- and the general solution of Hill's equation is

$$x(s) = \sqrt{\varepsilon} \cdot \sqrt{\beta(s)} \cdot \cos[\psi(s) + \phi] \quad . \tag{I.3.27}$$

4.4 Emittance and the phase space ellipses

Without doubt, the β-function is a somewhat abstract parameter that results from all focusing and defocusing elements in the ring. However, the integration constant ε on the other side has a well-defined physical interpretation. Given the solution of Hill's equation (Eq. I.3.27) and its derivative

$$x'(s) = -\frac{\sqrt{\varepsilon}}{\sqrt{\beta(s)}} \cdot \{\sin[\psi(s) - \phi] + \alpha(s)\cos[\psi(s) + \phi]\} \tag{I.3.28}$$

we can solve Eq. I.3.27 to re-write the expression for the cos-term

$$\cos[\psi(s)] = \frac{x(s)}{\sqrt{\varepsilon\beta(s)}}$$

and insert this into I.3.28 to get an expression for the integration constant ε

$$\varepsilon = \gamma(s)x^2(s) + 2\alpha(s)x(s)x'(s) + \beta(s)x'^2(s). \tag{I.3.29}$$

Here we have followed the usual convention and introduced the two beam dynamics parameters

$$\alpha(s) = -\frac{1}{2}\beta'(s)$$

and

$$\gamma(s) = \frac{1 + \alpha^2(s)}{\beta(s)}$$

which are basically used for more compact and - at least in a mathematical sense - more beautiful equations.

For those familiar with math, the expression Eq. I.3.29 will ring a bell: we obtain for ε a parametric representation of an ellipse in the *(x, x')* "phase space", which, according to Liouville's theorem, is a constant of motion, as long as only conservative forces are considered. The mathematical integration constant ε thus gains physical meaning. In fact, it describes the space occupied by the particle in the transverse *(x, x')*- or *(y, y')*- phase space (simplified here to a two-dimensional situation). More specifically, the area in this *(x, x')* space that is covered by the particle is given by

$$\text{Area} = \pi \cdot \varepsilon$$

and, as long as we consider only conservative forces acting on the particle, this area is constant. Here we take these facts as given, but we should point out that, as a direct consequence, the so-called emittance ε cannot be influenced by any external fields: it is a property of the beam, and we have to take it as given and handle with care.

To be more precise, and following the usual textbook treatment of accelerators, we can draw the ellipse of the particle's transverse motion in phase space; see, for example, Fig. I.3.25. Although the shape and orientation are determined by the optics function β and its derivative, α, and so will change as a function of the position s in the ring, the area covered in phase space is constant. In Fig. I.3.25, expressions for the dependence of the beam size and divergence and, as a consequence, the shape and orientation of the

phase space ellipse are included. Referring again to the single-particle trajectory discussed above (see Fig. I.3.18), but now plotting for a given position *s* in the ring the coordinates *x* and *x'* turn by turn, we obtain the phase space coordinates of the particle marked as dots in the figure. These coordinates follow the fringe of the ellipse and will do so as long as only conservative forces are taken into account. The emission of photons, a quantum effect, scattering at the rest gas molecules and—most severe—beam collisions are not conservative processes and so in a real machine the emittance slowly will increase. A pity, even if we have to admit that it is the beam collisions that in the end we are paid for.

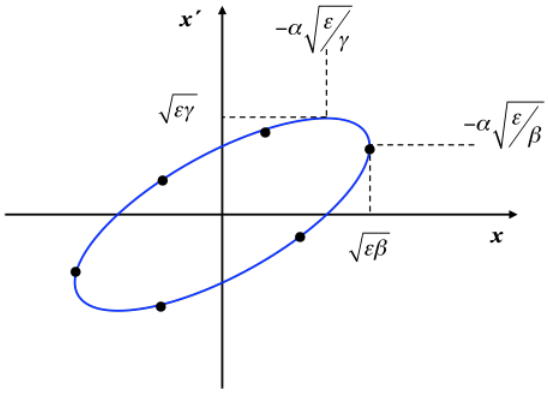

Fig. I.3.25: Plotting turn by turn the values of x and x' in a so-called phase space diagram, the particle's coordinates will follow the form of an ellipse whose shape and orientation is determined by the optics parameters, α, β and γ.

Let's take the general solution of our equation of motion Eq. I.3.29 as given for a moment - we will come back to it in more detail in two pages. The question is allowed how the shape and orientation of the phase space ellipse is defined by the optics parameters. For the maximum amplitude of the particle's oscillation that's easy

$$\hat{x} = \sqrt{\varepsilon \cdot \beta} \quad .$$

So far so good. What is now the angle x' at that position? To answer this question we put the expression for $\hat{x}$ into Eq. I.3.29,

$$\varepsilon = \gamma\varepsilon\beta + 2 \cdot \alpha\sqrt{\varepsilon\beta}x' + \beta x'^2$$

and solve for x'

$$x' = -\alpha \cdot \sqrt{\varepsilon/\beta} \quad .$$

Two comments to clarify the things:

- A high beta-function means a large beam size, and at the same time a small beam divergence. Et vice versa: small beams at a certain position in the ring will create large beam divergence, which turns out to be one of the fundamental limits of the performance of a particle collider, as we will see.
- In the middle of a quadrupole the beta-function reaches in most cases a local maximum (or minimum), so $\alpha = 0$. And so $x' = 0$ and the ellipse in phase space is flat (or upright).

And now for the maximum angle x': we start again with the general solution Eq. I.3.29, and replace the

α and γ by their original definitions

$$\varepsilon = \frac{x^2}{\beta} + \frac{\alpha^2 x^2}{\beta} + 2\alpha x x' + \beta x'^2$$

which we solve for x'

$$x'_{1,2} = \frac{-\alpha x \pm \sqrt{\varepsilon\beta - x^2}}{\beta}$$

and determine $\hat{x'}$ via $\frac{dx'}{dx} = 0$ to get for the maximum value

$$\hat{x'} = \sqrt{\varepsilon\gamma}$$

and the amplitude at that position

$$x_{\hat{x'}} = \pm\alpha\sqrt{\varepsilon/\beta} \qquad .$$

These values are introduced in the phase space plot Fig. I.3.25 and clarify the usual statement that the shape and orientation of the phase space ellipse is determined by the Twiss parameters α, β and γ.
Going through this contemplation now for an ensemble of many particles (sometimes called *"the beam"*) we realise that each and every particle will be defined by its individual coordinates *x, x'*, and so we get a manifold of single particle ellipses in phase space, each of them defined in the same manner in shape and orientation by the Twiss parameters. Clearly: for conservative systems the individual ellipses will never cross, but lie one surrounding the other in the *x-x'* coordinate system, as schematically shown in Fig. I.3.26. As indicated in the figure, the area of each single particle ellipse is defined by the emittance

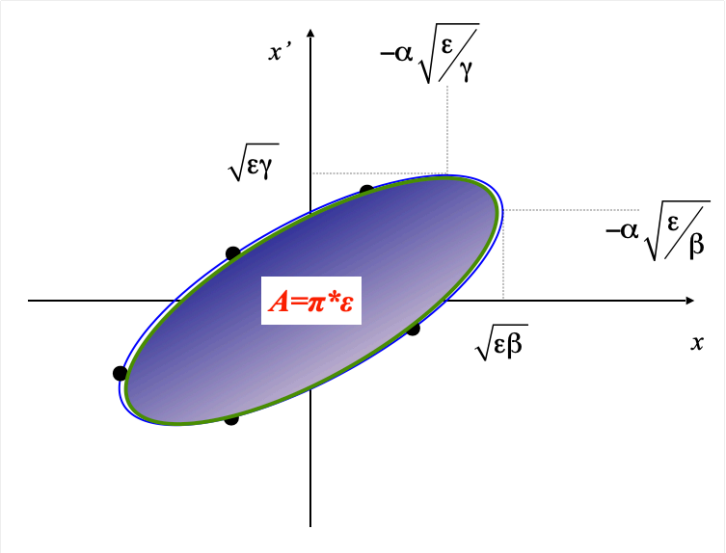

Fig. I.3.26: The *x,x'* coordinates of each article will form a manifold of ellipses, surrounding each other, and that follow the typical transverse Gaussian density distribution.

via $A = \pi \cdot \varepsilon$. So, summarising we state that: the emittance of a beam is related to the phase-space area that it occupies as an ensemble of many particles.

4.5 . . . and finally the beam size

It is a fair question, after all that math, how the *beam* actually will look like. What is its size and how can we influence it and even better, how can we calculate it? So, let us talk a little more about the beam as an ensemble of many particles: in LHC every bunch consists of typically 10^{11} protons. Referring to Eq. I.3.27, at a given position in the ring the maximum amplitude of a particle oscillation and so in the end the beam size is defined by the emittance, ε, which is constant, and the amplitude function $\beta(s)$ which is determined by the focusing properties and depends on the position s. Thus, at a certain moment in time, at a given position s the cos term in the equation will be equal to one and the amplitude of the trajectory will reach its maximum value. Now, a practical definition of the beam emittance requires a choice for the limiting ellipse that defines the phase-space area of the beam. If e.g. we consider a particle at one standard deviation (σ) of the transverse density distribution, then by using the emittance of this reference particle we can calculate the size of the complete beam, in the sense that the complete phase space area (within 1 σ) of all particles in the *(x, x')* phase space is surrounded (and thus defined) by our 1-σ candidate. This is visualised in Fig. I.3.27, which shows the particle density in the transverse plane, measured with a thin wire that is moved across the beam. As expected the particle density is highest in the centre and follows in quite good approximation a Gaussian distribution. The 1-σ particle is marked with an arrow in green in the figure and usually this is used to describe the beam size, knowing that there is more in nature than 1 σ. However we have to define a way to express the beam size and this is the usual definition.

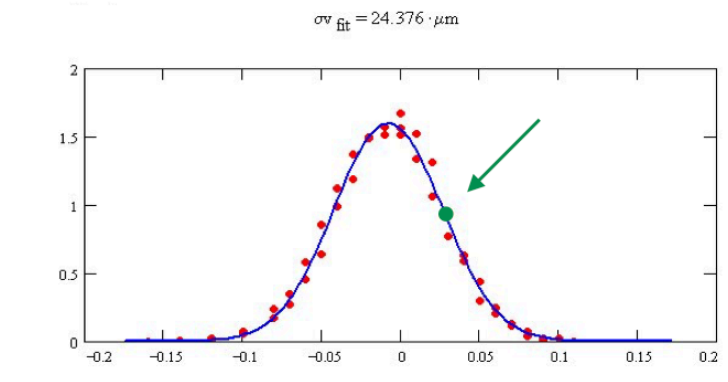

Fig. I.3.27: Measurement of the transverse profile of a typical particle beam with a thin wire that is moved fast across the beam. The horizontal axis shows the position of the wire, and the vertical one the corresponding measured intensity of the scattered events marked as red points. The line is a Gaussian fit and the green particle corresponds to 1 σ of the distribution, acting as reference value for the complete particle ensemble.

As a numerical example, we shall use the values for the LHC proton beam. In the periodic pattern of the arc, the β–function is equal to $180\,\mathrm{m}$ and the emittance at the flat-top energy is roughly $\varepsilon = 5 \cdot 10^{-10}\,\mathrm{rad\,m}$. The resulting typical beam size is therefore $0.3\,\mathrm{mm}$. Now, clearly, we would not design a vacuum aperture for the machine based on a one-sigma beam size; typically, an aperture requirement corresponding to 12 σ is a good rule to guarantee a sufficient beam lifetime, allowing for tolerances arising from magnet misalignments, optics errors, orbit fluctuations, and operational flexibility (due to

too many coffees of the operation team). In Fig. I.3.28 the LHC vacuum chamber is shown, including the beam screen used to protect the cold bore from synchrotron radiation; the free aperture available for the beam includes extra margins to exclude direct hits of the protons on the vacuum chamber wall, which would provoke immediately a quench of the super conducting magnets and corresponds to a minimum beam size of 18 σ.

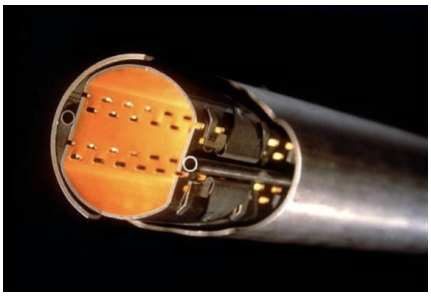

Fig. I.3.28: Vacuum chamber of the LHC storage ring, with the beam screen for photon absorption. The available free aperture corresponds to about 18 σ size.

Up to now everything looks sweet soft and easy going. And just to avoid the feeling that life of an accelerator physicist is always a bed of roses we invite the reader to have a look at Fig. I.3.29. Once more we plot the $x - x'$ space picture of the beam, however now including the effect of the strong beam-beam interaction [9]. During collision of the two counter rotating beams in a particle collider, each particle feels the space charge force of the opposing beam, which has a tremendous effect. In first approximation the particles get a kick, i.e. a short but very strong deflection that depends in a non-linear manner on the individual particle's amplitude at the collision point. And as this is by far not a conservative situation, the phase space distribution of the beam is distorted, tails in the transverse distribution are developing and if pushed to far, we will observe particle loss. It is the job of the beam dynamics experts to optimise the situation, maximising the performance of the collider while keeping the beam-beam effects within tolerable limits.

5 The Twiss parameters

As we have seen, the emittance ε that occurs in the general solution of Hill's equation, I.3.27 has a well defined meaning. It refers to the area of the particle distribution in phase space and thus can be considered like a quality parameter of the beam (. . . a bit like entropy in thermodynamics). The Twiss parameters, on the other side, are more abstract and depend in a quite indirect manner on the focusing structure of the magnet lattice. Still, they provide an extremely powerful tool to describe the beam and we will show now how to calculate them.
We start once more with the general solution Eq. I.3.27. and it's derivative Eq. I.3.28.

Remembering the trigonometrical gymnastics $\sin(a+b) = \ldots$ etc. we can re-write

$$x(s) = \sqrt{\varepsilon} \cdot \sqrt{\beta(s)} \cdot \{\cos(\psi(s)\cos(\phi) - \sin(\psi(s)\sin(\phi)\}$$

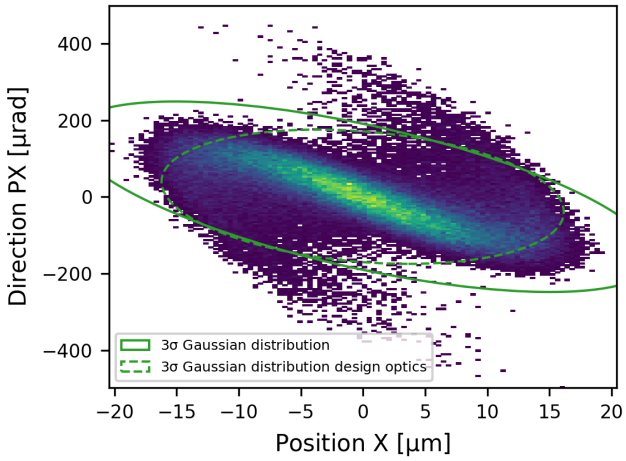

Fig. I.3.29: Phase space distribution of a particle beam, including the detrimental effect of beam-beam forces in a collider. The ellipses included in the graph show two approaches to fit a standard ellipse defined by the optics parameters of the lattice. The tails that result from the strong beam-beam effect clearly cannot be described in adequate manner in this case [9]. If pushed too far these particles will be lost.

and

$$x'(s) = -\frac{\sqrt{\varepsilon}}{\sqrt{\beta(s)}}\{\alpha(s)\cos(\psi(s)\cos(\phi)) - \sin(\psi(s))\sin(\phi) + \sin(\psi(s)\cos(\phi) + \cos(\psi(s)\sin(\phi)\} \quad .$$

Now, we define a starting position $s = s_0$, where we put the phase of the oscillation by definition to $\psi_{s=0} = 0$. This can be the injection point or the interaction point of two colliding beams or any arbitrary position in the ring. We get

$$\cos(\phi) = \frac{x_0}{\sqrt{\varepsilon\beta_0}} \quad , \quad \sin(\phi) = -\frac{1}{\sqrt{\varepsilon}}\left(x'_0\sqrt{\beta_0} + \frac{\alpha_0 x_0}{\sqrt{\beta_0}}\right)$$

where the subscript "0" refers clearly to the values at this starting point. Inserting above we obtain

$$\begin{aligned} x(s) &= \sqrt{\tfrac{\beta_s}{\beta_0}}\{\cos(\psi_s) + \alpha_0\sin(\psi_s)\} \cdot x_0 &&+\sqrt{\beta_s\beta_0} \cdot \sin(\psi_s) \cdot x'_0 \\ x'(s) &= \sqrt{\tfrac{1}{\beta_s\beta_0}}\{(\alpha_0 - \alpha_s)\cos(\psi_s) - (1 + \alpha_0\alpha_s\sin(\psi_s)\} \cdot x_0 &&+\sqrt{\tfrac{\beta_0}{\beta_s}} \cdot \{\cos(\psi_s) - \alpha_s\sin(\psi_s)\} \cdot x'_0. \end{aligned} \tag{I.3.30}$$

Here we arranged the terms in a way to emphasize the situation: starting from initial conditions in amplitude and angle, x_0, x'_0, we can calculate their values at any other place in the ring, provided we know the optics parameters at the two locations and the phase advance between them. Expressed more convenient in matrix form we get

$$\begin{pmatrix} x \\ x' \end{pmatrix}_{s1} = M \cdot \begin{pmatrix} x \\ x' \end{pmatrix}_{s0} \tag{I.3.31}$$

... which is the old story, however now the transfer matrix is expressed as a function of the optical

parameters

$$M_{s_0-s_1} = \begin{pmatrix} \sqrt{\frac{\beta_s}{\beta_0}}\cos(\psi_s) + \alpha_s \sin(\psi_s) & \sqrt{\beta_s \beta_0} \cdot \sin(\psi_s) \\ \sqrt{\frac{1}{\beta_s \beta_0}}(\alpha_0 - \alpha_s)\cos(\psi_s) - (1 + \alpha_0 \alpha_s \sin(\psi_s) & \sqrt{\frac{\beta_0}{\beta_s}} \cdot \cos(\psi_s) - \alpha_s \sin(\psi_s) \end{pmatrix} \quad .$$

So, basically the situation is the same as in Eq. I.3.15 and so by definition the numerical values of the matrix elements are the same. A fact that we can use as next step to indeed calculate the optics parameters. Before doing so, we would like to cite a colleague who expressed the facts in a wonderful manner, [10]: *" ... this rather formidable matrix simplifies considerably if we take into account one complete turn"*. Using the periodicity which is inherent in a ring type accelerator, and which means

$$\beta(s + L_0) = \beta(s) \tag{I.3.32}$$

$$\alpha(s + L_0) = \alpha(s) \tag{I.3.33}$$

$$\psi(s + L_0) = \psi_{\text{turn}} \tag{I.3.34}$$

with L_0 being the length of the periodic structure, we finally can write

$$M_{\text{turn}} = \begin{pmatrix} \cos(\psi_{\text{turn}}) + \alpha_s \sin(\psi_{\text{turn}}) & \beta_s \cdot \sin(\psi_{\text{turn}}) \\ -\gamma_s \sin(\psi_{\text{turn}}) & \cos(\psi_{\text{turn}} - \alpha_s \sin(\psi_{\text{turn}}) \end{pmatrix} \quad . \tag{I.3.35}$$

We know already that the phase advance depends on the β-function, and so we can write for the phase advance for one complete turn

$$\psi_{\text{turn}} = \int_s^{s+L_0} \frac{1}{\beta(s)} ds \quad .$$

Looking at the one-turn matrix, we get this information *"for free"* by just calculating the Trace of the one-turn map, Trace $= 2 \cdot \cos(\psi_{\text{turn}})$.

And as the tune of the machine is defined as the number of oscillations per turn, it corresponds to the phase advance in units of 2π:

$$Q = \frac{1}{2\pi} \oint \frac{1}{\beta(s)} ds \quad .$$

5.1 Stability of the betatron oscillations

It is a matter of fact, that whenever we design a storage ring lattice with a team of students, in 90 % of all cases there is no stable solution. The reason is twofold: due to a certain lack of experience and—more seriously—due to something called stability criterion: not every combination of magnet strength and arrangement leads to a stable solution. As always in life the beautiful moments are rare.
But there is hope: based on the equations that we have shown above, we can derive an equation that allows us to check for stability and determine the conditions for it.
We refer once more to the periodic situation, described by the one-turn-matrix, I.3.35. For convenience

we re-write it in a slightly modified way

$$\begin{aligned} M_{\text{turn}} &= \begin{pmatrix} \cos(\psi_{\text{turn}}) + \alpha_s \sin(\psi_{\text{turn}}) & \beta_s \cdot \sin(\psi_{\text{turn}}) \\ -\gamma_s \sin(\psi_{\text{turn}}) & \cos(\psi_{\text{turn}}) - \alpha_s \sin(\psi_{\text{turn}}) \end{pmatrix} \\ &= \cos(\psi_{\text{turn}}) \cdot \underbrace{\begin{pmatrix} 1 & 0 \\ 0 & 1 \end{pmatrix}}_{I} + \sin(\psi_{\text{turn}}) \cdot \underbrace{\begin{pmatrix} \alpha & \beta \\ -\gamma & -\alpha \end{pmatrix}}_{J} \end{aligned} \quad , \tag{I.3.36}$$

where - following literature, *I* is the unit matrix and *J* the matrix that contains the information about the optics parameters. So-far nothing has changed. The new way of writing however allows us in a very simple manner to deduce the stability of the motion. The transformation through *N* turns is described by *N*-times multiplying with the one-turn matrix. So, as the matrix for *N* turns is M^N, we can write

$$M^N = (I \cdot \cos\psi + J \cdot \sin\psi)^N = I \cdot \cos(N\psi) + J \cdot \sin(N\psi) \quad .$$

The last step follows from a generalisation of de Moivres formula.

Taking as example two consecutive turns we get, writing ψ_1 and ψ_2 for the phase advance of turn 1 and turn 2 respectively,

$$M^2 = \{I \cdot \cos\psi_1 + J \cdot \sin\psi_1\} \cdot \{I \cdot \cos\psi_2 + J \cdot \sin\psi_2\}$$

and multiplying out

$$M^2 = I^2 \cos\psi_1 \cos\psi_2 + IJ \cos\psi_1 \sin\psi_2 + JI \sin\psi_1 \cos\psi_2 + J^2 \sin\psi_1 \sin\psi_2 \quad .$$

Now for the matrices I and J we can show by simple multiplication that

$$I^2 = I \tag{I.3.37}$$

$$I \cdot J = J \cdot I \tag{I.3.38}$$

$$J^2 = -I \tag{I.3.39}$$

and so

$$M^2 = I \cdot \cos(\psi_1 + \psi_2) + J \cdot \sin(\psi_1 + \psi_2) \quad .$$

As we consider one complete turn the phase advance is the same, $\psi_1 = \psi_2$ and so

$$M^2 = I \cdot \cos(2\psi_{\text{turn}}) + J \cdot \sin(2\psi_{\text{turn}}) \quad .$$

We conclude that the motion for *N* turns remains bounded, if the elements of M^N remain bounded. And they do so, as long as ψ_{turn} is a real number. Or in other words we have to require that

$$\cos(\psi_{\text{turn}}) < 1$$

which means automatically that the Trace of our matrix, describing the periodic situation has to be smaller than 2

$$|\text{Trace}(M_{\text{turn}})| < 2$$

It couldn't be easier. The rule for stability is to calculate the one-turn matrix, determine its Trace and that's it. However, just an advice, don't forget that you need stability in both planes!
A little remark before we close this section: from the bare mathematical point of view the stability condition would be fulfilled even for $\text{Trace}(M_{\text{turn}}) = 2$. However in that case the phase advance per turn will be $\psi_{\text{turn}} = 90°$ and so the β-function, which is determined by the matrix element m_{12} in Eq. I.3.36 is undefined. So, ideed, we require $\text{Trace}(M_{\text{turn}}) < 2$.

5.2 Transformation of the Twiss parameters

Before we actually can design a storage ring lattice, we need a last ingredient, namely the rule of how to transform the Twiss parameters through a magnet structure, once we could determine them at a given point. In a certain way we are looking to the equivalent of the *x-x'* transformation through the single element matrices.
We start with the fact that the emittance is a constant of motion and can be expressed in parametric form,see Eq. I.3.29, as

$$\varepsilon = \gamma(s_1)x^2(s_1) + 2\alpha(s_1)x(s_1)x'(s_1) + \beta(s_1)x'^2(s_1). \tag{I.3.40}$$

We introduced here the index "s_1" as now we refer explicitly to a given position in the ring. Now we can repeat that but pointing to another position s_2

$$\varepsilon = \gamma(s_2)x^2(s_2) + 2\alpha(s_2)x(s_2)x'(s_2) + \beta(s_2)x'^2(s_2) \quad , \tag{I.3.41}$$

knowing perfectly well, that ε = const and so the numerical value is just the same. In Fig. I.3.30 we shown an example of the situation with the two points of interest marked in blue.

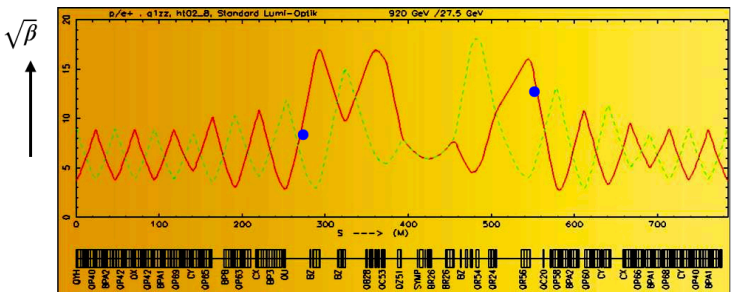

Fig. I.3.30: A typical beam optics in a synchrotron. Given the matrices of the single elements the transformation of the optics parameters between the two points marked in blue in the lattice can be calculated.

For the trajectory amplitude and angle we have the transformation rule

$$\begin{pmatrix} x \\ x' \end{pmatrix}_{\mathrm{s_2}} = M \cdot \begin{pmatrix} x \\ x' \end{pmatrix}_{\mathrm{s_1}} \tag{I.3.42}$$

with M being the product matrix of the lattice elements between s_1 and s_2

$$M_{\mathrm{s_1-s_2}} = \begin{pmatrix} C & S \\ C' & S' \end{pmatrix} \quad . \tag{I.3.43}$$

Now, thinking backwards, i.e. transferring from $s_2 \rightarrow s_1$ we apply the inverse matrix

$$\begin{pmatrix} x \\ x' \end{pmatrix}_{\mathrm{s_1}} = M^{-1} \cdot \begin{pmatrix} x \\ x' \end{pmatrix}_{\mathrm{s_2}} \tag{I.3.44}$$

with

$$M^{-1} = M_{\mathrm{s_2-s_1}} = \begin{pmatrix} S' & -S \\ -C' & C \end{pmatrix} \tag{I.3.45}$$

where we have used the fact that $\det(M) = 1$. So we can calculate the orbit values *x,x'* at position s_1 as a function of their values at position s_2

$$x_{\mathrm{s_1}} = S' \cdot x_{\mathrm{s_2}} - S \cdot x'_{\mathrm{s_2}} x'_{\mathrm{s_1}} = -C' \cdot x_{\mathrm{s_2}} + C \cdot x'_{\mathrm{s_2}}$$

which we insert into Eq. I.3.40 to end up with the two expressions for the (numerically same) emittances

$$\begin{aligned} \varepsilon &= \beta(s_2)x'^2 + 2\alpha(s_2) \cdot xx' + \gamma(s_2)x^2 \\ \varepsilon &= \beta(s_1) \cdot (Cx' - C'x)^2 + 2\alpha(s_1) \cdot (S'x - Sx')(Cx' - C'x) + \gamma(s_2)(S'x - Sx')^2 \quad . \end{aligned} \tag{I.3.46}$$

As both expressions have to give the same value, we can equalise them, sort via *x, x'*, compare the coefficients and get

$$\beta_{\mathrm{s_2}} = C^2\beta_{\mathrm{s_1}} - 2SC \cdot \alpha_{\mathrm{s_1}} + S^2 \cdot \gamma_{\mathrm{s_1}} \tag{I.3.47}$$

$$\alpha_{\mathrm{s_2}} = -CC'\beta_{\mathrm{s_1}} + (SC' + S'C) \cdot \alpha_{\mathrm{s_1}} - SS' \cdot \gamma_{\mathrm{s_1}} \tag{I.3.48}$$

$$\gamma_{\mathrm{s_2}} = C'^2\beta_{\mathrm{s_1}} - 2S'C' \cdot \alpha_{\mathrm{s_1}} + S'^2 \cdot \gamma_{\mathrm{s_1}} \tag{I.3.49}$$

$$\tag{I.3.50}$$

or as usual and more elegant and clear expressed in matrix form

$$\begin{pmatrix} \beta \\ \alpha \\ \gamma \end{pmatrix}_{s2} = \begin{pmatrix} C^2 & -2SC & S^2 \\ -CC' & SC' + CS' & -SS' \\ C'^2 & -2S'C' & S'^2 \end{pmatrix} \cdot \begin{pmatrix} \beta \\ \alpha \\ \gamma \end{pmatrix}_{s1} \quad . \tag{I.3.51}$$

Here we have to break for a cup of coffee and a few remarks:

– this expression is important!
– given the Twiss parameters α, β, γ at any point in the lattice we can transform them and calculate their values at any other point in the ring.
– the transfer matrix is given by the focusing properties of the lattice elements: the elements of M are just those that we used to calculate the single particle trajectories.

6 Calculation of the Twiss parameters

The optics parameters that have been introduced in the previous section represent a very efficient and powerful tool for the description and optimisation of the beam parameters in an accelerator. Unfortunately they have an uncomfortable disadvantage: we cannot calculate them analytically. The differential equation for the β-function can be established as we have shown in Eq. I.3.26, but it cannot be solved directly. And while the attentive reader will comment that he/she does not care too much, we would like to point out, that an analytical solution means - beyond the bare mathematics - a deeper understanding of the physics behind the story.
So we will have to find another method to determine the α-s, β-s and γ-s, and fortunately such a method exists. Let's summarise what we know already:

– the amplitude and angle of a particle trajectory can be calculated by a step by step matrix transformation of certain initial values, (x, x') via Eq. I.3.11, e.g.

$$\begin{pmatrix} x \\ x' \end{pmatrix}_{s_2} = M_{\text{quad}} \cdot \begin{pmatrix} x \\ x' \end{pmatrix}_{s_1} \tag{I.3.52}$$

with M_{quad} describing the focusing or defocusing effect of the magnet,

$$M_{\text{foc}} = \begin{pmatrix} \cos(\sqrt{|K|} \cdot l_q) & \frac{1}{\sqrt{|K|}} \sin(\sqrt{|K|} \cdot l_q) \\ -\sqrt{|K|} \cdot \sin(\sqrt{|K|} \cdot l_q) & \cos(\sqrt{|K|} \cdot l_q) \end{pmatrix}$$

where we refer in this case to a focusing lens.
– the matrices of all magnet elements (including the drift, which is not really magnetic, but never mind) can be combined via matrix multiplication to form the transfer matrix of a longer lattice structure, or even the whole ring

$$M_{\text{total}} = M_{\text{foc}} \cdot M_{\text{drift}} \cdot M_{\text{bend}} \cdot M_{\text{drift}} \cdot M_{\text{defoc}} \cdot M_{\text{drift}} \ldots$$

– and - more convenient - we get exactly the same transfer matrix if we express it as a function of the optics parameters, α, β and γ

$$M = \begin{pmatrix} \sqrt{\frac{\beta_{s_2}}{\beta_{s_1}}}(\cos(\psi_{21} + \alpha_{s_1} \sin\psi_{21}) & \sqrt{\beta_{s_2}\beta_{s_1}} \sin\psi_{21} \\ \frac{(\alpha_{s_1} - \alpha_{s_2})\cos\psi_{21} - (1 + \alpha_{s_1}\alpha_{s_2})\sin\psi_{21}}{\sqrt{\beta_{s_2}\beta_{s_1}}} & \sqrt{\frac{\beta_{s_1}}{\beta_{s_2}}}(\cos\psi_{21} - \alpha_{s_2}\sin\psi_{21}) \end{pmatrix} \quad .$$

– the last ingredient that we need to determine the numerical values of the Twiss family is their

transformation in a magnet structure, namely

$$\begin{pmatrix} \beta_{s_2} \\ \alpha_{s_2} \\ \gamma_{s_2} \end{pmatrix} = \begin{pmatrix} C^2 & -2SC & S^2 \\ -CC' & SC' + S'C & -SS' \\ C'^2 & -2C'S' & S'^2 \end{pmatrix} \cdot \begin{pmatrix} \beta_{s_1} \\ \alpha_{s_1} \\ \gamma_{s_1} \end{pmatrix} \tag{I.3.53}$$

where the indices s_1 and s_2 refer to the starting point in the lattice and the position where we want to determine the parameters. The C and S are just a shorter way of writing the cos-like and sin-like solutions, as explained above, Eqs. I.3.16 and I.3.17 but now clearly for the product matrix of the lattice elements between the two points.

To start on an easy going level and make the things as clear as possible, we apply these equations to a drift, which is indeed not the most complicated case.
The single element matrix of a drift is given by

$$M = \begin{pmatrix} C & S \\ C' & S' \end{pmatrix} = M = \begin{pmatrix} 1 & l_d \\ 0 & 1 \end{pmatrix} \tag{I.3.54}$$

which clearly means that a particle trajectory is a straight line defined by the initial amplitude, x_0 and angle x'_0,

$$\begin{pmatrix} x \\ x' \end{pmatrix}_{l_d} = \begin{pmatrix} 1 & l_d \\ 0 & 1 \end{pmatrix} \cdot \begin{pmatrix} x \\ x' \end{pmatrix}_0$$

and so,

$$\begin{aligned} x(l_d) &= x_0 + x'_0 \cdot l_d \\ x'(l_d) &= x'_0 \quad . \end{aligned}$$

Applying now the transfer rule for the Twissies, Eq. I.3.53 we get for the most important case of the β-function, the transformation

$$\beta(s) = \beta_0 - 2 \cdot s \cdot \alpha_0 + s^2 \cdot \gamma_0$$

where as usual s has been chosen as the general independent variable. At the end of the drift space we clearly get $s = l_d$; but we do not have to mention that explicitly.

For the fun of it, let's determine the stability criterion for this drift:

$$\text{Trace}(M) = \text{Trace} \begin{pmatrix} 1 & l_d \\ 0 & 1 \end{pmatrix} = 1 + 1 = 2 \quad ,$$

which is not strictly smaller than two; even only a tiny bit too large. So, unfortunately in a situation where the storage ring is built out of only drifts, no magnets, no nothing, the situation is not stable. It's a pity, ... would have been a cheep machine.

Now, more seriously: the magnets in an accelerator can be arranged in different ways, depending

on the beam optics that we aim for. In the case of high energy colliders, the so-called FoDo is the lattice cell, that is most commonly used. It provides the highest dipole fill factor and has at the same time the very special feature that it can easily be calculated on a piece of paper. Figure I.3.31 represents the beam optics of a typical particle collider. Concentrating on the upper part of the figure, the β-function is shown throughout the $6.3\,\mathrm{km}$ ring. The regular pattern of the optics in the four arcs reflects the periodic focusing structure, namely the FoDo.

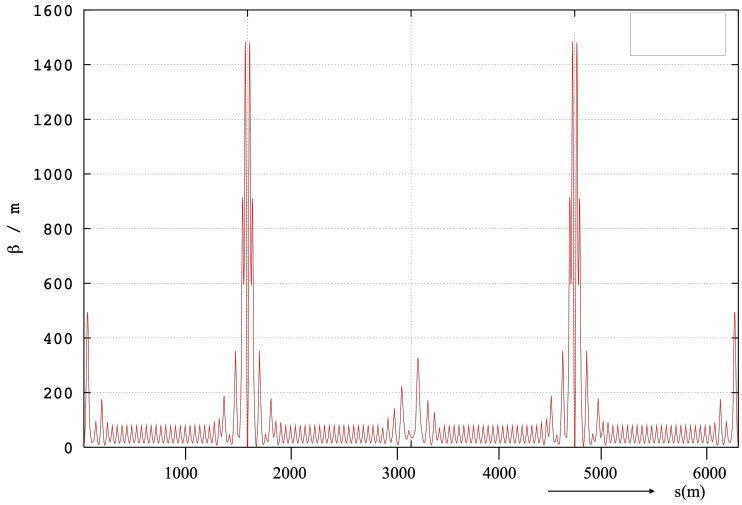

Fig. I.3.31: Luminosity optics of a particle collider: the regular pattern of the β-function in the arcs is usually a FoDo based structure and connects the straight sections where insertions like RF systems, injection / extraction of the beams and finally the physics detectors are located.

Schematically such a FoDo is shown in Fig. I.3.32. We will treat this kind of lattice structure in more detail in the section on lattice design. Here the "take-home-message" is that we have a focusing quadrupole lens and a defocusing one and nothing in between (yes, later dipoles will fill the gap, and corrector magnets and sextupoles and so on, however even then we are allowed to treat them as drifts, on a certain level).

The β-functions of such a FoDo cell - as calculated by an optics code—in the horizontal and vertical plane—are shown in Fig. I.3.33. Now, before we go into the detail of calculating the optics parameters, let's see what our optics program tells us. For convenience we start the calculation in the middle of a (focusing) quadrupole. Here the α is zero and for symmetry reasons the situation is simpler. In any case, due to the symmetry of the cell, we expect the largest beta-function in the given plane at the quadrupole, focusing in that plane.

Table I.3.2: Results of an optics calculation for a single FoDo cell.

element	length (m)	k-strength (m^{-2})	β_x (m)	α_x	ϕ_x (1/2π)	β_y (m)	α_y	ϕ_y (1/2π)
QFH	0.25	-0.54	11.6	0	0	5.3	0	0
QD	0.5	0.54	5.3	0	0.07	11.6	0	0.007
QFH	0.25	-0.54	11.6	0	0.125	5.3	0	0.125

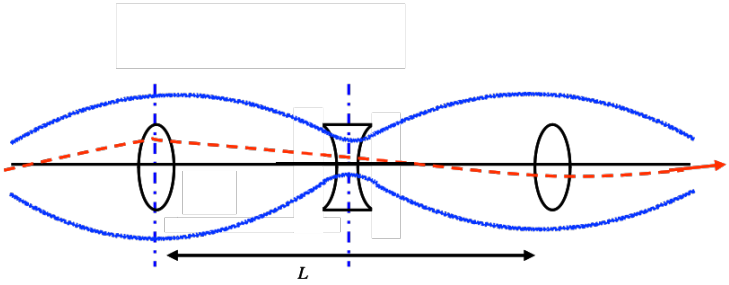

Fig. I.3.32: Schematic drawing of a FoDo structure: focusing and defocusing lenses are located at (in most cases) equidistant manner, leading to a well defined regular beam optics. The blue shape indicates the beam envelope, as defined by the β-function and beam emittance and the red dashed line a possible single particle trajectory. The blue dash-dotted lines mark the centre of the quadrupoles, where for symmetry reasons the optics function α is zero and β reaches maximum or minimum values.

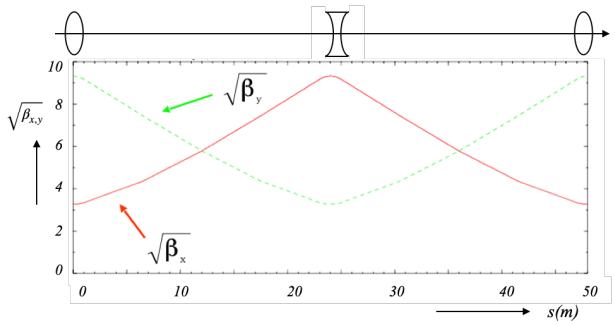

Fig. I.3.33: Beam optics of a regular FoDo cell: if powered symmetrically the β-functions will be equal at equivalent places in the two transverse planes. For symmetry reasons the optics functions start in the middle of a focusing quadrupole, where $\alpha = 0$; and so the first and last element of the cell is a half-quadrupole.

We admit that the case described in Table I.3.2 is a very simple, or better a *simplified* one. The FoDo is absolutely symmetric, with the quadrupoles located equidistantly in the cell and their strength of equal but opposite sign. While we will rarely find this in reality, it allows us an easy analytical calculation and understanding. As direct consequence, the β-functions in both planes are "anti-symmetric", with the same numerical values occurring for $\beta_{\max}$ and $\beta_{\min}$ in the corresponding quadrupoles, and the phase advance, expressed in units of $2 \cdot \pi$ adds up over the cell in both planes to $0.125 \cdot 2\pi = 90°$.
The crucial question is now: "Can we understand what the optics code is doing?" To answer that we establish the product matrix of the cell.
With $k = \pm 0.54\,\mathrm{m}^{-2}$, the length of the focusing and defocusing quadrupoles $l_q = 0.5\,\mathrm{m}$ and the length of the drift between the quadrupoles $l_d = 2.5\,\mathrm{m}$ we get, using the expressions Eqs. I.3.12 and I.3.14, and multiplying out the product matrix of the FoDo

$$M_{\mathrm{FoDo}} = M_{\mathrm{QFH}} \cdot M_{\mathrm{ld}} \cdot M_{\mathrm{QD}} \cdot M_{\mathrm{ld}} \cdot M_{\mathrm{QFH}} \quad .$$

As already mentioned, we prefer to start in the middle of a focusing quadrupole (and also end there), and

so the first matrix in the product is the one for half a quadrupole (which is a quadrupole with half the length). With the help of a pocket calculator (or a pen, a piece of paper and a bit of patience) we obtain

$$M_{\mathrm{FoDo}} = \begin{pmatrix} 0.707 & 8.206 \\ -0.061 & 0.707 \end{pmatrix} \quad .$$

And now the same story, however the product matrix of the cell expressed in Twiss-form and as we have a periodic situation we use $\beta_0 = \beta_s$ etc, which simplifies the expression

$$M = \begin{pmatrix} \cos\psi_{\mathrm{cell}} + \alpha_0 sin\psi_{\mathrm{cell}} & \beta_0 \sin\psi_{\mathrm{cell}} \\ -\gamma_0 sin\psi_{\mathrm{cell}} & \cos\psi_{\mathrm{cell}} + \alpha_0 \sin\psi_{\mathrm{cell}} \end{pmatrix} \quad .$$

As usual the subscript "0" refers to the beginning of the cell, which is in the middle of the QF quadrupole, which is the same as at the end of the cell, which is once more the centre of the QF.

Both expressions have to be equivalent if it comes to their numerical values. And so we can determine the Trace of the matrix to calculate the phase advance

$$\cos(\psi_{\mathrm{cell}}) = \frac{1}{2}\mathrm{Trace}(M) = 0.707$$

$$\psi_{cell} = 45^\circ \quad .$$

Knowing that we get the β-function from the matrix element m_{12}

$$\beta = \frac{m_{12}}{\sin\psi_{\mathrm{cell}}} = \frac{8.206}{\sin 45^\circ} = 11.6\,\mathrm{m}$$

which we can use, together with m_{11} to find α

$$\alpha = \frac{m_{11} - \cos\psi_{\mathrm{cell}}}{\sin\psi_{\mathrm{cell}}} = 0.0$$

which are exactly the same values as our optics code (MAD-X) told us. We conclude razor-sharply that MADX is doing a good job.

We admit that the gymnastics with hyperbolic trigonometrical functions is not everybody's darling. And in case that you do not really know the value of $\cosh(0.738492)$, there is an easier way: we can use quite often the thin lens approximation to get a first idea; and we will do now to show you the power of that approach.

We remember that in thin lens approximation we can replace the quadrupole matrix for a focusing matrix by

$$M_{\mathrm{foc}} = \begin{pmatrix} 1 & 0 \\ \frac{-1}{f} & 1 \end{pmatrix}$$

and

$$M_{\mathrm{defoc}} = \begin{pmatrix} 1 & 0 \\ \frac{1}{f} & 1 \end{pmatrix}$$

for a defocusing one, with f being the focal length, $f = \frac{1}{|k_q| \cdot l_q}$. We will calculate now, just as before, the product matrix of the FoDo in thin lens approximation. To make life a bit easier we can however start with half the cell, bringing us from the centre of the QF at the beginning of the cell to the centre of the QD, see Fig. I.3.34.

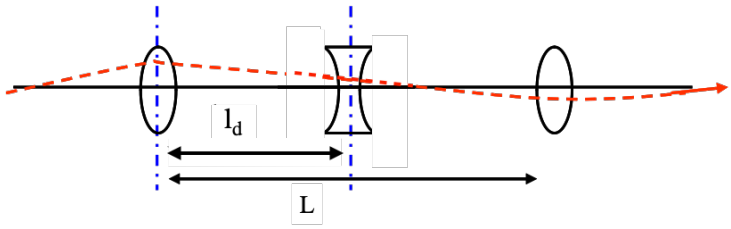

Fig. I.3.34: Thin lens representation of a FoDo cell to calculate the product matrix for the half-cell: the blue dashed lines mark the centre of the quadrupoles and as we refer to thin lens approximation the distance l_D between the quadrupoles corresponds to half the cell length L. The red dashed line shows schematically a particle trajectory.

$$M_{\text{halfcell}} = M_{\text{QD}/2} \cdot M_{\text{ld}} \cdot M_{\text{QF}/2}$$

$$M_{\text{halfcell}} \begin{pmatrix} 1 & 0 \\ 1/\tilde{f} & 1 \end{pmatrix} \cdot \begin{pmatrix} 1 & l_d \\ 0 & 1 \end{pmatrix} \cdot \begin{pmatrix} 1 & 0 \\ -1/\tilde{f} & 1 \end{pmatrix}$$

$$M_{\text{halfcell}} = \begin{pmatrix} 1 - \frac{l_d}{\tilde{f}} & l_d \\ \frac{-l_d}{\tilde{f}^2} & 1 + \frac{l_d}{\tilde{f}} \end{pmatrix} \quad ,$$

where we have introduced the focal length of a half quadrupole, $\tilde{f} = 2 \cdot f$ (...a half quadrupole is focusing half as strong and so has double the focal length)!
For the second part of the FoDo we get the same product matrix, with inverted sign of f, so

$$M_{\text{FoDo}} = \begin{pmatrix} 1 - \frac{l_d}{\tilde{f}} & l_d \\ \frac{-l_d}{\tilde{f}^2} & 1 + \frac{l_d}{\tilde{f}} \end{pmatrix} \cdot \begin{pmatrix} 1 + \frac{l_d}{\tilde{f}} & l_d \\ \frac{-l_d}{\tilde{f}^2} & 1 - \frac{l_d}{\tilde{f}} \end{pmatrix}$$

$$M_{\text{FoDo}} = \begin{pmatrix} 1 - \frac{2l_d^2}{\tilde{f}^2} & 2l_d(1 + \frac{l_d}{\tilde{f}}) \\ 2(\frac{l_d^2}{\tilde{f}^3} - \frac{l_d}{\tilde{f}^2}) & 1 - \frac{2l_d^2}{\tilde{f}^2} \end{pmatrix} \quad . \tag{I.3.55}$$

You will agree that this looks indeed much easier than the fully correct but also fully complicated story above.

As before we calculate the phase-advance of the cell via the Trace of the matrix

$$\cos\psi_{\text{cell}} = \frac{1}{2}\text{Trace}(M) = \frac{1}{2} \cdot (2 - \frac{4l_d^2}{\tilde{f}^2}) \quad .$$

Remembering primary school and the trigonometrical magic, namely

$$\cos(x) = \cos^2(x/2) - \sin^2(x/2) = 1 - 2 \cdot \sin^2(x/2)$$

we again refer to the equivalence of the matrices and write

$$\cos(\Psi_{\text{cell}}) = 1 - 2 \cdot \sin^2(\Psi_{\text{cell}}/2) = 1 - \frac{2l_d^2}{\tilde{f}^2} \;\rightarrow\; \sin(\Psi_{\text{cell}}/2) = l_d/\tilde{f} = \frac{L_{\text{cell}}}{2\tilde{f}}$$

and so we get

$$\sin(\Psi_{\text{cell}}/2) = \frac{L_{\text{cell}}}{4f} \qquad .$$

The phase advance is given by just the ratio of the cell length and the focal length; a remarkably simple result.
Coming back to our example,

$$L_{\text{cell}} = l_{QF} + l_d + l_{QD} + l_d$$

$$L_{\text{cell}} = 0.5m + 2.5m + 0.5m + 2.5m = 6m$$

and

$$1/f = k \cdot l_q = 0.5\,\text{m} \cdot 0.54\,\text{m}^{-2} = 0.27\,\text{m}^{-1}$$

$$\rightarrow f = 3.7\,\text{m} \qquad .$$

So - given these values - we can calculate the phase advance per cell

$$\frac{\Psi_{\text{cell}}}{2} = \sin^{-1}(\frac{L_{\text{cell}}}{4f}) \qquad .$$

Comparing the results (see Table I.3.3) we are indeed pretty close to the exact calculation.

Table I.3.3: FoDo cell

	thin lens	exact
Ψ_{cell}	47.8°	45°
β	11.4 m	11.6 m

We will still stay for a moment in the thin lens world, to get a rule for the stability of the motion. Stability requires $|\text{Trace}(M)| < 2$. Applying this to Eq. I.3.55 we get

$$|\text{Trace}(M)| = |2 - \frac{4l_d^2}{\tilde{f}^2}| < 2$$

which means that

$$f > \frac{L_{\text{cell}}}{4} \qquad .$$

So, please don't focus too strong, when building a lattice: as long as the focal length of the quadrupole is larger than a quarter of the cell length, we are in a stable situation. Once more an astonishingly simple

and straight forward result.

6.1 Exercise V

Show that for the cell defined above the stability condition is fulfilled.

The stability condition, described here has a simple interpretation: it is well known in optics that an object at a distance of $a = 2f$ from a focusing lens has its image at $b = 2f$ behind the lens, see Fig. I.3.35. The defocusing lens in that case has no effect, if a point like object is located exactly on the axis at a distance 2f from the focusing lens, because it is traversed without offset. If however the defocusing lens is shifted further apart, $L > 4f$ or - equivalently - the focal length of the QF is shorter, this is no more true and the divergence of the beam is increased by every defocusing lens. So, in short ...don't focus too strong !!

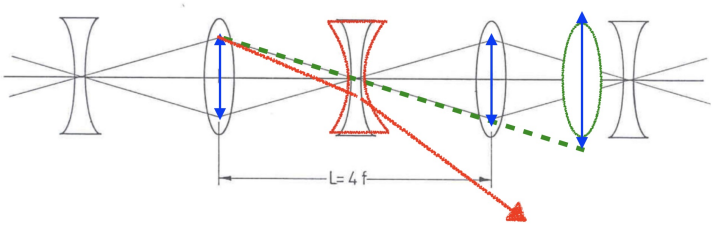

Fig. I.3.35: Geometric explanation of the stability condition in a FoDo structure. The dashed green line shows the trajectory for maximum allowed focusing strength. Increasing the gradient even more, or equivalent to that increasing the distance between the quadrupoles, leads to the situation marked as red line: due to the over-focusing the amplitude of the trajectory is steadily increasing and the particle will be lost.

6.2 Scaling laws of optics parameters

Meanwhile being familiar with the thin lens approximation, there is indeed more that we can get out of it. We come back to the thin lens description of a FoDo, however now we stop at QD, i.e. in the middle of the cell schematically shown as point 1 and 2 in Fig. I.3.36 The matrix for the half cell, bringing us from the centre of the QF to the centre of the QD, we know already

$$M_{\text{halfcell}} = \begin{pmatrix} 1 - \frac{l_d}{f} & l_d \\ \frac{-l_d}{f^2} & 1 + \frac{l_d}{f} \end{pmatrix} \quad .$$

We can - that's routine now for us - express the same story as a function of the Twiss parameters: given two locations in the ring, point *1* and point *2* in Fig. I.3.36, we can express the transfer matrix as a function of the Twiss parameters at these two points. In general, we write

$$M = \begin{pmatrix} \sqrt{\frac{\beta_2}{\beta_1}}(\cos\psi_{12} + \alpha_1 \sin\psi_{12}) & \sqrt{\beta_1\beta_2}\sin\psi_{12} \\ \frac{(\alpha_1 - \alpha_2)\cos\psi_{12} - (1+\alpha_1\alpha_2)\sin\psi_{12}}{\sqrt{\beta_1\beta_2}} & \sqrt{\frac{\beta_1}{\beta_2}}\cos\psi_{12} - \alpha_2 \sin\psi_{12}) \end{pmatrix} \quad .$$

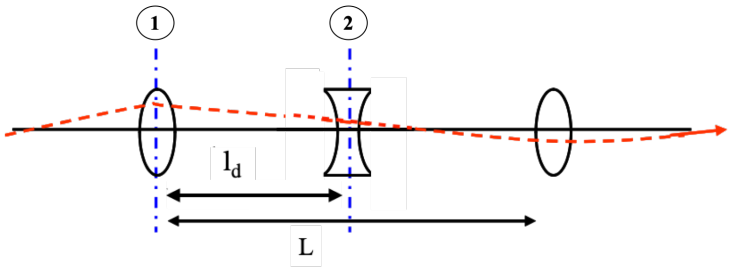

Fig. I.3.36: Schematic drawing of a FoDo structure to calculate the optics functions at the QF and QD quadrupole: we refer once more to Fig. I.3.34, indicating now the points of interest—centre of the focusing and de-fousing quadrupole—as *"1"* and *"2"* in the figure as well as in the text. At these positions the β-function will reach the maximum and minimum value, see Eqs. I.3.56 and I.3.57.

For symmetry reasons we have in the middle of a foc (defoc) quadrupole $\alpha = 0$, and so the half cell will lead us from $\beta_{\max}$ to $\beta_{\min}$. At the same time we write for the phase advance from position *1* to *2*, $\psi_{12} = \frac{\psi_{\text{cell}}}{2}$ which leads us to

$$M = \begin{pmatrix} \sqrt{\frac{\beta_{\min}}{\beta_{\max}}}\cos\frac{\psi_{\text{cell}}}{2} & \sqrt{\beta_{\min}\beta_{\max}}\sin\frac{\psi_{\text{cell}}}{2} \\ \frac{-1}{\sqrt{\beta_{\min}\beta_{\max}}}\sin\frac{\psi_{\text{cell}}}{2} & \sqrt{\frac{\beta_{\max}}{\beta_{\min}}}\cos\frac{\psi_{\text{cell}}}{2} \end{pmatrix} \quad .$$

Due to the equivalence of the product matrix and the Twiss matrix, we get the two conditions

$$\frac{m_{22}}{m_{11}} = \frac{\beta_{\max}}{\beta_{\min}} = \frac{1 + l_d/\tilde{f}}{1 - l_d/\tilde{f}} = \frac{1 + \sin\frac{\psi_{\text{cell}}}{2}}{1 - \sin\frac{\psi_{\text{cell}}}{2}}$$

and

$$\frac{m_{12}}{m_{21}} = -\beta_{\max} \cdot \beta_{\min} = -\tilde{f}^2 = -\frac{l_d^2}{\sin^2\frac{\psi_{\text{cell}}}{2}}$$

that we can solve for

$$\beta_{\max} = \frac{(1 + \sin\frac{\psi_{\text{cell}}}{2})\, L}{\sin\left(\psi_{\text{cell}}\right)} \tag{I.3.56}$$

$$\beta_{\min} = \frac{(1 - \sin\frac{\psi_{\text{cell}}}{2})\, L}{\sin\left(\psi_{\text{cell}}\right)} \quad . \tag{I.3.57}$$

The maximum and minimum values of the β-function in a FoDo cell (which is the value at the QF and QD quadrupoles) are determined by the cell length L and its phase advance ψ_{cell}.

You might argue that somewhere there should appear the focusing strength of the magnets. And, yes, it does, hidden in a sophisticated way, behind the phase advance. These equations, Eqs. I.3.56 and I.3.57, are extremely useful for the first steps of a accelerator design. It allows us to create a reasonable (i.e. feasible) starting point for the lattice structure, which results in well determined β-s, so beam sizes and guarantees stability of the dynamics. Clear enough, we will use an optics code for the fine-tuning

and *matching* of the optics. However in general we are within 10% of a good solution.
We would like to complete this discussion of lattice cells with - you might guess it - once more having a look at the phase space picture. As the β-function in a focusing quadrupole is maximum, in a defocusing is minimum, which means $\alpha = 0$ at these locations, we expect a flat or upright phase space ellipse in the QF and QD. In Fig. I.3.37 the phase space picture is plotted for a number of positions inside the FoDo cell. In between these places the ellipse is tilted, its orientation and shape determined by the Twiss parameters, however the area covered in phase space will always be constant.

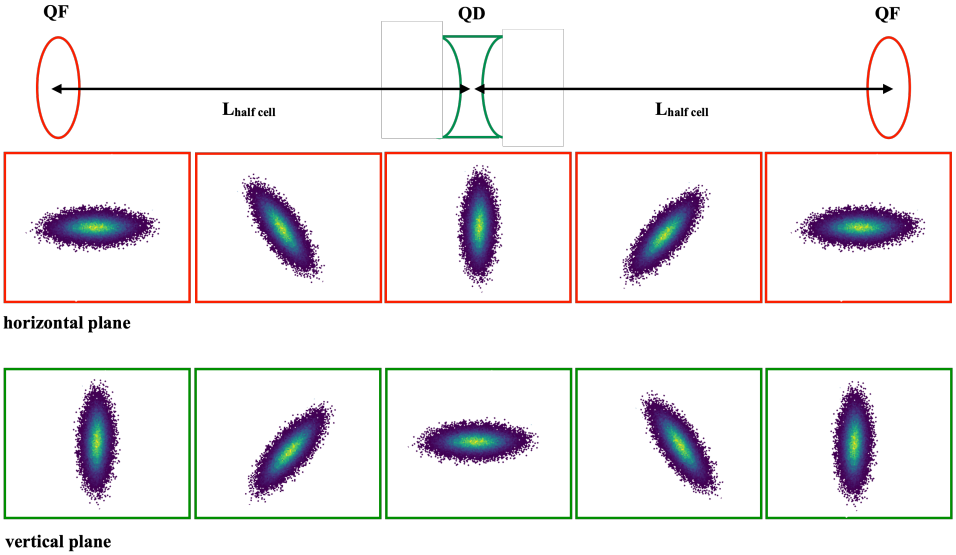

Fig. I.3.37: Schematic view of the phase space ellipse in different locations of the FoDo cell. In the centre of the quadrupoles $\alpha = 0$ and so the ellipse is flat or upright.

6.3 Non-periodic structures

In the previous section, the Twiss parameters, α, β, γ and the phase advance ψ have been derived for a periodic situation, namely a storage ring, or a lattice cell. The condition of periodicity is essential for the definition of the β-function. It is imposed by Hill's equation and its solution. More clear, a β-function is *not* defined in a non-periodic lattice. Often enough, however, we face such a non-periodic situation: a transfer line, where the beam passes only once from e.g. one accelerator to the next, or - by definition - a linear accelerator. Nonetheless we are clearly interested in quantities like beam envelopes and divergences and we would like to use the powerful language that we presented above to treat and optimise these structures as well.
We can do so, as long as we can determine the optics functions at the beginning of our e.g. transfer-line. Principally they are not uniquely determined as we do not have the condition of periodicity. However the transfer-line might connect two rings and so, the initial α, β and γ will be given by the optics properties of this ring. And we will apply the rule for transferring the Twissies, as given in Eq. I.3.53.
Such a situation is quite common and shown as an example for the ELSA ring [11] in Fig. I.3.38. An electron beam is accelerated in the booster-ring, which is clearly periodic and so has a well defined β-function. Reaching the flat top energy of 1.6 GeV, the beam is extracted into the transfer-line which

connects the Booster and the so-called Stretcher ring for further acceleration. The optics of the transfer-line is matched on one side to the periodic solution (i.e. the α-s and β-s of the booster) and on the other to the values of the high energy ring, and a certain number of independent quadrupoles is needed to achieve perfect matching conditions. *"a certain number"* means at least four on both sides of the transfer line, namely for fulfilling the optics conditions of α and β in both planes, and in case dispersion matching is required in addition (see Chapter I.14 on accelerator design), we have to add another bunch of magnets.

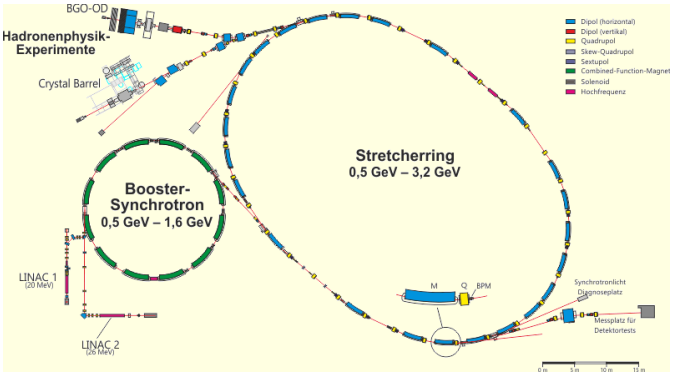

Fig. I.3.38: The two rings, booster and stretcher of the ELSA accelerator complex are connected by a transfer line that has to fulfill the matching conditions on both sides.

In the absence of a ring-type pre-accelerator (a small synchrotron or damping ring) the only chance is to *guess*. Based on measurements (or guts feeling) we have to determine by educated guess and fit the beam emittance and optics parameters that we will use as starting values for the optics calculations, sometimes through km-long accelerator structures in a linear collider.

7 The not-so ideal world: acceleration and momentum spread

A synchrotron, storage ring or what ever circular accelerator we might consider, is a nice and robust machine with well defined beam parameters. The only thing that makes the story complicated is *the acceleration !* As soon as we start to increase the beam energy—which is unfortunately what we are paid for—things get quite a bit more *interesting*. Interesting in this context might be replaced by complicated. However let's start with a little reminder on the phase space properties, that we discussed before. At a given location in the storage ring, the phase space ellipse of a particle is defined in shape and orientation by the optics parameters α, β, γ. Three typical situations are shown in Fig. I.3.39. The parameter ε is given by the equation $\varepsilon = \gamma(s) + 2\alpha(s)x(s)x'(s) + \beta(s)x'^2(s)$. It is a remarkable fact that while all ingredients in the above equation depend actually on the coordinate s, the emittance does not. We summarize once more the basic facts:

- ε defines the area covered in phase space, via $A = \varepsilon \cdot \pi$;
- it describes en ellipse in the $x - x$' phase space, which is defined for each particle. In case we describe the beam as an ensemble of many particles, ε is a quality factor for the whole beam;

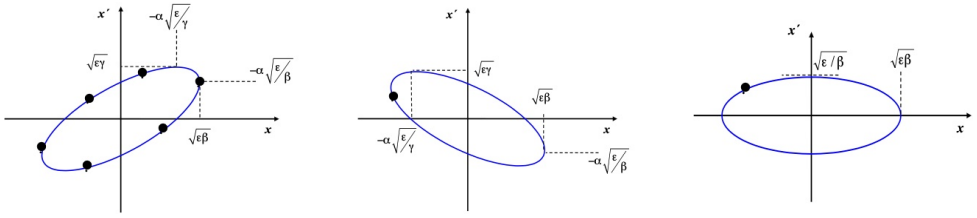

Fig. I.3.39: Phase space ellipse of a particle in a ring, at three different positions. Shape and orientation are defined by the optics parameters, while the area $A = \pi \cdot \varepsilon$ is constant.

– shape and orientation of the phase space ellipse are given by the optics parameters;
– Following Liouvilles theorem, ε is constant.

All nice and clear, but , so sorry, that's wrong

$$\varepsilon \neq \text{const} \quad .$$

In classical mechanics we refer to two canonical coordinates, which in our case are position x and momentum p_x. And referring for a moment to the horizontal plane, Liouville's theorem tells us that the area in the phase space of canonical coordinates, is constant.

$$\int p_x dx = \text{const} \quad .$$

For convenience, in other words because we are lazy bones, we however refer to x and x', the position and angle. And - a bit more serious - we do so for good reasons, as we want to know position and angle of a particle trajectory. So, clearly the angle *x'* and the transverse momentum p_x are related parameters. But they are not the same.

$$x' = \frac{dx}{ds} = \frac{dx}{dt} \cdot \frac{dt}{ds} = \frac{\beta_{rel_x}}{\beta_{rel}} = \frac{p_x}{p} \quad .$$

(Attention: here we refer to Albert's, $\beta_{rel} = v/c$, not Bernhard's!! Unfortunately most physicists only know the first three Greek letters which sometimes leads to confusion). Now our definition of the phase space the area is

$$A = \varepsilon \cdot \pi = \int x' dx = \frac{p_x dx}{p} \propto \frac{\text{const}}{m_0 c\, \gamma_{rel} \beta_{rel}} \quad ,$$

where we have explicitly used the relativistic correct expression for the momentum, $p = \gamma_{rel} \beta_{rel} m_0 c$.

So, the beam emittance as we define it still is constant, but only as long as the beam energy does not change. As soon as we start to accelerate, the observed emittance seems to shrink. And it does indeed,

$$A = \varepsilon \cdot \pi = \int x' dx \propto \frac{1}{\beta_{rel} \gamma_{rel}} \quad .$$

Schematically the situation is visualised in Fig. I.3.40. During acceleration the longitudinal momentum will increase while the transverse momentum, p_x will stay the same. As direct consequence the divergence, *x'*, will shrink. We conclude immediately, that at lowest energy the beam will have the highest emittance, for a given optics (i.e. β), which means it will have the largest size and so will need the largest

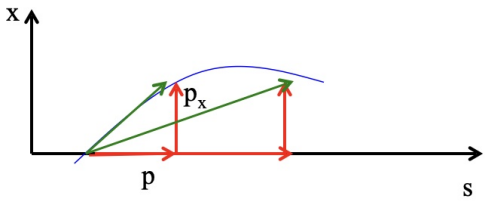

Fig. I.3.40: Schematic explanation of the adiabatic shrinking: During acceleration the longitudinal momentum will increase while the transverse components stay unchanged, leading to a reduction of the corresponding angles, *x'* resp. *y'*.

magnet aperture. The situation can be quite drastic. Figure I.3.41 shows the 7 σ beam envelope inside the mini-beta magnet of the HERA collider. In red the beam size is plotted, in green the geometry of the vacuum chamber (designed as clover-shape to squeeze out more space between the pole shoes of the magnet) and in white dotted the hyperbolic shape of the iron pole shoes. On the left side the situation is shown at 40 GeV injection energy and the beam barely fits in. We had a lifetime of a few hours only (well . . . the beam rather than we) and we were very eager to push the button to "take off". At flat top, near 1 TeV energy, the emittance got so small, that the beam envelope—calculated for the same optics—hardly is seen in the same magnet. Lifetime was close to infinite and life was easy.

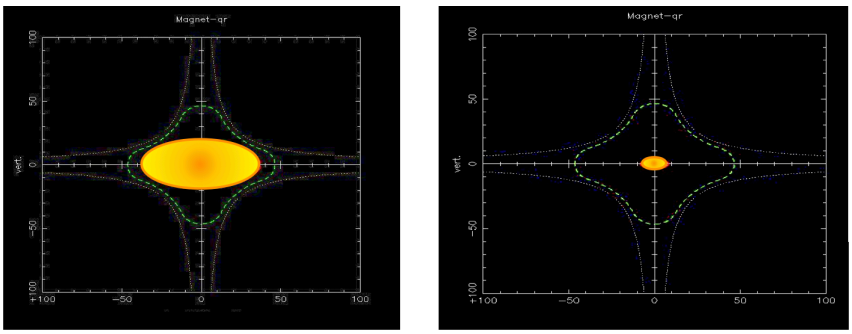

Fig. I.3.41: Calculated beam size corresponding to 7 σ in a quadrupole magnet of a storage ring. *left*: at injection energy (40 eV), *right* for the same optics at flat top energy (920 GeV). Due to the reduction of the beam emittance the available free aperture increases considerably during the acceleration process.

A few concluding remarks on that topic:

- A proton machine . . . or an electron linac . . . needs the highest aperture at injection energy!!!
- As soon as we start to accelerate the beam size shrinks as $\sigma \propto \frac{1}{\sqrt{\gamma}}$ in both transverse planes.
- At lowest energy the machine will have the major aperture problems $\rightarrow$ here we have to minimise the values of β as much as possible.
- We will need different beam optics adopted to the energy.

Finally, for good reasons, in literature "our" *x-x'-phase* space is sometimes called *trace space*, to mark a clear difference to the real x - p_x *phase space*.

In conclusion we summarise that protons or electrons in a linear accelerator shrink during accel-

eration, as well as protons or heavy ions do in a synchrotron.
Electrons in a circular accelerator do not!!! They grow, and their emittance behaves like $\varepsilon_e \propto \gamma^2$. But that's another story and will be told in another context. These facts have a serious and immediate consequence for the optics calculations of a storage ring: if the beam emittance is indeed shrinking during acceleration this is a nice effect. However it means that at low energy (typically at injection) the beam will have its largest emittance and the optics designer will have to earn his/her money to establish a focusing pattern, that limits the β-function to low values; low enough that the beam dimension, $\sigma = \sqrt{\varepsilon \cdot \beta}$ fits at any location into the aperture, defined by the vacuum chamber and magnets. It is as easy as that: at low energy the beam is big anyway and we cannot afford large β-functions. Figure I.3.42 demonstrates this situation quite drastically. At injection (left side of the figure) a special optics is shown that had been established for injection and the low energy steps of the LHC. Values of maximum $550\,\mathrm{m}$ for both betas (β_x, β_y) are the absolute limit to avoid particle losses. On the right hand side - at high energy - the collision optics is shown, where due to the fact that the energy had been increased by a factor of 16 (!) and thus due to the much smaller emittance, β values up to $4.5\,\mathrm{km}$ are acceptable. We also will conclude that there has to be somehow a way to bring the beam from the left part of the figure to the right one ... very carefully, adiabatic and applying about a dozen intermediate optics steps to guarantee at any moment stable conditions. The procedure is usually called *beta-squeeze* and takes nearly as long as the whole acceleration procedure, namely 30 min.

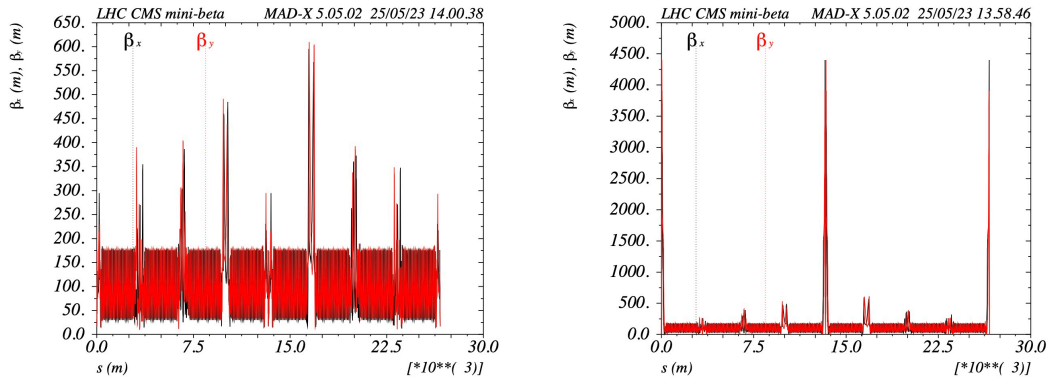

Fig. I.3.42: Injection optics *(left, 450 GeV)* and collision optics *(right, 7 TeV)* of the LHC. Due to the larger emittance at injection energy the *beta*-function has to be limited to guarantee sufficient free aperture.

8 Dispersion and momentum spread

An ideal accelerator would be a device that accelerates an infinite amount of particles to an infinitely high energy with infinitely sharp energy spread.
Well, you will agree that this is too much asking for in real world. Still, at least in parts of these requests we are close. Figure I.3.43 shows an electrostatic accelerator, that—based on a DC voltage of 12 MV—brings basically all particles injected from the source (on the right side of the picture) to the very same energy ($12\,\mathrm{MeV}$) with an energy spread of $\Delta E/E \approx 10^{-5}$ or better.

Fig. I.3.43: A perfect accelerator if we consider the energy spread: due to the DC-voltage all particles see the same potential difference resulting in very narrow momentum spread of the beam.

Unfortunately these wonderful devices are very limited in the available acceleration voltage. The potential difference can only be applied once. And—alas—in order to gain higher energies we have to apply *time varying* electric fields, as produced in so-called resonators or RF-cavities or in a Widerøe structure as shown in Fig. I.3.44. Here we can create a fast oscillating electromagnetic field between the drift tubes whose (longitudinal) electric field component is used to accelerate the beam. The longitudinal

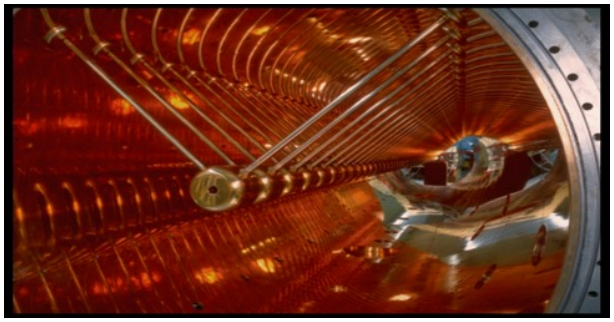

Fig. I.3.44: Typical drift tube structure of a Wideroe Linac (Courtesy of GSI).

beam dynamics and the techniques to build these devices are explained in Chapter I.4 on longitudinal beam dynamics. Here we only refer to the problem that applying time varying longitudinal electric fields creates a certain amount of trouble for us. In fact due to the changing fields the typical momentum spread in a storage ring is on a level that cannot be ignored anymore.

Up to now, we have treated the beam and the equation of motion as a mono-energetic problem. Unfortunately, in the case of a realistic beam, we have to deal with a considerable distribution of the particles with respect to energy or momentum. A typical value is in the order of $\Delta p/p \approx 10^{-3}$. This momentum spread leads to several effects concerning the bending of the dipole magnets and the focusing strength of the quadrupoles. It turns out that the equation of motion, which has been a homogeneous differential equation until now, acquires a non-vanishing term on the right-hand side (r. h. s.). In the development of the equation of motion, we assumed ideal conditions for the particle momentum, which means that in Eq. I.3.7 and as a consequence in Eq. I.3.8 the momentum was ideal and the same for every

particle. For convenience we repeat the equation here once more

$$x'' - \frac{1}{\rho} + \frac{x}{\rho^2} = -\frac{B_0}{p/e} + \frac{xg}{p/e} \quad . \tag{I.3.58}$$

Now, unfortunately, we have to introduce a certain momentum spread and so we replace

$$p \to p_0 + \Delta p$$

but still we stay with the linear approximation and take only dipole and quadrupole fields into account. However, we consider in our endless optimism only small momentum errors, $\Delta p \ll p_0$, which is indeed a realistic assumption and allows to make the approximation

$$\frac{1}{p} = \frac{1}{p_0 + \Delta p} \approx \frac{1}{p_0} - \frac{\Delta p}{p_0^2} \quad .$$

Inserting this into the equation above we can write

$$x'' - \tfrac{1}{\rho} + \tfrac{x}{\rho^2} \approx \underbrace{-\frac{eB_0}{p_0}}_{-\frac{1}{\rho}} + \tfrac{\Delta p}{p_0^2} eB_0 + \underbrace{\frac{xeg}{p_0}}_{x \cdot k} - \underbrace{x \cdot e \cdot g \frac{\Delta p}{p_0^2}}_{\approx 0} \quad . \tag{I.3.59}$$

The first term on the r.h.s. is as before the bending strength of the dipole field. The third term describes the corresponding quadrupole contribution and the last term is the product of two small quantities, *x* and Δp, which we ignore. However there is a term that does not vanish and after slight re-arrangement we get

$$x'' + x(\frac{1}{\rho^2} - k) = \frac{\Delta p}{p_0} \frac{1}{\rho} \quad .$$

The momentum spread of the beam adds a non-vanishing term on the r.h.s. of the equation of motion. The general solution of our now in-homogeneous differential equation is therefore the sum of the solution of the homogeneous equation of motion and a particular solution of the in-homogeneous equation

$$x(s) = x_h(s) + x_i(s).$$

Here x_h is the solution that we have discussed up to now and x_i is an additional contribution that still has to be determined. To be clear: the momentum error adds an additional oscillation amplitude to the ideal trajectories that we described before and it depends (in our approximation) linearly on the actual momentum deviation of the individual particle. For convenience, we usually normalize this second term and define a special function, the so-called dispersion

$$D(s) := \frac{x_i(s)}{\Delta p / p_0} \quad .$$

This equation describes the dependence of the additional amplitude of the transverse oscillation on $\Delta p/p$,

$$x_i''(s) + K(s) \cdot x_i(s) = \frac{1}{\rho} \cdot \frac{\Delta p}{p_0} \quad .$$

The dispersion function is defined by the magnet lattice and is usually calculated by optics programs in the context of the calculation of the usual optical parameters; it is of equal importance. Analytically, it can be determined for single elements via the expression

$$D(s) = S(s) \cdot \int \frac{1}{\rho(\tilde{s})} C(\tilde{s}) d\tilde{s} - C(s) \cdot \int \frac{1}{\rho(\tilde{s})} S(\tilde{s}) d\tilde{s} \quad , \tag{I.3.60}$$

where $S(s)$ and $C(s)$ correspond to the sin-like and cos-like elements of the single-element matrices or of the corresponding product matrix if there are several elements considered in the lattice. Although all this sounds somewhat theoretical, we would like to stress that it is just the good old spectrometer (or prisma-) effect, as schematically shown in Fig. I.3.45. However the dispersion has to be taken serious as

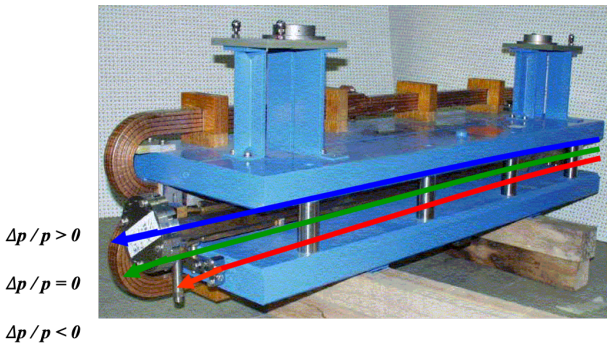

Fig. I.3.45: Spectrometer effect of a beam with finite momentum spread passing a dipole: the dispersion leads to different trajectories for particles that have different momenta.

the typical values for the beam size and dispersive effect in the case of a high-energy storage ring are of the same order, e.g.

$$x_h = 1 \ldots 2 \text{ mm}, \quad D(s) \approx 1 \ldots 2 \text{ m} \quad .$$

Thus, for a typical momentum spread of $\Delta p/p_0 = 1 \cdot 10^{-3}$, we obtain an additional contribution to the beam size from the dispersion function that is of the same order as that from the betatron oscillations. A typical example of a high-energy beam optics including the dispersion function is shown in Fig. I.3.46. It should be pointed out that the dispersion describes the special orbit that an ideal particle would have in the absence of betatron oscillations ($x_\beta = x'_\beta = 0$) for a momentum deviation of $\Delta p/p = 1$. Nevertheless, it describes "just another particle orbit" and so it is subject to the focusing forces of the lattice elements, as seen in the figure.

Now, we definitely are aware of the fact that this is a bit an abstract story. And—if the highly esteemed reader allows—we will try to visualise the facts in a simplified manner.
We start once more with the idealised situation, and a particle that is circulating in the little toy storage ring, introduced above. The ring consists only out of dipole and focusing,and defocusing quadrupole magnets, see Fig. I.3.47 (left part), and idealising quite a bit for the moment we assume that the dipole

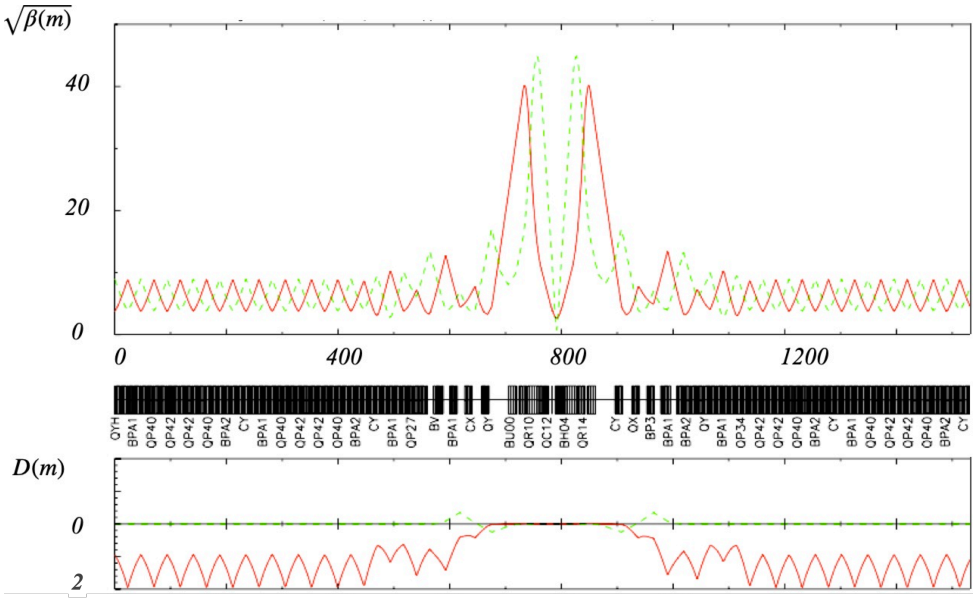

Fig. I.3.46: Beam optics of a collider: the two arcs - left and right side of the plot - are connected by a mini-beta insertion. *Upper part*: the horizontal and vertical β-function is shown (red and green curve respectively). The periodic pattern, following the regular FoDo structure of the arcs is clearly seen as well as the Interaction Point (IP) of the beams where smallest β-values are created. *Lower part*: ror. (red) and vert. (green) dispersion, once more following the regular pattern in the arc structure. For obvious reasons the dispersion has to vanish at the collision point and reaches indeed zero values in both planes at the IP.

field acts as it were present allover the place, in a kind of cyclotron type arrangement. That's not really the case in a synchrotron, however it helps to understand the underlying principle (and it makes the drawings much easier to do). An ideal particle without any amplitude or angle, $x = x' = 0$, and with perfect momentum, $\Delta p = 0$ will follow the ideal circle, marked in blue, see middle part of the figure. The fact that we draw a circle and not a polygon, defined by the dipole magnets, shows that we are really super idealising here. In case the particle still has the perfect momentum, however it starts with a certain amplitude and/or angle, $x \neq 0$ or $x' \neq 0$ it will perform oscillations around the ideal orbit. And so the trajectory will follow the betatron oscillations, defined by the focusing and defocusing forces of the quadrupoles, sketched as black dashed line and marked as x_β in the plot. So-far so good.
Now, our particle has on top of amplitude and angle a certain momentum deviation, $\Delta p/p \neq 0$ and so it will run on a larger (or smaller) circle - depending on the sign of the momentum error, and its betatron oscillations will be centred around *this* new closed orbit. The difference in radius between the ideal circle and the one for the off-momentum particle is defined by the dispersion function, via $x_D(s) = D(s) \cdot \Delta p/p$, as indicated in the figure. And its betatron oscillations will zig-zag around its new closed orbit, which is defined by the dispersion—*right part of the figure*.

The only part which is not included in the drawings is the fact that, the dispersion, being just-another-orbit is subject to the focusing fields of the quadrupoles, as any other orbit. And so it will oscillate under the mutual influence of the focusing and defocusing fields and go instead of a perfect circle in a zig-zag like manner around the ring, as is indeed shown in Fig I.3.46. However we considered

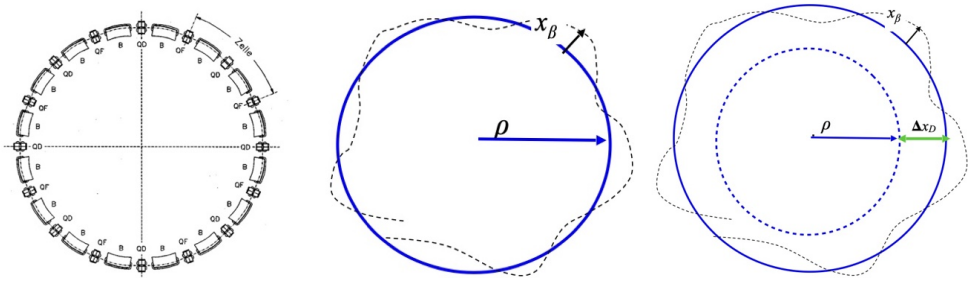

Fig. I.3.47: The (periodic) dispersion is the closed orbit of a particle with momentum error. The well known betatron oscillations—treated so far—will oscillate around this new closed orbit.

that too much zig-zag for a simple drawing and leave it to the fantasy of the reader to complete the picture.

9 Dispersion and beam size

Now, to be a little bit more exact in our mathematical description, we realize that we cannot simply add the contribution from the dispersion to the betatron amplitude. Both—momentum spread as well as the betatron amplitude—follow in good approximation a Gaussian distribution and so we have to add them as superposition.

It is correct that for a single particle trajectory the dispersion just adds another piece of amplitude, that depends on the actual momentum deviation.

$$x(s) = x_\beta(s) + D(s) \cdot \frac{\Delta p}{p} \quad .$$

Looking at the beam as a ensemble of many particles, however, things change slightly. And in order to determine the beam size we have to "fold" the two distributions and get

$$\sigma_x = \sqrt{\sigma_{x\beta}^2 + (D \cdot \frac{\sigma_p}{p})^2} = \sqrt{\varepsilon \cdot \beta + D^2(s) \cdot \frac{\sigma_p^2}{p^2}} \quad ,$$

where σ_p describes the standard deviation of the particles' momentum spread. This straight forward expression deserves a few remarks:

- in order to keep the beam small at the collision points the dispersion should vanish at the IP.
- as the dispersion represents the link between longitudinal and transverse dynamics, and possibly will lead to coupling between these two worlds, it should also vanish at the location of the RF structures, where the beam sees a sudden increase of its energy (or momentum). If not suppressed at the cavities, we will realise that new resonances will be created, *synchro-betatron* resonances, see Chapter I.8 on transverse linear imperfections , making life of the operators team even more difficult as the free space in the machine's working diagram is more and more limited.
- when designing a lattice for a storage ring, therefore, special magnet arrangements will be needed that suppress the dispersion. These so-called dispersion suppressor schemes will be explained in a

later section, on lattice design.

Before we introduce the audience to real world and confront the still enthusiastic student with the problems of chromaticity and dynamic aperture and all those little adversities and problems that define the life of an accelerator physicist, we will spend a moment to fill the concept of dispersion with numbers, at least in a few examples.
Again, starting on the lowest possible level, let's have a look at a drift

$$M_{\text{drift}} = \begin{pmatrix} 1 & l_d \\ 0 & 1 \end{pmatrix} \quad .$$

The rule to calculate the dispersive terms had been given in Eq. I.3.60, where now for obvious reasons the expression $1/\rho$ in both terms is zero, and so is *D(s)* and *D'(s)*.
In full beauty the 3×3 matrix of a drift is

$$M_{\text{drift}} = \begin{pmatrix} 1 & l_d & 0 \\ 0 & 1 & 0 \\ 0 & 0 & 1 \end{pmatrix} \quad ,$$

... which is indeed not too sophisticated. A bit more interesting is the story for a dipole sector magnet—which has, as we know already, a weak focusing component in the plane of bending. In general a focusing matrix looks like

$$M_{\text{foc}} = \begin{pmatrix} \cos(\sqrt{|K|} \cdot l_q) & \frac{1}{\sqrt{|K|}} \sin(\sqrt{|K|} \cdot l_q) \\ -\sqrt{|K|} \cdot \sin(\sqrt{|K|} \cdot l_q) & \cos(\sqrt{|K|} \cdot l_q) \end{pmatrix} \tag{I.3.61}$$

with $K = 1/\rho^2 - k$ combining the weak focusing of the dipole and the strong focusing of a quadrupole magnet. In case of a pure dipole magnet the second term is zero, and so we remain with the weak focusing $1/\rho^2$ and get *for the focusing properties* of the dipole magnet

$$M_{\text{foc}} = \begin{pmatrix} C & S \\ C' & S' \end{pmatrix} = \begin{pmatrix} \cos(\frac{l_b}{\rho}) & \rho \cdot \sin(\frac{l_b}{\rho}) \\ -\frac{1}{\rho} \cdot \sin(\frac{l_b}{\rho}) & \cos(\frac{1_b}{\rho}) \end{pmatrix} \quad . \tag{I.3.62}$$

To avoid confusion, we introduced for the length of the dipole (i.e. bending)-magnet the parameter l_b to distinguish it from the quadrupole length l_q and the drift space l_d.
We can use this matrix now to calculate the dispersive terms via Eq. I.3.60

$$D(s) = S(s) \cdot \int_{s1}^{s2} \frac{1}{\rho} C(\tilde{s}) d\tilde{s} - C(s) \cdot \int_{s1}^{s2} \frac{1}{\rho} S(\tilde{s}) d\tilde{s} \quad ,$$

where the longitudinal coordinate s_1 refers to the beginning of the bending magnet and $s_2 = s_1 + l_b$ to the end and assume a constant bending radius within the dipole magnet

$$D(s) = (\rho \cdot \sin\frac{l_b}{\rho}) \cdot \frac{1}{\rho} \cdot (\rho \cdot \sin\frac{l_b}{\rho}) - (\cos\frac{l_b}{\rho}) \cdot \frac{1}{\rho} \cdot \rho \cdot (-\cos\frac{l_b}{\rho} + 1) \cdot \rho$$

$$D(s) = (\rho \cdot \sin^2\frac{l_b}{\rho}) + \rho \cdot (\cos\frac{l_b}{\rho}) \cdot \rho \cdot (\cos\frac{l_b}{\rho} - 1) \quad ,$$

and so finally we get

$$D(s) = \rho \cdot (1 - \cos\frac{l_b}{\rho}), \quad D'(s) = \sin\frac{l_b}{\rho} \qquad .$$

Our 3×3 matrix is now complete and the rule for transferring particles with momentum deviation is

$$\begin{pmatrix} x \\ x' \\ \Delta p/p_0 \end{pmatrix}_{s2} = \begin{pmatrix} C & S & D \\ C' & S' & D' \\ 0 & 0 & 1 \end{pmatrix} \cdot \begin{pmatrix} x \\ x' \\ \Delta p/p_0 \end{pmatrix}_{s1} \tag{I.3.63}$$

$$\begin{pmatrix} x \\ x' \\ \Delta p/p_0 \end{pmatrix}_{s2} = \begin{pmatrix} \cos(\frac{l_b}{\rho}) & \rho \cdot \sin(\frac{l_b}{\rho}) & \rho \cdot (1 - \cos\frac{l_b}{\rho}) \\ -\frac{1}{\rho} \cdot \sin(\frac{l_b}{\rho}) & \cos(\frac{1}{\rho}) & \sin(\frac{l_b}{\rho}) \\ 0 & 0 & 1 \end{pmatrix} \cdot \begin{pmatrix} x \\ x' \\ \Delta p/p_0 \end{pmatrix}_{s1} \qquad . \tag{I.3.64}$$

Nota bene:
even an ideal particle with $x = x' = 0$ will start to oscillate if it passes a dipole magnet and has a momentum error $\Delta p/p$. A dispersion trajectory will obey the same focusing forces (i.e. will be transferred by the same matrices) as a normal betatron oscillation.

In principle we could calculate the *D* and *D'* terms for each and every magnet in the lattice. However, if they did not exist yet, we would invent computers to do that job for us. And so a usual optics code not only calculates the β-function for us but also the *D* and *D'*.
There is a last point that we have to mention: usually we talk about synchrotrons, or storage rings or what-so-ever rings. And these have by definition an intrinsic periodicity: after one turn we end up at the very same little blue dipole magnet that we saw a few micro seconds before. In the case of the β-function this periodicity is required (mathematically) for a uniquely determined β-function.
Now for the dispersion it is more or less the same problem. A particle without betatron oscillations but with momentum spread will follow a closed orbit, which is the *periodic* dispersion, the blue circle on the right part of Fig. I.3.47. To be periodic—for one turn or in case of periodic lattice cells for one periodic structure—we have to require the periodicity condition

$$\begin{pmatrix} \eta \\ \eta' \\ 1 \end{pmatrix} = \begin{pmatrix} C & S & D \\ C' & S' & D' \\ 0 & 0 & 1 \end{pmatrix} \cdot \begin{pmatrix} \eta \\ \eta' \\ 1 \end{pmatrix} \qquad . \tag{I.3.65}$$

Here we have used as before *D* and *D'* for the dispersion trajectory part of the transfer matrix. In a counter play between these dispersion creating terms of the matrix and the focusing properties of the lattice we get—using this periodicity condition—the periodic dispersion of the lattice and its derivative called η and η'. And—just like for the β-function—we can use the condition to calculate this periodic dispersion in a lattice structure. We will do so now, not a big surprise, for our highly esteemed FoDo cell.

9.1 Dispersion in a FoDo cell

It is instructive to repeat the procedure that we have done before for the β-function in a FoDo-cell, and calculate the dispersion. As we have to introduce the dispersion driving elements (i.e. the dipole magnets) we refer our calculation once more to the schematics shown in Fig. I.3.48, where now the dipoles located between the focusing and defocusing quadrupole magnets are marked in blue. We still neglect the weak

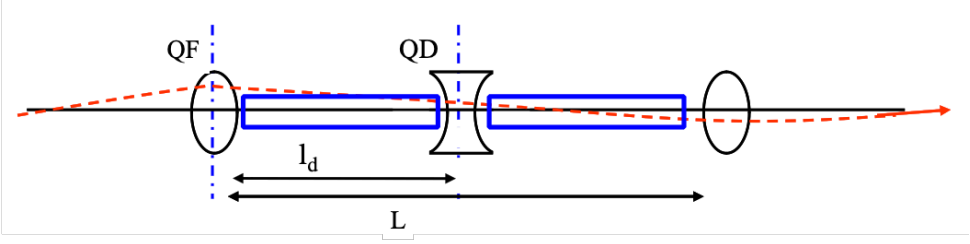

Fig. I.3.48: Schematic drawing of a FoDo structure to calculate the optics functions at the QF and QD quadrupole: we refer once more to Fig. I.3.36, including now the dipole magnets—schematically shown as blue boxes—as dispersion driving elements in the lattice cell. The dashed lines refer again to the points of interest, i.e. the centre of the quadrupoles where the dispersion will reach its max. or min. values.

focusing contribution $1/\rho^2$, as it is negligible anyway compared to the quadrupole gradient, but we take into account the driving term $1/\rho$ to determine the dispersion effect and we assume that the length of the dipole corresponds to half the length of the FoDo, $l_b = l_d = \frac{L}{2}$.
We will work in thin lens approximation and so this assumption is quite ok. The matrix that brings us from the centre of the focusing quadrupole to the centre of the defocusing one (blue cursor lines in the figure), thus describing the half-cell is

$$M_{\text{halfcell}} = M_{\text{QD}/2} \cdot M_d \cdot M_{\text{QF}/2}$$

which is with $f = 1/(k \cdot l_q)$ as focal length of the quadrupoles

$$M_{\text{halfcell}} = \begin{pmatrix} 1 & l_q \\ \frac{-1}{\tilde{f}} & 1 \end{pmatrix} \cdot \begin{pmatrix} 1 & l_d \\ 0 & 1\cdot \end{pmatrix} \cdot \begin{pmatrix} 1 & l_q \\ \frac{1}{\tilde{f}} & 1 \end{pmatrix} \quad .$$

As before we set $\tilde{f} = 2 \cdot f$ for the focal length of half a quadrupole, as we start the calculation for symmetry reasons (which means to save some ink) in the middle of the quadrupole. Multiplying out we get

$$M_{\text{halfcell}} = \begin{pmatrix} C & S \\ C' & S' \end{pmatrix} = \begin{pmatrix} 1 - \frac{l_d}{\tilde{f}} & l_d \\ \frac{-l_d}{\tilde{f}^2} & 1 + \frac{l_d}{\tilde{f}} \end{pmatrix} \quad .$$

So far nothing is new. But now we calculate the dispersive terms of the cell, using the expression I.3.60

$$D(s) = S(s) \cdot \int \frac{1}{\rho(s)} C ds - C(s) \cdot \int \frac{1}{\rho(s)} S ds$$

$$D(l_d) = \underbrace{l_d}_{S(s)} \cdot \frac{1}{\rho} \cdot \int_0^{l_d} \underbrace{(1 - \frac{s}{\tilde{f}})}_{C(s)} ds \quad \underbrace{-(1 - \frac{l_d}{\tilde{f}})}_{C(s)} \cdot \int_0^{l_d} \underbrace{s}_{S(s)} ds \tag{I.3.66}$$

$$D(l_d) = \frac{l_d}{\rho}(l - \frac{l_d^2}{2\tilde{f}}) - (1 - \frac{l_d}{\tilde{f}}) \cdot \frac{1}{\rho} \cdot \frac{l_d^2}{2} \quad ,$$

which gives

$$D(l_d) = \frac{l_d^2}{2\rho} \quad ,$$

and in full analogy for D'

$$D'(l_d) = \frac{l_d}{\rho}(1 + \frac{l_d}{2\tilde{f}}) \quad ,$$

and we get the complete matrix including the dispersion terms D, D'

$$M_{\text{halfcell}} = \begin{pmatrix} C & S & D \\ C' & S' & D' \\ 0 & 0 & 1 \end{pmatrix} = \begin{pmatrix} 1 - \frac{l_d}{\tilde{f}} & l_d & \frac{l_d^2}{2\rho} \\ \frac{-l_d}{\tilde{f}^2} & 1 + \frac{l_d}{\tilde{f}} & \frac{l}{\rho}(1 + \frac{l}{2\tilde{f}}) \\ 0 & 0 & 1 \end{pmatrix} \quad .$$

In analogy to the determination of the amplitude function, β, we know that the half-cell brings us from the maximum dispersion, $D_{\max}$ to the minimum $D_{\min}$, as visualised schematically in Fig I.3.49. So we

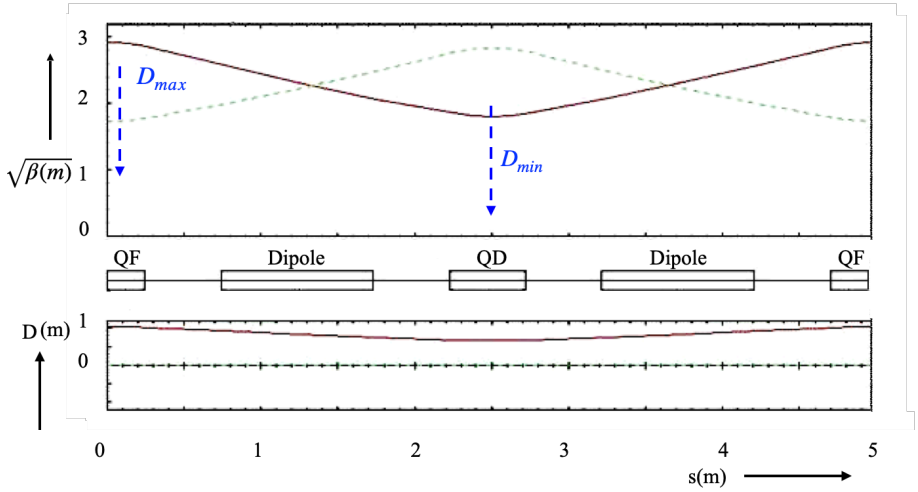

Fig. I.3.49: FoDo cell with the maximum and minimum values of the dispersion (marked by the arrows).

can write (remembering that D' is zero at the beginning of the cell as well as in the centre)

$$\begin{pmatrix} D_{\min} \\ 0 \\ 1 \end{pmatrix} = M_{\text{half-cell}} \cdot \begin{pmatrix} D_{\max} \\ 0 \\ 1 \end{pmatrix} \quad .$$

Multiplying out we get

$$D_{\min} = D_{\max} \cdot (1 - \frac{l_d}{\tilde{f}}) + \frac{l_d^2}{2\rho}$$

and

$$0 = -D_{\max} \cdot \frac{l_d}{\tilde{f}^2} + \frac{l_d}{\rho}(1 + \frac{l_d}{2\tilde{f}}) \quad .$$

So we have two equations that we can solve for the two parameters $D_{\max}$ and $D_{\min}$

$$D_{\max} = \frac{l_d^2}{\rho} \cdot \frac{1 + \frac{1}{2}\sin\frac{\psi_{\text{cell}}}{2}}{\sin^2\frac{\psi_{\text{cell}}}{2}}$$

$$D_{\min} = \frac{l_d^2}{\rho} \cdot \frac{1 - \frac{1}{2}\sin\frac{\psi_{\text{cell}}}{2}}{\sin^2\frac{\psi_{\text{cell}}}{2}} \quad .$$

For the last transformation we have once more used the relation $l/f = \sin(\psi/2)$, that we derived above and ψ_{cell} describes the phase advance for the full cell.
We conclude that the dispersion in the FoDo depends—apart from the obvious bending radius—only on the phase advance (which is clear as it describes the focusing strength) and the length of the cell. In other words, if you want a smaller dispersion, make your cell shorter and increase the focusing strength of the quadrupoles. However, don't forget the limits set by the stability criterion. Figure I.3.50 visualises the effect. It shows the maximum and minimum dispersion as a function of the phase advance per cell. And it turns out that quite opposite to the β-function the dispersion can be made smaller and smaller by increasing the phase advance. Well ... until we run into problems of keeping the β-function limited or the beam dynamics stable.

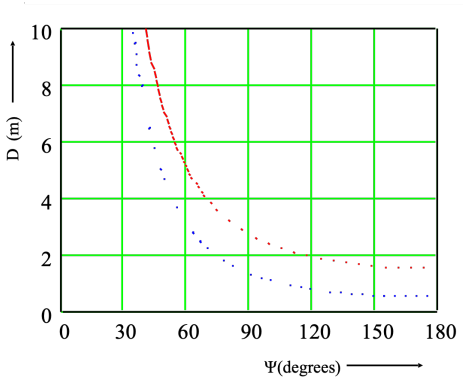

Fig. I.3.50: Dispersion in a FoDo cell as function of the phase advance of the cell: an increase of the phase advance per cell, which means stronger focusing, leads to a general decrease of the dispersion function. At the location of the focusing (red curve) as well as at the defocusing quadrupole (blue) the corresponding dispersion values reduce.

We mentioned already that the dispersion should vanish at the collision point of the two counter-rotating beams. Unless it would lead to the quite uncomfortable situation that due to the natural momentum spread, the beam size—that should be as small as we can technically achieve—would be diluted.

Other reasons might exist to get rid of the dispersion—at least for a certain part in the lattice. Techniques of how to do that in a storage ring exist and will be treated in the section on lattice design. Here we just refer to Fig. I.3.51 which shows the principle. Starting from the *IP*, the dispersion is zero in the straight section where the collisions take place and the particle detector is located. We see the sharp increase of the β-function due to the mini-beta insertion but apart from that everything is easy going. However as soon as we enter the arc, i.e. as soon as the beam feels the bending field of the first dipole magnet, the dispersion takes off and is increased step by step in every dipole. Due to the focusing forces of the lattice quadrupoles we finally reach a situation where due to the counter-play of the dispersion driving dipoles and the restoring force of the lattice quadrupoles the dispersion follows a zig-zag like curve between $\hat{D}$ and $\check{D}$, as we have calculated above.

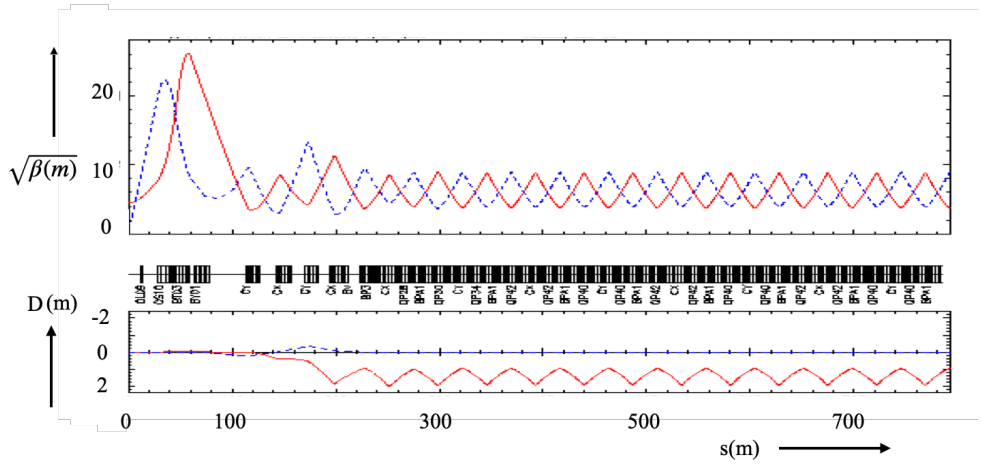

Fig. I.3.51: Beam optics starting at a collision point with $D = D' = 0$. As soon as the first dipole magnet is encountered at the beginning of the arc, the dispersion starts to rise and is oscillating in the arc as a result of the focusing quadrupoles and the dispersion driving force of the dipoles.

Finally a last point: dispersion is actually visible. There is a famous effect in lepton machines, where the beam—due to the considerable energy loss due to synchrotron light—is running on a dispersive orbit, until it regains the lost energy in the RF sections. This give and take of the energy leads to—guess what—another zig-zag behaviour, this time of the closed orbit, and is called saw-tooth effect. Figure I.3.52 shows the closed orbit of the electron beam in the Large Electron Positron collider (LEP). It is running from right to left, and the green bars are Beam Position Monitor (BPM) measurements. Starting more or less well centred the beam looses energy due to synchrotron radiation and so shifts to the inner side of the ring. Until it regains energy in the RF straight section, shoots over, because it got more energy than would fit to the ideal situation, looses again etc. We conclude that LEP had four RF stations and—knowing the dispersion function in the arc—we even could calculate the energy lost in each arc.

9.2 Exercise VI

Figure I.3.53 shows the result of an orbit measurement during a dispersion measurement campaign. After applying a dedicated momentum (or energy) change to the beam the horizontal and vertical orbit of a

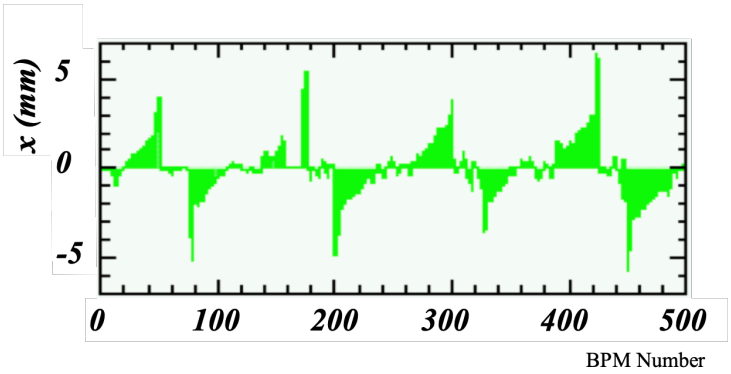

Fig. I.3.52: The famous *saw tooth* effect at LEP: the beam is loosing energy in the arc due to synchrotron radiation, which is replenished in the RF sections. The corresponding horizontal orbit oscillation, caused by the dispersion in the ring and measured at the beam position monitors (BPM) forms the special pattern that led to the name of the phenomenon.

proton beam are displayed with reference to a stored orbit that had been taken for the ideal beam energy. These beam manipulations are used to determine the actual dispersion in the storage ring as a function of the position s.

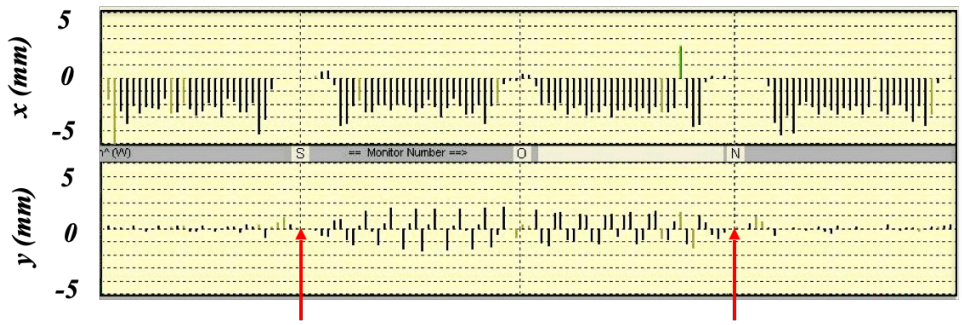

Fig. I.3.53: Orbit difference in the hor. and vert. plane between the ideal beam and a beam with shifted momentum.

Calculate the shift in momentum that has been applied during the measurement.

Was the beam momentum shifted to lower or higher values?

In Fig. I.3.51 we realise in addition to the expected orbit change in the horizontal plane a small change in the vertical orbit. Can you explain where this might come from?

10 The momentum compaction factor

In a formula one race, those running at higher speed are driven by the centrifugal force to an outer orbit. Now, assume that they would actually run at the speed of light, which seems to be constant. Then, due to the longer orbit on their circle, they would arrive at the gas-station (if there were one) a bit later. In synchrotrons this effect is called—quite unfortunately—*momentum compaction factor,* α_p. To make a

clear statement here: we do not compact any momentum. And the famous factor α_p should indeed be called *dispersion-driven-orbit-lengthening-factor*. ... ok, ok, doesn't really sound better. So let's talk mathematics instead.

We know already that a particle with momentum deviation will run on a dispersive orbit, i.e. its overall oscillation amplitude is defined via the betatron oscillations (the solution of the homogeneous equation of motion) plus an additional term defined by the dispersion:

$$x(s) = x_\beta(s) + D(s) \cdot \frac{\Delta p}{p_0} \quad .$$

We already had a look at the story, that is shown schematically in Fig. I.3.54.

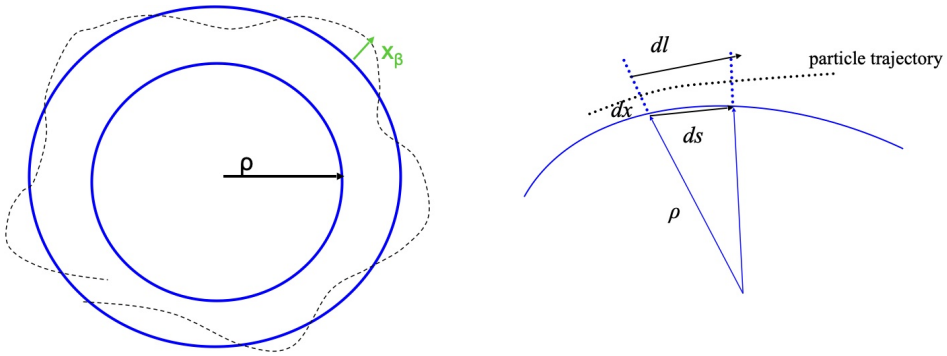

Fig. I.3.54: Periodic dispersion and—zoomed in—a part of the particle trajectory for $\Delta p/p_0 > 0$. Due to the dispersion, the off-momentum-particle will run on a longer trajectory.

It shows on the left side the simple effect that a particle with higher momentum is running on a larger radius. The r.h.s. is a zoomed in picture of a part of the arc. Given the ideal bending radius ρ the ideal particle will pass an infinitesimal distance *ds*. The off-momentum particle will be off-set in radius by the amount dx and thus pass the little larger distance *dl*, with

$$\frac{dl}{ds} = \frac{\rho + dx}{\rho}$$

which we can solve for the additional orbit lengthening *dl*

$$dl = (1 + \frac{dx}{\rho(s)})ds \quad .$$

Integrating around the ring gives us the overall length of the off-momentum particle

$$L_{\Delta p} = \oint dl = \oint (1 + \frac{dx}{\rho(s)})ds$$

and we obtain for the difference between off- and on-momentum orbit

$$\delta L = L_{\Delta p} - L_0 = \frac{\Delta p}{p_0} \oint \frac{D(s)}{\rho(s)} ds \quad ,$$

where we have introduced explicitly the dependency on the local position s: both, dispersion and bending

radius of the magnets will depend on the location in the ring. All in all we conclude that the lengthening of the orbit for off-momentum particles is given by the dispersion function and the bending radius.
The momentum compaction factor is defined now as the ratio between relative momentum deviation and relative orbit difference (or "orbit lengthening")

$$\frac{\delta L}{L_0} = \alpha_p \cdot \frac{\Delta p}{p_0}$$

with L_0 and p_0 being the ideal orbit length and ideal momentum.
For first estimates let's assume that all dipoles have the same bending radius, $\rho = \text{const}$. Replacing as a second approximation the integral by the sum over the length of the dipole magnets (in all places that are not bending magnets we have $1/\rho = 0$ anyway)

$$\int D(s)ds \approx \Sigma(l_{\text{dipoles}}) \cdot < D >_{\text{dipole}}$$

$$\rightarrow \alpha_p \approx \frac{1}{L_0} \cdot l_{\text{dipoles}} \cdot < D > \cdot \frac{1}{\rho}$$

and with $\Sigma(l_{\text{dipoles}}) = 2\pi\rho$ we get

$$\alpha_p \approx \frac{2\pi}{L_0} < D >= \frac{< D >}{R}$$

where *R* is the geometric radius of the machine, $L_0 = 2\pi R$. As last approximation let's assume finally that all particles are running at the speed of light, $v \approx c$, so with the same velocity ... which is nearly true in high energy beams. In this case we can write

$$\frac{\delta t}{T_0} = \frac{\delta l}{L_0} = \alpha_p \cdot \frac{\Delta p}{p_0} \quad .$$

Thus the momentum compaction factor determines the relative orbit length for a off-momentum particle and so it does for the relative time difference. And therefore it defines the arrival time of an off-momentum particle at e.g. the location of the RF cavities, that will accelerate the beam. And as a direct consequence it is the dispersion that—via α_p—determines the longitudinal dynamics of the beam. It is one of the few moments where longitudinal and transverse beam dynamics come together.

11 The not-at-all ideal world

Or in other words, welcome to reality.
Following a strong request from the editors, I have to clarify the title of this section a bit more. So, let's call it *"errors in field and gradient"*.
Indeed, during the operation of a real particle collider, in the middle of data taking of the experiments, the beam parameters started to flip around and beam orbit, tunes and for the experiments most important the background rates in the detector modules were anything but tolerable. After careful investigation on beam and then in the tunnel we found a magnet that due to overheating of the coils developed a short cut, clearly visible in Fig. I.3.55. In this section we will study the impact of such a lovely event on the beam

dynamics.

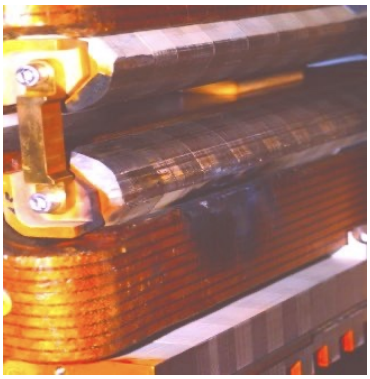

Fig. I.3.55: Dramatic event in the life of a storage ring: due to failure of cooling water several coil-windings caught fire and developed a short-cut of the magnet current. For both, the fire-brigade and the beam dynamics colleagues such an event is thrilling.

The problem is that we have to face the issue that nothing is perfect and even if we are not always encountering problems as serious as the one in Fig. I.3.55, small field errors add up and we cannot ignore them. As in the case of the dipole magnets it is first of all the momentum spread of the beam that is of concern here. Dispersion was the name of the effect for the bending magnets and you will not be surprised to hear that in the case of the quadrupole lenses we encounter a very similar problem. But let's start from scratch.

Amplitude x and angle x' of a particle trajectory are transformed through the individual lattice elements via the matrix transformation

$$\begin{pmatrix} x \\ x' \end{pmatrix}_{s1} = M_{\text{quadrupole}} \cdot \begin{pmatrix} x \\ x' \end{pmatrix}_{s0}$$

with $M_{\text{quadrupole}}$ describing the focusing or defocusing effect of the magnet,

$$M_{\text{foc}} = \begin{pmatrix} \cos(\sqrt{|K|} \cdot l_q) & \frac{1}{\sqrt{|K|}} \sin(\sqrt{|K|} \cdot l_q) \\ -\sqrt{|K|} \cdot \sin(\sqrt{|K|} \cdot l_q) & \cos(\sqrt{|K|} \cdot l_q) \end{pmatrix} \quad .$$

We refer once more to the horizontal plane and have chosen a focusing magnet, as example. On the other side, we can express the matrix for one complete turn in Twiss form, as we have shown above (see Eq. I.3.35).

$$M(s) = \begin{pmatrix} \cos(\psi_{\text{turn}}) + \alpha_s \sin(\psi_{\text{turn}}) & \beta \sin(\psi_{\text{turn}}) \\ -\gamma \sin(\psi_{\text{turn}}) & \cos(\psi_{\text{turn}}) - \alpha_s \sin(\psi_{\text{turn}}) \end{pmatrix} \quad ,$$

where ψ_{turn} describes the phase advance integrated through the complete machine, which is clearly, normalised to 2π, the tune, $Q = \psi_{\text{turn}}/2\pi$. In case of a gradient error, this ideal one-turn-matrix is disturbed. Let's assume we have only a small error, so that we can introduce it as thin-lens matrix (if the error is large the beam is gone anyway). So we write for the distorted matrix including the gradient error (see Fig. I.3.56)

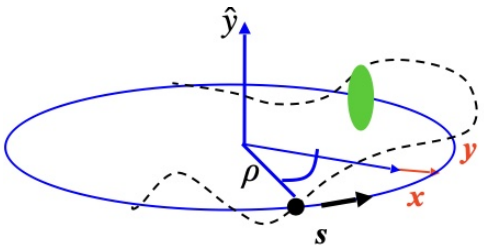

Fig. I.3.56: Description of a quadrupole error introduced as thin lens quadrupole magnet.

$$M_{\text{dist}} = M_{\Delta k} \cdot M_{\text{ideal}} = \begin{pmatrix} 1 & 0 \\ -\Delta k ds & 1 \end{pmatrix} \cdot \begin{pmatrix} \cos(\psi_{\text{turn}}) + \alpha \sin(\psi_{\text{turn}}) & \beta \sin(\psi_{\text{turn}}) \\ -\gamma \sin(\psi_{\text{turn}}) & \cos(\psi_{\text{turn}}) - \alpha \sin(\psi_{\text{turn}}) \end{pmatrix} \quad .$$

Here we explicitly introduced the subscript *dist* for the distorted matrix that includes the error, and following the sign convention introduced above, a negative sign for the k-value corresponds to a focusing quadrupole, which means that in this example we indeed introduce a focusing quadrupole error. Multiplying out we get for the new, distorted one turn matrix

$$M_{\text{dist}} = \begin{pmatrix} \cos\psi_0 + \alpha \cdot \sin\psi_0 & \beta \cdot \sin\psi_0 \\ -\Delta k ds \cdot (\cos\psi_0 + \alpha \sin\psi_0) - \gamma \cdot \sin\psi_0 & -\Delta k ds \cdot \beta \sin\psi_0 + \cos\psi_0 - \alpha \sin\psi_0 \end{pmatrix} \quad .$$

The rule for getting the tune out of the one turn matrix is via its trace, which is in this case

$$\text{Trace}(M_{\text{dist}}) = 2\cos\psi = 2\cos\psi_0 - \Delta k \beta ds \cdot \sin\psi_0 \quad .$$

As usual the index "0" refers to the ideal situation and so the new phase advance for the complete ring is

$$\psi = \psi_0 + \Delta\psi$$

with $\Delta\psi$ the phase change caused by the gradient error. Inserting we get

$$\cos\psi = \cos(\psi_0 + \Delta\psi) = \cos\psi_0 - \frac{\Delta k ds \beta \sin\psi_0}{2} \quad .$$

Now remembering the old fashioned trigonometric stuff and assuming that the error is small we can re-write the l.h.s.

$$\cos\psi_0 \cdot \underbrace{\cos(\Delta\psi)}_{\approx 1} - \sin(\psi_0) \cdot \underbrace{\sin(\Delta\psi)}_{\approx \Delta\psi} = \cos\psi_0 - \frac{\Delta k ds \beta \sin\psi_0}{2} \tag{I.3.67}$$

and so a small error in gradient Δk leads to a change of the phase advance per turn of

$$\Delta\psi = \frac{\Delta k ds \beta}{2}$$

or for the tune, $Q = \psi/2\pi$ we get a tune change of

$$\Delta Q = \int_{s0}^{s0+l_q} \frac{\Delta k(s)\beta(s)ds}{4\pi} \quad .$$

This fact is worth summarising a few statements:

- a gradient error will always lead to a tune shift,
- the tune shift is proportional to the size of the error which is defined by the product of gradient-error and length of the quadrupole, $\Delta k \cdot l_q$,
- the tune shift is also proportional to the β-function at the place where the error occurs.

In this sense the β-function is not only indicating the beam size, via $\sigma = \sqrt{\varepsilon\beta(s)}$ but also the *"sensitivity"* of the beam with respect to external errors. Field errors in quadrupole at places where the β-function is high are much more serious and lead to much stronger distortions than at places of low β.
We can use this fact to measure on beam the value of the β-function in different locations of the ring. In case we have individually powered quadrupoles, we can deliberately change their gradient (one by one), measure the corresponding tune drift and thus determine the β-function (in both planes) at the location of the quadrupole lens.

11.1 Gradient errors and beta-beat

A gradient error will always create a distortion in the focusing properties of our ring. And thus—as explained before—it will naturally lead to a tune shift. However there is more to come. We cannot allow for a gradient error and expect that our beam dimensions remain the same. More precisely, as tune and β-function are related,

$$Q = \frac{1}{2\pi} \oint \frac{ds}{\beta(s)}$$

we cannot have a tune change without any influence on β. So, for a given single gradient error, Δk somewhere in the ring, we get

$$\frac{\Delta\beta(s_0)}{\beta(s_0)} = -\frac{1}{2\sin 2\pi Q} \cdot \int_{s1}^{s1+lq} \beta(\tilde{s})\Delta k(\tilde{s}) \cdot \cos\{2(\psi_{\mathrm{s1}} - \psi_{\mathrm{s}}) - 2\pi Q)\} ds \quad .$$

The derivation of this equation is a bit tedious, see Chapter I.8 for more details. What we can conclude, however, is that like in the case of the tune shift, the effect on the beam, i.e. the size of the β-beat, depends on the β-function at the position of the gradient error, s_1. The β-beat oscillates around the ring with twice the phase advance of our system, thus it will be visible at any position s. And finally, there is a resonance denominator, $\sin(2\pi Q)$ that eventually amplifies the problem in case we are running the machine close to a integer or half-integer tune. We know already that resonances have to be avoided and this is the mathematical expression for it. For more details about this topic see Chapter I.9 on nonlinear effects.

11.2 Chromaticity

While dispersion is a problem that describes the non-ideal bending effect of dipoles in the case of a momentum error (or spread) among the particles, the careful reader will not be surprised to learn that a similar effect exists for the quadrupole focusing. We call this *chromaticity*. The chromaticity Q' describes an optical error of a quadrupole lens in an accelerator: for a given magnetic field, i.e., gradient of the quadrupole magnet, particles with a smaller momentum will feel a stronger focusing force, and particles with a larger momentum will feel a weaker force. The situation is shown schematically in Fig. I.3.57. As a consequence, the tune of an individual particle will change, and the chromaticity Q' relates the resulting tune shift to the relative momentum error of the particle. By definition, we write, in

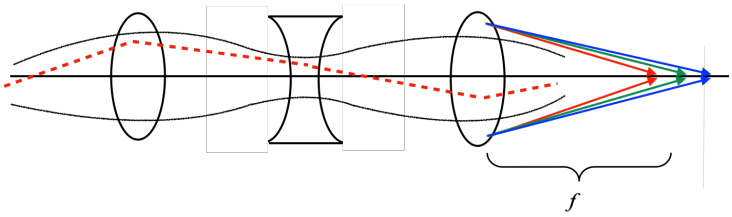

Fig. I.3.57: Schematic visualisation of the chromatic effect: focusing and defocusing quadrupole of a FoDo cell are shown with the beam envelope (black) and a particle trajectory (red). Due to the momentum spread in the beam the focal length of the structure is larger for higher momentum particles (blue arrow) than for lower momentum particles (red arrow).

linear approximation,

$$\Delta Q = Q' \cdot \frac{\Delta p}{p_0} \quad ,$$

where we assume a purely linear relation between momentum error and tune. For small errors (a few $\Delta p/p_0 \approx 10^{-4} \ldots 10^{-3}$) this is indeed usually a good approximation; as soon as larger momentum deviations have to be considered, e.g. in electron beams that are highly dominated by the emission of synchrotron light, non-linear terms will have to be taken into account. In any case, Q' is a consequence of the focusing properties of the quadrupole magnets and is thus given by the characteristics of the lattice. For small momentum errors $\Delta p/p_0$, the focusing parameter k which is normalised to the momentum of the beam can be approximated as

$$k(p) = \frac{g}{p/e} = \frac{ge}{p_0 + \Delta p} \quad ,$$

where g denotes the gradient of the quadrupole lens, p_0 denotes the design momentum, and the term Δp refers to the momentum error. If Δp is small, as we have assumed, we can write in a first-order approximation

$$k(p) \approx \frac{ge}{p_0}\left(1 - \frac{\Delta p}{p_0}\right) \quad . \tag{I.3.68}$$

This describes a quadrupole error

$$\Delta k = -k_0 \cdot \frac{\Delta p}{p_0} \quad . \tag{I.3.69}$$

The negative sign indicates that a positive momentum deviation leads to a weaker focusing strength and,

accordingly, to a negative tune shift. In the end it's just like in music where a weaker "tuning" of the guitar string leads to a lower frequency of the sound

$$\Delta Q = \frac{1}{4\pi} \int \Delta k \, \beta(s) \, \mathrm{d}s, \tag{I.3.70}$$

$$\Delta Q = -\frac{1}{4\pi} \frac{\Delta p}{p_0} \int k_0 \beta(s) \, \mathrm{d}s. \tag{I.3.71}$$

Thus this so-called "natural" chromaticity Q' of a lattice is given by

$$Q' = -\frac{1}{4\pi} \int k_0(s) \beta(s) \, \mathrm{d}s, \tag{I.3.72}$$

and it tells us by how much higher momentum particles are shifted in their tune to smaller values.
The question that arises now is: *what's wrong about chromaticity?*
Well ... unfortunately, while the dispersion created in the dipole magnets requires nothing more than some additional aperture in the vacuum chamber, the chromaticity of the quadrupoles has an influence on the tune of the particles and so can lead to dangerous resonance conditions. Particles with a particular momentum error will be pushed into resonances and be lost within a very short time. A look at the tune spectrum visualizes the problem. Whereas an ideal situation leads to a well-compensated chromaticity and the particles oscillate with basically the same frequency (Fig. I.3.58), a non-corrected chromaticity (Q' = 20 units in the case of Fig. I.3.59) broadens the tune spectrum and a number of particles are pushed towards dangerous resonance lines.

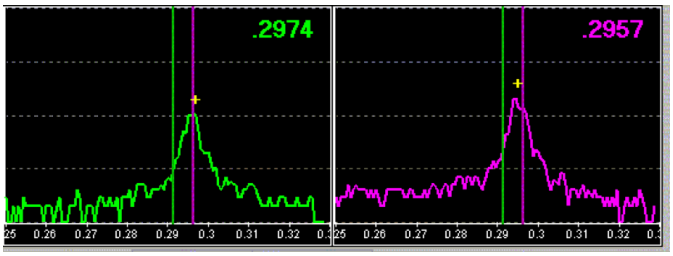

Fig. I.3.58: Tune spectrum of a proton beam with a well-corrected chromaticity $Q' \approx 1$.

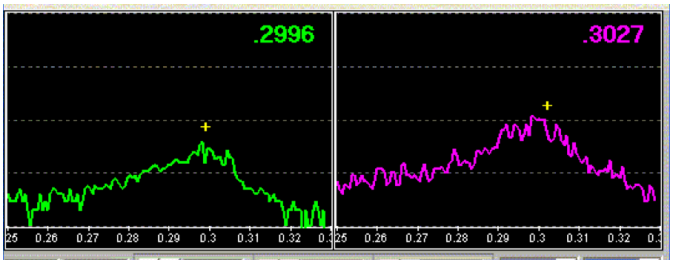

Fig. I.3.59: Tune spectrum of a proton beam with a poorly matched chromaticity $Q' \approx 20$.

It is a challenge for the operation team of a large collider to find an optimum working point, i.e. to adjust the tune in both transverse planes in a way to avoid dangerous resonance lines. Having a

well compensated chromaticity and thus only a small spread in the particles' tunes, there is a certain chance to do the job and the beam lifetime is ok. For a large spread in tunes, due to non-compensated chromaticity, it is basically impossible and a large part of the particles will be lost as their tune will be on resonance lines. Figure I.3.60 visualises the problem. The yellow cross shows the actual measured tune in x and y, located within a pattern of forbidden resonance lines, that are calculated and displayed up to seventh order ... not the easiest job for the operator to find an adequate working point.
In the case of the LHC (luminosity optics) the so-called *natural* chromaticity, which is just another word for the uncompensated situation, is $Q' = -250$. Given the momentum spread of the proton beam of $\Delta p/p_0 \approx 2 \cdot 10^{-4}$ we obtain a tune spread of the beam of

$$\Delta Q = 0.256 \ldots 0.361,$$

which crosses several resonance lines in Fig. I.3.60. In large storage rings and synchrotrons in particular,

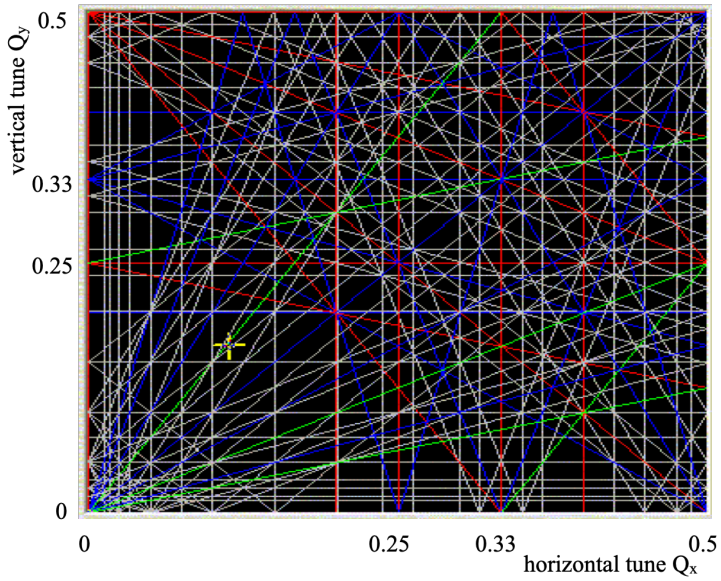

Fig. I.3.60: The working diagram of a storage ring: it shows—marked as yellow cross in the graph—the transverse tunes of the beam in a $Q_x - Q_y$ diagram. In addition to the actual measured tunes, lines show resonances of different order that must be avoided to guarantee sufficient beam lifetime. Careful adjustment of the quadrupole gradients is needed to optimise the working point (Q_x, Q_y) *on beam* and find sufficient space between the forbidden resonance lines.

this problem is crucial and represents one of the major factors that limit machine performance: because of the strong focusing of the quadrupoles and the large size, the chromaticity can reach considerable values.
A chromaticity correction scheme is therefore indispensable. What we would need is a series of individual little quadrupole magnets that provide additional focusing for each individual particle, depending on its individual momentum deviation. Schematically shown in Fig. I.3.61.

Wow, with a particle bunch of $N_p = 2 \cdot 10^{11}$ protons, this means we would need more than 10^{11} little quadrupoles, ... a hopeless task.

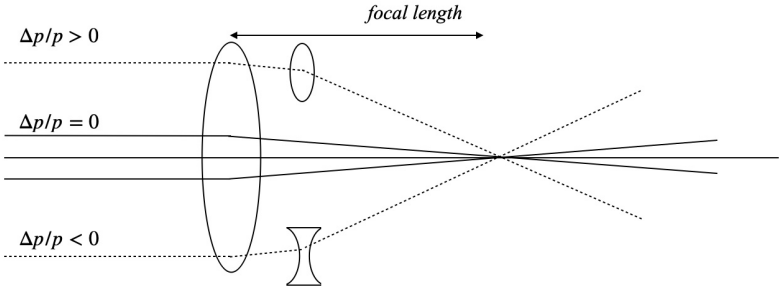

Fig. I.3.61: The idea of chromaticity correction: we have to add additional focusing fields to those particles with higher momentum—running due to dispersion at the outer lane; and we must reduce the focusing fields for those with lower momentum at the inner lane. Schematically this is indicated by little focusing and defocusing quadrupoles. Technically sextupole magnets are installed to provide the extra focusing fields; details see text.

But here is another way to go: the trick is performed in three steps, and the first step is already implicitly shown in the figure above.

- We sort the particles in the horizontal plane according to their momentum. This is provided whenever we have a non-vanishing dispersion, for example close to the focusing quadrupoles in the arc, where both the dispersion and the β-function reach high values and the particle trajectories are determined by the well-known relation $x_{\mathrm{D}}(s) = D(s) \cdot \Delta p/p_0$.
- At these places, we create magnetic fields that have a position-dependent focusing strength, in other words, fields that represent a position-dependent gradient. Sextupole magnets have exactly this property: if $\tilde{g}$ describes the strength of the sextupole field, we get

$$B_x = \tilde{g} \cdot xy \tag{I.3.73}$$

for the horizontal field component and

$$B_y = \tilde{g} \cdot \frac{1}{2}(x^2 - y^2) \tag{I.3.74}$$

for the vertical component. The resulting gradient in both planes is obtained as

$$\frac{\partial B_x}{\partial y} = \frac{\partial B_y}{\partial x} = \tilde{g} \cdot x \qquad . \tag{I.3.75}$$

- We now only have to adjust the strengths of two sextupole families (one to compensate the horizontal and another to compensate the vertical chromaticity) to get an overall correction in both planes.

In Fig. I.3.62 we visualise schematically the way the trick goes. It shows the cross section of a quadrupole magnet and its corresponding sextupole and the field direction in the horizontal plane. On the left side, where the low-momentum particles are located, the sextupole field points opposite to the quadrupole field lines, so weakens its focusing effect. On the right side of the magnet both field lines add up leading to a position dependent linear increasing quadrupole contribution of the sextupole which we

adjust exactly to the need of the higher momentum parties.

Figure I.3.63 shows a photo of such a sextupole magnet with the six (hic) pole shoes clearly visible.

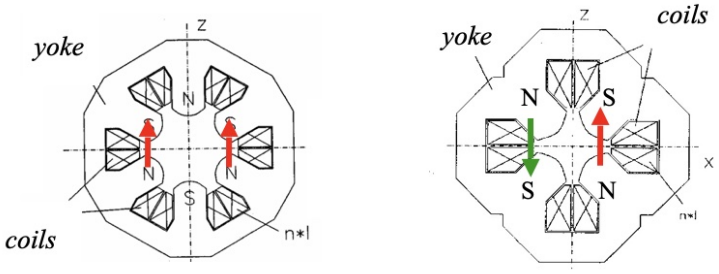

Fig. I.3.62: Schematic design of a quadrupole magnet and its corresponding sextupole. On the right hand side of the magnet aperture, where due to dispersion the higher momentum particles are passing, the fields of quadrupole and sextupole add and increase the focusing effect. On the left hand side it's just the other way round.

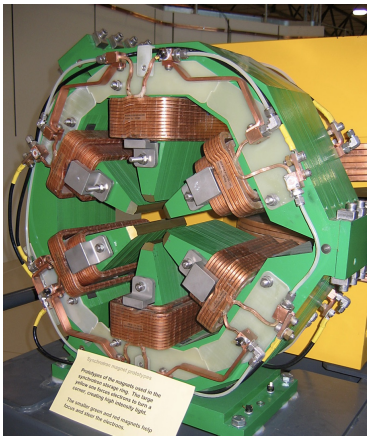

Fig. I.3.63: Sextupole magnet in a typical storage ring (Courtesy: Australian synchrotron).

In a little more detail, and referring again to normalized gradients, we can write

$$k_{\text{sext}} = \frac{e}{p}\,\tilde{g}\cdot x, \tag{I.3.76}$$

which leads for a given particle amplitude

$$x_{\text{D}} = D\cdot\frac{\Delta p}{p} \tag{I.3.77}$$

to the normalized focusing strength (of the sextupole magnet)

$$k_{\text{sext}} = \frac{e}{p}\,\tilde{g}\cdot D\frac{\Delta p}{p}. \tag{I.3.78}$$

The combined effect of the so-called natural chromaticity created by the quadrupole lenses (see Eq. (I.3.72)) and the compensation by the sextupoles leads to an overall chromaticity budget,

$$Q' = -\frac{1}{4\pi} \oint [(k(s) - \frac{e}{p}\, \tilde{g}(s) \cdot D(s))]\beta(s)\, \mathrm{d}s \tag{I.3.79}$$

and needs to be adjusted to zero in both transverse planes.

To summarize and make things as crystal clear as possible, the focusing properties of the magnet lattice lead to restoring forces in both transverse planes. The transverse motion of a particle is therefore a quasi-harmonic oscillation as the particle moves through the synchrotron, and the tune describes the frequency of these oscillations. As we cannot assume that all particles have exactly the same momentum, we have to take into account the effect of the momentum spread in the beam: the restoring forces are a function of the momentum of each individual particle and so the tune of each particle is different. We have to correct for this effect, and we do so by applying sextupole fields in regions where a non-vanishing dispersion distributes the off-momentum particles in the horizontal plane.
As easy as that!
Well ... not quite. In the very same manner as a focusing quadrupole does something good in one plane but something not-so-good in the other, we will need two sextupoles to do a proper job, namely to compensate the chromaticity in the two planes. And each of them will make things better in one plane and worse in the other. So we get two equations, with the two sextupole strengths as free parameters and so we can solve the problem, i.e. optimise Q' in both planes.

$$\begin{aligned} Q'_x = & -\tfrac{1}{4\pi} \oint \beta_x(s)\, [+k_q(s) & - m^F \cdot l_{\mathrm{sext}}\, D_x(s) + m^D \cdot l_{\mathrm{sext}} D_x(s)]\, ds \\ Q'_y = & \underbrace{-\frac{1}{4\pi} \oint \beta_y(s)\, [-k_q(s)}_{\textit{natural chromaticity}} & \underbrace{+\, m^F \cdot l_{\mathrm{sext}}\, D_x(s) - m^D \cdot l_{\mathrm{sext}} D_x(s)]}_{\textit{sextupole correction}}\, ds \end{aligned} \quad . \tag{I.3.80}$$

We realise that—by the nature of the problem—the terms for the hor. and vert. sextupoles differ in sign.

11.3 Gradient errors and beta-beat

It is quite clear that a quadrupole error will not only influence the oscillation frequency, aka "tune" but also the β function. Just like *tuning* a race car: a stronger restoring force will lead to higher frequencies and smaller amplitudes.
As before, we introduce a small focusing error in our storage ring, as schematically shown in Fig. I.3.64. From a certain starting point in the ring, s_0, we define a transfer matrix A up to the error, and from there on another matrix B that completes the turn.

The ideal ring is then described by

$$M_{\mathrm{turn}} = B \cdot A$$

and including the error that we describe in thin lens approximation we write

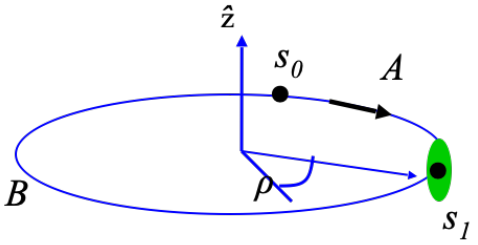

Fig. I.3.64: Schematics to introduce a small quadrupole error in the mathematical description of a lattice structure. The one turn matrix is split into two matrices, *A* and *B* with the quadrupole lens describing the error in between.

$$M^* = B \cdot \begin{pmatrix} 1 & 0 \\ -\Delta k ds & 1 \end{pmatrix} \cdot A$$

where the "*" refers to the distorted matrix, including the error. As before we refer here to a focusing lens, thus the negative sign of Δk. For the matrices A and B we write without going into any details for the time being

$$A = \begin{pmatrix} a_{11} & a_{12} \\ a_{21} & a_{22} \end{pmatrix}$$

and

$$B = \begin{pmatrix} b_{11} & b_{12} \\ b_{21} & b_{22} \end{pmatrix} \quad .$$

Multiplying out we get first

$$M^* = B \cdot \begin{pmatrix} a_{11} & a_{12} \\ -\Delta k ds \cdot a_{11} + a_{12} & -\Delta k ds \cdot a_{21} + a_{22} \end{pmatrix}$$

and then

$$M^* = B \cdot \begin{pmatrix} \square & b_{11}a_{12} + b_{12}(-\Delta k ds a_{12} + a_{22}) \\ \square & \square \end{pmatrix} \quad . \tag{I.3.81}$$

In order to save some ink and as we do not need them in the following we replaced three out of four elements by $\square$. The remaining matrix element however, m_{12} will give us the beta function which is in Twiss form for the undisturbed case, as we have seen above, $m_{12} = \beta_0 \cdot \sin(2\pi Q)$. Including the error we obtain from I.3.81

$$m_{12}^* = b_{11}a_{12} + b_{12}a_{22} - b_{12}a_{12}\Delta k ds$$

where the first term refers to the ideal case, and so we can write

$$m_{12}^* = \beta_0 \cdot \sin(2\pi Q) - b_{12}a_{12}\Delta k ds \quad .$$

Now, as M^* is still a matrix for one complete turn we still can express the element m_{12}^* in Twiss form:

$$m_{12}^* = (\beta_0 + \Delta\beta) \cdot \sin[2\pi(Q + dQ)] \qquad .$$

Equalising the last two equations and assuming a small error we get

$$\beta_0 \sin(2\pi Q) - a_{12} b_{12} \Delta k ds = (\beta_0 + \Delta\beta) \cdot \sin 2\pi (Q + dQ)$$

$$\beta_0 \sin(2\pi Q) - a_{12} b_{12} \Delta k ds = (\beta_0 + \Delta\beta) \cdot \{\sin 2\pi Q \underbrace{cos 2\pi dQ)}_{\approx 1} + \cos 2\pi Q \underbrace{\sin 2\pi dQ)}_{\approx 2\pi dQ}\} \tag{I.3.82}$$

where we have assumed a small error and thus a small tune change dQ.
Now we multiply out,

$$\beta_0 \sin(2\pi Q) - a_{12} b_{12} \Delta k ds = \beta_0 \sin 2\pi Q + \beta_0 2\pi dQ \cdot \cos(2\pi Q) + d\beta \sin(2\pi Q) + d\beta 2\pi dQ \cdot \cos(2\pi dQ)$$

ignore the second order term

$$d\beta \; 2\pi \; dQ \; cos(2\pi dQ) \approx 0$$

so we get

$$-a_{12} b_{12} \Delta k ds = \beta_0 2\pi dQ cos(2\pi Q) + d\beta_0 sin(2\pi Q)$$

and remember that the tune shift is created by a quadrupole error, $dQ = \frac{\Delta k \beta_1 ds}{4\pi}$

$$-a_{12} b_{12} \Delta k ds = \frac{\beta_0 \Delta k \beta_1 ds}{2} \cos(2\pi Q) + d\beta_0 \sin(2\pi Q) \qquad .$$

This expression we can finally solve for $d\beta$

$$d\beta = \frac{-1}{2\sin(2\pi Q)} \{2 a_{12} b_{12} + \beta_0 \beta_1 \cos(2\pi Q)\} \Delta k ds \qquad .$$

The last equation gives us the change of the beta-function under the influence of a quadrupole error in a storage ring with tune Q.
As last step we refer back to the transport matrix in Twiss form,

$$M = \begin{pmatrix} \sqrt{\frac{\beta_s}{\beta_0}} (\cos(\psi_s + \alpha_0 \sin\psi_s) & \sqrt{\beta_s \beta_0} \sin\psi_s \\ \frac{(\alpha_0 - \alpha_s)\cos\psi_s - (1 + \alpha_0 \alpha_s)\sin\psi_s}{\sqrt{\beta_s \beta_0}} & \sqrt{\frac{\beta_0}{\beta_s}} (\cos\psi_s - \alpha_s \sin\psi_s) \end{pmatrix}$$

and following Fig. I.3.64 we know that in our example the matrix A brings us from the starting point s_0 to the location of the error, with the phase advance $\Delta\psi = \psi_1 - \psi_0$; while matrix B covers the remaining part, namely from the error location around the ring back to s_0 and so $\Delta\psi = 2\pi Q - \psi_1 - \psi_0$. Inserting this and writing for the phase advance ψ_{01} for $\psi_1 - \psi_0$ we get

$$d\beta = \frac{\beta_0}{2\sin(2\pi Q)} 2\sin(\Delta\psi_{01} \sin(2\pi Q - \Delta\psi_{01}) + \cos(2\pi Q) \Delta k ds \qquad .$$

After some last TLC transformations (i.e. using the usual trigonometrical tricks) we obtain the final result:

$$\frac{\Delta\beta}{\beta_0} = \frac{1}{2\sin(2\pi Q)} \int_{s1}^{s1+l_q} \beta(s1)\Delta k \cos\{2(\psi_{s1} - \psi_{s0}) - 2\pi Q\} ds \quad .$$

And that's it.

Nota bene: (which can be translated as *watch out*)

- the so-called beta-beat, $\Delta\beta/\beta$ which is just the relative error of the β-function, is proportional to the strength of the error Δk, which is not a surprise,
- and it is proportional to the β-function at the place of the error,
- and there is a resonance denominator, $\sin(2\pi Q)$ which tells us that we should not run on half-integer values of the tune.

The last statement of this list is of extreme importance. It tells us about conditions in the ring, where due to resonance effects the whole beam will be lost, as any (!) small focusing error in the storage ring will lead to an infinite increase of the beam size and an immediate loss of the complete beam. We will encounter similar conditions for a manifold of multipoles, driving such resonance situations.

12 Colliding beams and luminosity

We finally come to the marginal problem of bringing the beams together. In other words we have to prepare the storage ring lattice to collide the two counter rotating particle beams and hope for sufficient actual single particle collisions so that we obtain a decent event rate, sufficiently high for e.g. a Nobel prize.

As the number of Nobel prizes is small, we conclude that the cross section of interesting events in physics is not huge, and so we have to do something to increase the probability of protons to collide. We refer once more to the beam optics, shown above in Fig. I.3.31 that we repeat here for convenience (see Fig. I.3.65). It shows a typical lattice of a collider ring which consists of a number of arc sections (four in this case) where a regular quadrupole structure provides a periodic focusing of the beam. We learned already that for high energy colliders the FoDo is most appropriate as it allows for highest dipole fill factor, which means nothing else than largest integrated dipole fields around the ring and thus highest energy of the stored beam.

All in all the lattice design will always consist of such a regular arc structure, where we observe a periodic beam optics, where the dipole magnets are located that define—via the beam rigidity—the momentum of the particle beam and where we control the tune, chromaticity and other general parameters of the machine. The four arcs are connected by straight sections where the β-function shows strange excursions to reach—in the middle of the so-called *insertion*—very small values. In the straights we find usually dispersion free regions, with long drift spaces for the RF structures, injection and extraction of the beams and the high energy particle detectors, if we cannot avoid them. Before we go into the details of such a design, we would like to emphasize two basic principles in accelerator design:

- fixed target machines, where the accelerated particle beam hits a solid, liquid or even gas target

tender-loving-careful transformations

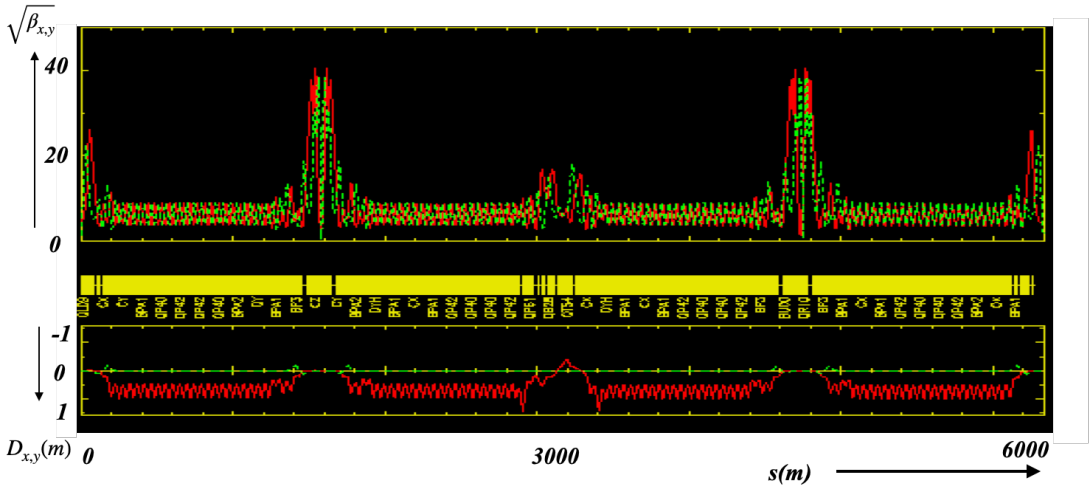

Fig. I.3.65: Luminosity optics of a particle collider: upper part shows the β-function in both planes, the lower part the dispersion. The regular pattern of the optics functions in the arcs is combined with straight sections where the beam dimension (i.e. the β-function) is reduced as much as possible to increase the luminosity. As direct consequence we observe very high values of β in the mini-beta quadrupoles before and after the collision point.

– two beam colliders where we bring two counter rotating beams into collision.

Examples of event pictures in both cases are shown in Fig. I.3.66 and I.3.67.

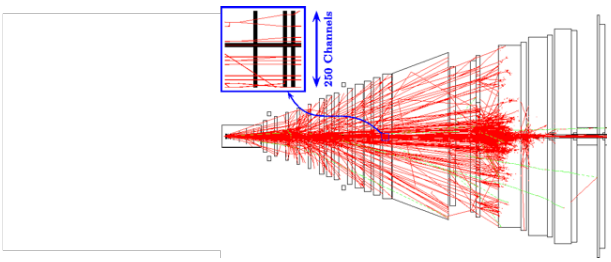

Fig. I.3.66: Fixed target event observed in the HERA-B experiment. The high density of the solid state target (tungsten in that case) leads to a large number of "events" and thus to a manifold of tracks that can be analysed by the particle detector.

The difference is striking: in a fixed target experiment the accelerated beam will hit a target that has such a high density of matter that in most cases the complete beam is stopped inside the target and a large number of events (visible as tracks in the figure) is created. In other words, if you had not enough coffee in the morning and crash with you car into your dust bin in front of the house you will always be happy to get a hit. On the other side, the available energy in such a case is limited. For basic reasons of kinematics, in the centre of mass system, the energy for physics is a function of the square root of the beam energy, see e.g. Ref. [12],

$$E_{\mathrm{cm}} \propto \sqrt{E_{\mathrm{beam}}} \quad .$$

Much more efficient therefore—as soon as we talk about high-energy physics—is the direct colli-

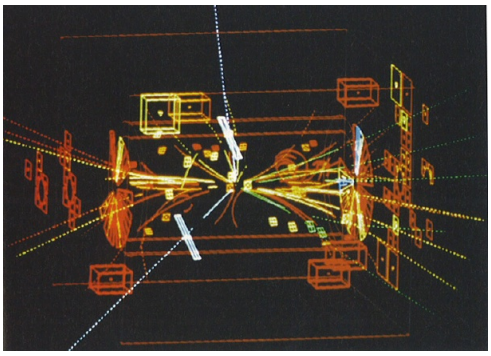

Fig. I.3.67: A typical event (Z_0 production and decay into lepton/anti-lepton pairs) observed in a particle collider. Due to the limited number of particles in the colliding bunches, the event rate is much smaller than in the fixed target case.

sion of two counter rotating beams schematically shown in Fig. I.3.68. Here, at least in the case of equal

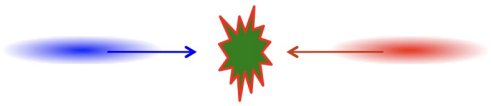

Fig. I.3.68: Schematic view of two colliding beams: particle colliders are the tool to obtain highest energy in the centre of mass system, E_{cm}.

particle beams and energies, we just add up the beam energies,

$$E_{\mathrm{cm}} = E_{\mathrm{beam1}} + E_{\mathrm{beam2}} \quad .$$

In the ideal situation (which is the most common one), the two counter rotating beams have equal energies and so the available energy in the centre of mass system is just twice the beam energy

$$E_{\mathrm{cm}} = 2 \cdot E_{\mathrm{beam}} \quad .$$

However, as you might have expected, the story in such a case is quite a bit more challenging, which brings us to the topic of "lattice insertions".

12.1 Lattice insertions

We start with a trivial case, namely the drift, and ask the question "*What will happen to the beam parameters α, β, γ, if we stop focusing for a while?*" We know that the transfer rule for the optics parameters is given by Eq. I.3.53

$$\begin{pmatrix} \beta \\ \alpha \\ \gamma \end{pmatrix}_s = \begin{pmatrix} C^2 & -2SC & S^2 \\ -CC' & SC' + S'C & -SS' \\ C'^2 & -2S'C' & S'^2 \end{pmatrix} \cdot \begin{pmatrix} \beta \\ \alpha \\ \gamma \end{pmatrix}_0$$

where once more we use the abbreviations C and S for the single matrix elements, describing the focusing properties of the lattice (see Eq. I.3.16). In the case of a drift, the situation is quite simple and with

$$M_{\text{drift}} = \begin{pmatrix} C & S \\ C' & S' \end{pmatrix} = \begin{pmatrix} 1 & s \\ 0 & 1 \end{pmatrix}$$

where we use the general expression s for the position inside the drift and so at the end of the drift we clearly would set $s = l_{\text{drift}}$. Thus the optics parameters develop from their in initial values at $s = 0$ in front of the drift as

$$\begin{aligned} \beta(s) &= \beta_0 - 2\alpha_0 \cdot s + \gamma_0 \cdot s^2 \\ \alpha(s) &= \alpha_0 - \gamma_0 \cdot s \\ \gamma(s) &= \gamma_0 \,. \end{aligned}$$

There are already a few nice rules to develop which make life as a storage ring lattice designer easier:

– Location of a waist:

Given arbitrary initial conditions at the beginning of the drift, we can determine the location of an eventual waist inside the drift space, schematically drawn in Fig. I.3.69.

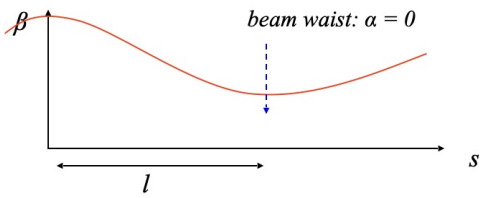

Fig. I.3.69: Starting from a focusing situation, right after a quadrupole, β will reduce and reach somewhere in the drift a minimum that can be determined in position and size.

Expressed more scientifically, given the initial conditions $\alpha_0,\ \beta_0,\ \gamma_0$, we want to determine the point of smallest beam dimension inside the drift: at which location occurs the beam waist? Now, at a beam waist the β-function will reach a minimum and so we require

$$\alpha_{\text{waist}} = 0$$

which means that the waist will occur (if at all) at the well defined position

$$s_{\text{waist}} = \frac{\alpha_0}{\gamma_0}$$

and with $\gamma(s) = \gamma_0,\ \alpha(s) = 0$ the beam size at the location of the waist is

$$\beta(s) = \frac{1}{\gamma_0}$$

. . . all nice and simple.

– Of special importance is the situation in the middle of a symmetric drift, i.e. at the waist point with symmetric drift lengths on both sides, e.g. like in Fig. I.3.70. This is clearly the situation that we (or better our beam) will face at the IP of a collider.

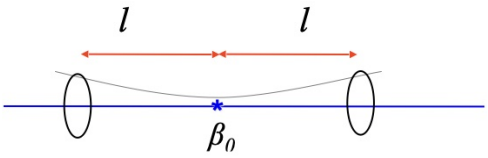

Fig. I.3.70: β-function in a symmetric drift: in the absence of focusing fields, the β-function in a symmetric drift is increasing quadratically with the distance *l* from the symmetry point.

Given the development of the optics functions, described above, we obtain for β, starting at the location of a waist where $\alpha_0 = 0$,

$$\beta(s) = \beta_0 + \frac{s^2}{\beta_0} \quad . \tag{I.3.83}$$

There are three statements to make about that:

– this is a direct consequence of Liouville's theorem and the conservation of the phase space area, which is a very fundamental law of nature ... and so there is no way out.
– this is very bad, as it leads eventually to very high beam sizes at the end of the drift, where usually our first quadrupoles will be located.
– and it means that the effect is larger the smaller the β-function at the waist is.

Now, if we cannot fight against Liouville's theorem ... at least we can optimise and find the β at the center of the drift that leads to the lowest maximum β at the end and so to the smallest aperture need in our magnets. Taking the derivative of Eq. I.3.83 we can determine that β at the waist that will lead to smallest $\beta(l_d)$. So we require

$$\frac{d\beta(l_d)}{\beta_0} = 1 - \frac{l_d^2}{\beta_0^2} = 0$$

and obtain as optimised starting condition:

$$\beta_0 = l_d \quad \rightarrow \quad \beta(l_d) = 2\beta_0 \qquad .$$

So, we get the smallest possible beam size at the location of our first quadrupole after the drift, if we start with a β-function that equals the length of the drift space; and in this optimised case the beta function just doubles inside the drift until we reach the first focusing element. In any case we conclude that we should keep the β-function as small as possible, wherever we are in order to limit the aperture need of the beam and thus the idea is to keep drift-space short.

Well ... unfortunately some devices in our machine need drift spaces that are considerably larger than we might prefer: They are called *Particle Detectors* and they are typically located at a symmetric beam waist. Figure I.3.71 gives an impression of how such a modern detector looks like. The ATLAS

detector installed at CERN's LHC collider is the largest detector built so-far. And the drift space that has to be provided in the straight section has to extend to $23\,\mathrm{m}$ on both sides of the IP.

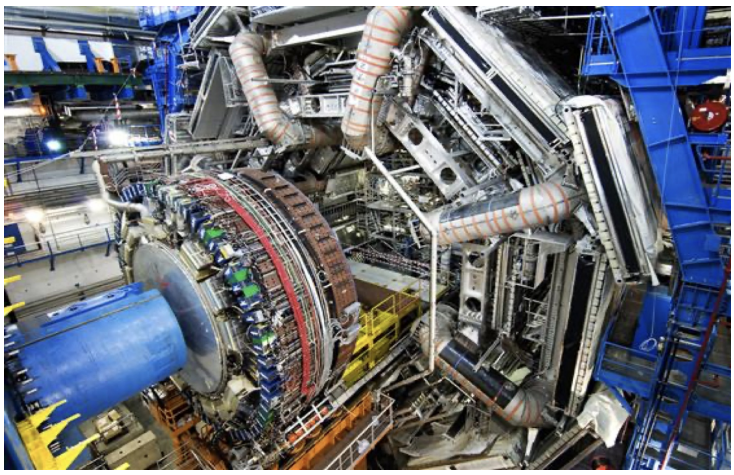

Fig. I.3.71: The particle detector ATLAS, installed at Interaction Point 1 of the LHC collider.

There is a second complication, that comes into the game: the probability to find an interesting (i.e. Nobel prize winning) event is small. For the case of the Higgs event, the situation is shown in Fig. I.3.72. It shows the cross section of the Higgs production in hadronic collisions, which is clearly the typical situation in the LHC collider. Without going too much into the detail of the different production channels, we conclude that all in all the cross section is somehow in the range of a *pico barn*. Now, as

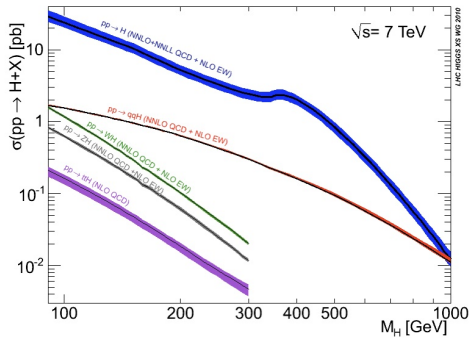

Fig. I.3.72: Hadronic cross section for Higgs production: it's in the range of pico-barn.

this sounds a kind of funny unit, we better translate: A barn in particle physics stands for $10^{-24} cm^2$ and a pico is 10^{-12}. A pico barn in other words is

$$1\,\mathrm{pb} = \frac{1}{\mathrm{mio}} \cdot \frac{1}{\mathrm{mio}} \cdot \frac{1}{\mathrm{mio}} \cdot \frac{1}{\mathrm{mio}} \cdot \frac{1}{\mathrm{mio}} \cdot \frac{1}{10000}\,\mathrm{mm}^2$$

which can for normal people be replaced up to high orders of approximation by *zero*; and the only chance we have to get a decent number of *Higgsens* produced is to compress the transverse beam size at the IP as much as possible to increase the density of the colliding proton clouds ... which brings us to problem number three: In typical solid materials the distance between the atoms or molecules is in the

order of Ångstroms. Figure I.3.73 shows the image of a silicon crystal, taken by a raster tunnel electron microscope. And the distance of the well structured atoms is defined by the Bohr radius, $R_B = 0.74$ Å. In most solid materials we speak about $1 \ldots 5 \cdot 10^{-10}$ m as inter atom distance. We realise this fact when—as explained above—we hit the dust bin in front of our house, or if we have a look at the manifold of tracks in Fig. I.3.66.

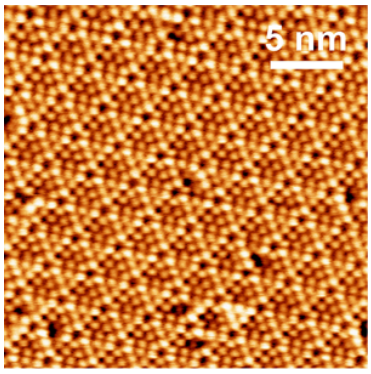

Fig. I.3.73: Raster electron microscope picture of a silicon array, showing the nice arrangement and typical dimensions of such a crystal (Courtesy: Forschungszentrum Juelich).

Particle bunches in accelerators are much more diluted: the typical distance of two protons in the arc of LHC is 3000 Å. And thus the only chance that we have to produce a sufficiently large number of physics events is to squeeze the beam size down as much as possible. Expressed in our language: we have to install a mini- (or nowadays even called micro-) beta insertion, to push the performance or "luminosity" of the collider to highest possible values. In the case of the LHC, the main parameters are summarised in Tab. I.3.4, where n_b refers to the number of stored bunches, f_0 then revolution frequency and I_p to the overall current per beam. And the luminosity—written in a slightly simplified expression is given by

$$L = \frac{1}{4\pi e^2 f_0 n_b} \cdot \frac{I_{\mathrm{p1}} I_{\mathrm{p2}}}{\sigma_x \, \sigma_y} \quad .$$

This expression refers to the most simple situation, namely equal beam sizes of the colliding beams in both planes, head on collisions and no reduction factors due to eventual offsets or the so-called hourglass effect. For more sophisticated situations we refer to [13]. In short, we need highest possible bunch currents and smallest possible β-functions at the IP. Given a certain luminosity, the event rate for a physics

Table I.3.4: Main parameters of the LHC in collider mode and the corresponding luminosity

$\beta_{x,y}$	55	cm
$\varepsilon_{x,y}$	$5 \cdot 10^{-10}$	rad m
$\sigma_{x,y}$	16.6	µm
I_p	0.584	A
f_0	11.245	kHz
n_b	2808	
$L = 10^{34}\mathrm{cm}^{-2}\mathrm{s}^{-1}$		

reaction then is simply defined as the product of L and the cross section Σ of the reaction considered,

$$R_{\text{react}} = \Sigma \cdot L \qquad .$$

12.2 Mini beta-insertion

The practical realisation of an Interaction Region (IR) has considerable impact on the beam dynamics of the storage ring. Figure I.3.74 shows such a mini-beta insertion in a typical storage ring. Embedded in the straight section between two arcs, the structure has to provide the flexibility to optimise—starting from the periodic solution of the FoDo in the arc—at least eight optics parameters: the two β-functions, the two α-s, hor. and vert. dispersion in both planes and its derivative D, D'. Often enough there are beyond these requirements additional constraints for phase advance or additional space for beam diagnostics and control. So we will need at least eight individually powered quadrupoles on both sides,

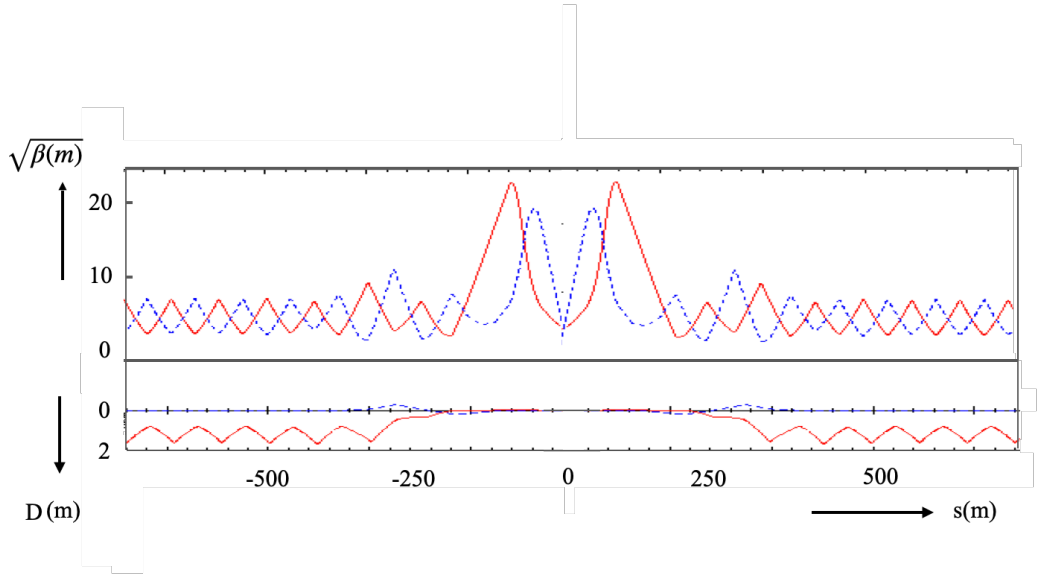

Fig. I.3.74: The collision optics of the typical particle collider embedded into the periodic arc structure. The horizontal axis shows in the usual manner the s- coordinate, expressed here as distance to the interaction point. The vertical axis shows in the upper part the square root of the hor. (red) and vert. (blue) $\beta-$function—thus indicating the beam size. In the lower part of the figure the dispersion function is shown. The mini-beta concept as well as the dispersion suppressor scheme are clearly visible and for obvious reasons (see text) the value of the dispersion is zero at the collision point.

to do the job. The details of such a structure are explained in Chapter I.14 on accelerator design. Here we would like to concentrate on the impacts on beam dynamics. Starting at the IP, in the middle of the plot, the beta function increases drastically on both sides, being pushed by the β^* and the length of the drift space needed, called l^* sometimes. As close as possible we install the first quadrupole magnets, to counteract the increasing β. For obvious reasons these magnets are called *mini-beta-quadrupoles*. They are followed by a sufficiently large number of quadrupoles to match the optics and to support the dispersion suppressor scheme. As a matter of fact, the mini-beta quads are the magnets with the largest aperture need and at the same time here the highest field quality is required. And so they are usually the most expensive devices in the ring.

Figure I.3.75 shows a picture of the LHC mini-beta arrangement. Three super-conducting quadrupoles form an optical triplet to counteract the sharply increasing optics functions in both planes.

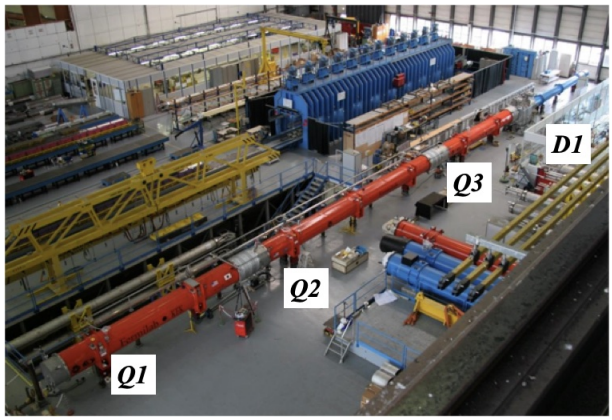

Fig. I.3.75: Quadrupole triplet of the LHC: the quadrupoles Q1, Q2 and Q3 are seen by both proton beams, forming an optically anti-symmetric triplet, while D1 refers to the dipole magnet that guides the two counter-rotating beams into their separate arc structure.

Figure I.3.76 shows the complete beam optics of the LHC, with the high-luminosity regions in IP1 and IP5, where the ATLAS and CMS detectors are located. Two other straight sections, IR2 and IR8 are dedicated for beam collisions as well, however with reduced luminosity, therefore larger β^*s and a more moderate increase of the β-functions in the direct vicinity of the IP.

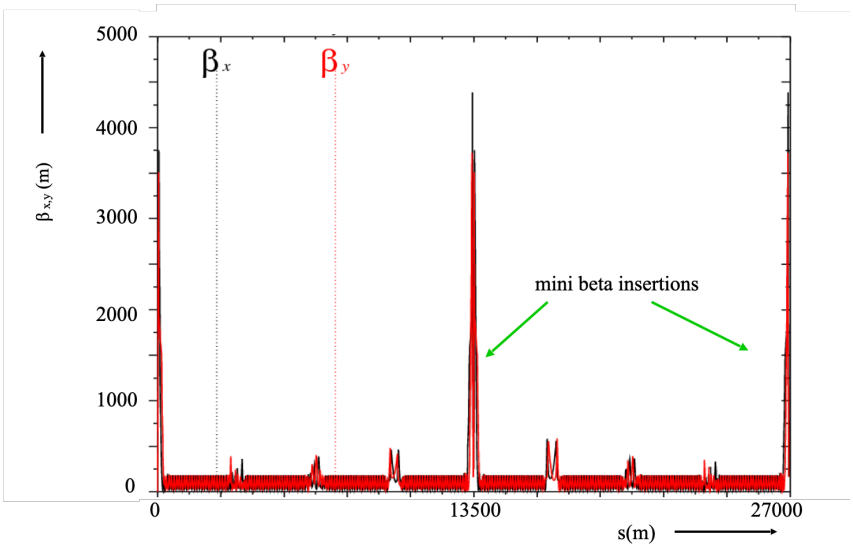

Fig. I.3.76: Beam optics of the LHC for collider operation: small beta-functions at the interaction points IP1 and IP5 lead to large beam dimensions in the mini-beta triplet quadrupoles before and after the interaction point.

In this context it is worth to have a look at the phase space picture. We know that the area of the phase space ellipse has to be constant, and the ellipse—somewhere in a typical location of the accelerator—will look reasonably shaped and reasonable tilted. Now, when focusing the beam size

will shrink to smallest values at the IP, where $\alpha = 0$ and so the phase space ellipse—still having the same area—will be upright, *very* thin in the *x*-coordinate and *very* large in the *x'* coordinate. We cannot reduce the transverse size in hor. or vert. plane without increasing the beam divergence to large values. Figure I.3.77 shows the situation. And as we talk about a very fundamental concept, namely Liouville's theorem, there is no way out. The enormous aperture need at the end of our interaction region drift space is the price to pay for reducing the transverse beam size and for achieving high luminosities.

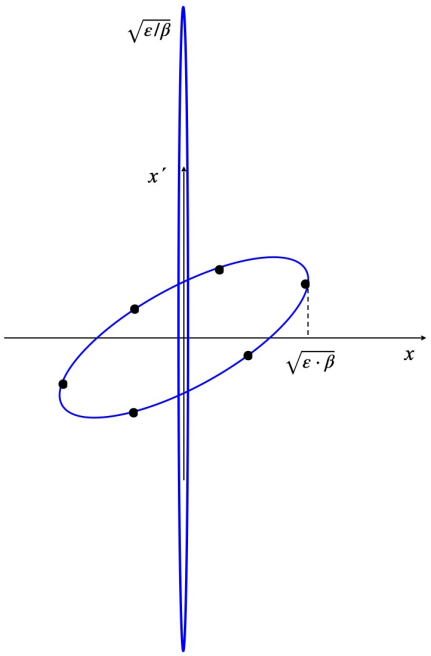

Fig. I.3.77: Phase space ellipse in a standard location (e.g. the arc) compared to the extreme situation at the IP where the ellipse is upright and small beam sizes and large divergence are obtained. Still the area of both ellipses has to be the same.

The lattice designer will include the mini-beta-insertion into the storage ring lattice, starting from the optics conditions at the IP (which will be usually $\beta = \beta^*, \alpha = 0$) and matching the optics towards the periodic solution in the arc structure. The LHC luminosity optics in Fig. I.3.76 with the two high luminosity experiments in IP1 and IP5 and their mini beta concept leads to extreme values of the beta-function in the triplet quadrupoles: the maximum values obtained, $\hat{\beta} = 4500\,\mathrm{m}$ and the corresponding aperture need in the mini-beta magnets represent one of the ultimate limits to the achievable luminosity.

12.3 Phase advance in the interaction region

There is a surprising feature concerning the phase advance through the interaction region: the phase advance in general in a storage ring lattice is defined by the inverse of the beta-function, namely

$$\Psi(s) = \int \frac{1}{\beta(s)} ds \qquad . \tag{I.3.84}$$

Now, we know that the β-function in a symmetric drift develops as

$$\beta(s) = \beta^* \cdot (1 + (\frac{s}{\beta^*})^2) \quad .$$

Putting this in Eq. I.3.84 we obtain for the phase advance in our drift

$$\begin{aligned} \Phi(s) &= \frac{1}{\beta^*} \int_0^{l_d} \frac{1}{1 + (s/\beta^*)^2} ds \\ &= \tan^{-1}(\frac{l_d}{\beta^*}) \quad . \end{aligned}$$

In Fig. I.3.78 we plot this function, with the ratio between drift length and β-function as hor. coordinate. For reasonably large drift lengths l_d and small β values at the waist, the phase advance adds up soon to $180°$. In other words, a typical mini-beta insertion increases the tune of the machine by half an integer! Even if there is not a single quadrupole located in this drift.

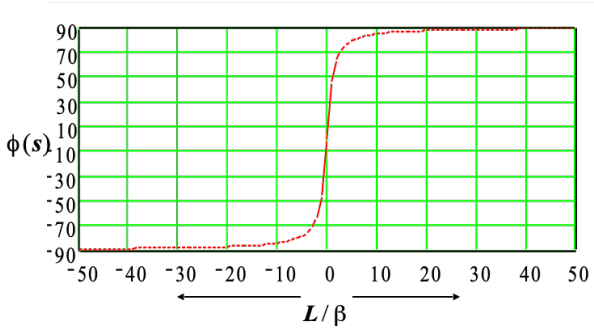

Fig. I.3.78: Phase advance in a long drift, as a function of the normalised drift length L/β. Very soon the phase advance approaches the limit of $90°$ on both sides. A long drift in combination with a low beta insertion will therefore increase automatically the tune by half an integer.

12.4 Dynamic aperture

We would not like to close this chapter without at least mentioning just another important concept that represents one of the fundamental limits of the collider performance. The keyword is *dynamic aperture*, a phrasing that leads usually to a certain level of confusion or even desperation of our detector colleagues. It refers to the chromaticity of a storage ring and the fact that Q' has to be compensated by sextupole magnets. Given a linear lattice, consisting out of focusing and defocusing quadrupoles, with drifts and dipole magnets in between, we face a linear situation and the equation of motion—being a quasi harmonic oscillation—can be solved analytically and everybody is happy. However—as explained in Section 11.2—in order to accept a certain momentum spread, which is always present in the beam, we have to introduce sextupole fields to compensate the chromatic error of the lattice. We repeat here Eq.I.3.72 which defines the chromaticity of a magnet lattice,

$$Q' = -\frac{1}{4\pi} \int k(s)\beta(s)\,\mathrm{d}s \quad .$$

It is given by the focusing strength of the quadrupoles and (!) the β-function at the location of the magnet. And so, while a typical arc structure will contribute on a more or less moderate level to Q', the mini-beta insertions will have a huge impact. We find the strongest quadrupole magnets there and by the nature of the problem we face the largest values of β. So, it is evident that the mini-betas have the strongest chromatic effect in the lattice. On the other side, the sextupoles can only be located in the arcs, as in the straight sections, namely at the insertions dedicated for beam collision, the dispersion has to be suppressed, and so sextupoles at these places, that might look promising for a local chromaticity correction, will be useless. As a consequence the strength of the sextupole fields in the arcs have to compensate the chromaticity in the arcs and the strong contribution from the interaction regions at the same time.
Which means in the end that these sextupole magnets have a very high field, adding uncomfortably strong non-linearities to our up-to-now linear problem. The topic is discussed on mathematical basis

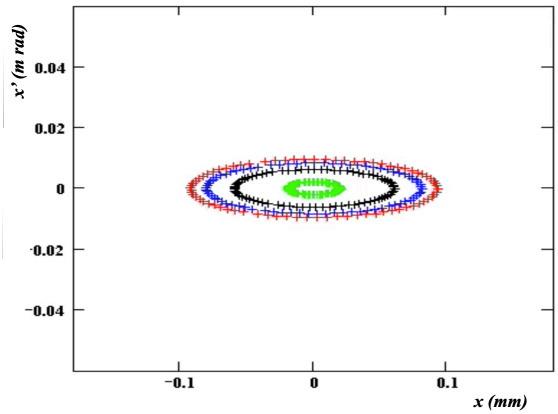

Fig. I.3.79: Phase space ellipse of four particles in a purely linear lattice.

in Chapters I.8 on transverse linear imperfections and I.9 on nonlinear effects. Here we just want to visualise the effect. In Fig. I.3.79 we show the result of a so-called tracking calculation in our purely linear toy-storage ring. And we are not surprised to find nice ellipses for the phase space curve of the four particles that have been chosen. The green ellipse corresponds to a particle close to the centre of the beam, black might be something like two sigma away, blue close to the edge and the red curve at a relatively large transverse amplitude, i.e. close to the aperture limit. Still, each and every particle in this idealised situation will run—in phase space—on its ellipse and the ellipses, being result of exactly the same focusing conditions will never cross or change shape.

In Fig. I.3.80 we refer to the same situation, however in order to compensate the chromaticity, we introduced a strong sextupole field, $B \propto x^2$ which changes the situation drastically. While the particles in the centre of the beam, i.e. having small orbit amplitudes, will not see much of the non-linear field, the red particle suffers turn by turn from the non-linearities and finally will increase its oscillation amplitude until the particle—hitting the vacuum chamber wall—will be lost. This onset of amplitude increase, where the non-linearities start to present a distortion that leads finally to particle loss is called *dynamic aperture*. And it will define in the end the final limit of the collider performance.

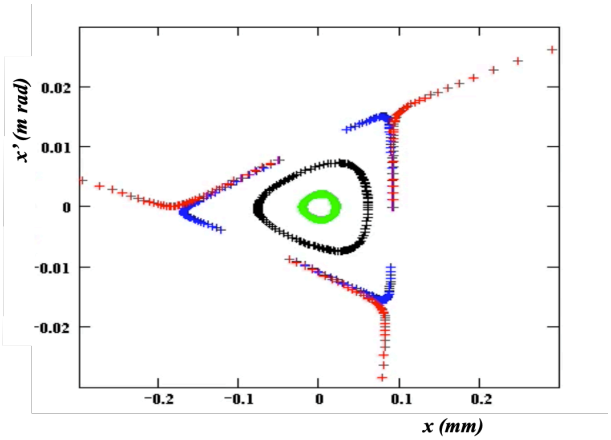

Fig. I.3.80: Phase space ellipse of four particles in a lattice with strong sextupole fields. The on-set of increasing oscillation amplitudes of the outermost particle (red dots) is called dynamic aperture and describes the limit of stability, determined by the non-linearity of the fields.

Solutions to the exercises

Exercise 1

The beam rigidity is obtained in the usual way by the golden rule:

$$\begin{aligned} B \cdot \rho\,[\mathrm{Tm}] = \frac{p}{e} &\approx \frac{1}{0.3} \cdot p\,[\mathrm{GeV}/c] \\ &\approx \frac{1}{0.3} \cdot 7000\,\mathrm{Tm} \\ &= 23\,350\,\mathrm{Tm} \end{aligned}$$

and knowing the magnetic dipole field of $B = 8.392\,\mathrm{T}$ *we get*

$$\rho = \frac{7000\,\mathrm{Tm}}{8.392\,\mathrm{T} \cdot 0.299792} = 2780\,\mathrm{m} \qquad .$$

For convenience we use in this ultra relativistic case the units $\frac{\mathrm{GeV}}{c}$ *for the momentum p. It follows that—in case the LHC were built out of dipole magnets only—the ring would have a circumference of*

$$\begin{aligned} \tilde{C}_0 &= 2\pi\rho \\ &= 18\,\mathrm{km} \qquad . \end{aligned}$$

Determine the number of dipoles that is needed in the machine. The bending angle for one LHC dipole magnet is given by

$$\alpha = \frac{l_B}{\rho} = \frac{14.2\,\mathrm{m}}{2780\,\mathrm{m}} = 5.108\,\mathrm{mrad}$$

and as we want to have a closed storage ring we require an overall bending angle of 2π*, which allows*

us to calculate the number of dipole magnets that are required

$$N_B = \frac{2\pi}{\alpha} = \frac{6.28\,\mathrm{rad}}{5.108\,\mathrm{mrad}} = 1232 \qquad .$$

Now we know that the actual circumference is $27\,\mathrm{km}$ *and so we conclude that there is more in a storage ring than dipole magnets. . . . which is indeed the topic of the following chapters.*

Exercise 2

Starting again with the golden rule of the beam rigidity, we all know: it is the momentum that defines the magnetic field

$$B \cdot \rho = \frac{p}{e} \qquad .$$

So we have to calculate the momentum of the electron beam first and—as it is neither ultra relativistic nor completely in the classical energy regime—we have to apply the full relativistic stuff.

- *Overall energy of a particle:* $E = \sqrt{p^2c^2 + m_0^2c^4}$
- *Rest energy of an electron:* $E_0 = m_0c^2 = 511\,\mathrm{keV}$
- *Kinetic energy of the beam:* $E_{\mathrm{kin}} = 10\,\mathrm{keV}$

And so we get for the total energy of the electrons: $E = 5.21 \cdot 10^5\ \mathrm{eV}$.
To calculate the momentum we write:

$$p^2c^2 = E^2 - m_0^2c^4$$

$$p = \frac{\sqrt{E^2 - m_0^2c^4}}{c} = \frac{\sqrt{(5.21 \cdot 10^5\ \mathrm{eV})^2 - (5.11 \cdot 10^5\ \mathrm{eV})^2}}{2.99792 \cdot 10^8\ \mathrm{m/s}}$$

to get

$$\frac{p}{e} = \frac{1.02 \cdot 10^5\ \mathrm{eV}}{2.99792 \cdot 10^8\ \mathrm{m/s} \cdot \mathrm{e}} = 3.4 \cdot 10^{-4}\ \frac{\mathrm{Vs}}{\mathrm{m}}.$$

Given the magnetic B-field, we can determine the bending radius,

$$\rho = \frac{p/e}{B} = \frac{3.4 \cdot 10^{-4}\ \mathrm{Tm}}{5 \cdot 10^{-5}\ \mathrm{T}} \qquad ,$$

$$\rho = 6.8\,\mathrm{m} \qquad .$$

It is astonishing: The storage ring is very small, or in other words: the magnetic field of the earth is quite strong and we conclude that

- *an energy of* $10\,\mathrm{keV}$ *is not really very much. Even if your dentist will use it to X-ray your teeth.*
- *the earth magnetic field, which is in the order of one Gauss, i.e.* $10^{-4}\ T$ *sounds pretty small, however usually it is on a level of tolerances that we have to take into account—and eventually*

compensate.

Finally, we still have to discuss the question in which direction you will have to inject the electrons to get a circulating beam. Here we have to be careful: electrons are negatively charged, this is well known. However the geographic North pole is a magnetic South. So we have to inject clockwise (if looking from a bird's view) to obtain a circulating beam.

Exercise 3

We can use the beam rigidity (or the particle momentum) to calculate the normalized quadrupole strength:

$$k = \frac{g}{B \cdot \rho} = \frac{g}{p/e}$$

$$k = 0.299792 \cdot \frac{g}{B \cdot \rho} = \frac{g}{p[\mathrm{GeV}/c]}$$

$$k = 0.299792 \cdot \frac{235\,\mathrm{T/m}}{7000\,\mathrm{GeV}/c} \approx 0.01\,\frac{1}{\mathrm{m}^2} \quad .$$

Exercise 4

Given the quadrupole parameters, listed in Table I.3.1, we obtained for g= $235\,\mathrm{T/m}$ *a value of*

$$k = 0.299792 \cdot \frac{235\,\mathrm{T/m}}{7000\,[\mathrm{GeV}/c]} \approx 0.01\,\frac{1}{\mathrm{m}^2} \quad .$$

And with the length of the quadrupole of

$$l_q = 5.5\,\mathrm{m}$$

we calculate the focal length of the lens as

$$f = \frac{1}{k \cdot l_q} = \frac{1}{0.01/\mathrm{m}^2 \cdot 5.5\,\mathrm{m}} = 18.2\,\mathrm{m} > l_q \quad .$$

The focal length of this magnet is still quite larger than the magnetic length l_q. So it is valid to treat that quadrupole in thin lens approximation, even if its actual hardware length of more than $5\,\mathrm{m}$ *is not really short.*

- *How does the matrix for such a (focusing) magnet look like?*
- *How would you establish a description of this magnet in thin lens approximation? Compare the matrix elements.*

The matrix of a focusing quadrupole is given by

$$M_{\text{foc}} = \begin{pmatrix} \cos(\sqrt{|K|}\cdot l_q) & \frac{1}{\sqrt{|K|}}\sin(\sqrt{|K|}\cdot l_q) \\ -\sqrt{|K|}\cdot\sin(\sqrt{|K|}\cdot l_q) & \cos(\sqrt{|K|}\cdot l_q) \end{pmatrix}$$

and using the values given in the exercise, we get

$$M_{\text{foc}} = \begin{pmatrix} 0.8525 & 5.22 \\ -0.0522 & 0.8525 \end{pmatrix}$$

In thin lens approximation we replace the matrix above by the much simpler expression

$$M_{\text{foc}} = \begin{pmatrix} 1 & 0 \\ \frac{-1}{|f|} & 1 \end{pmatrix}$$

with the focal length, as calculated above, $f = 18.2\,\text{m}$.

But we should not forget the overall length of the magnet: the thin lens description has to be completed by the matrix of a drift space of half the quadrupole length in front and after the thin lens quadrupole. The appropriate description is therefore—as shown in Fig. I.3.81

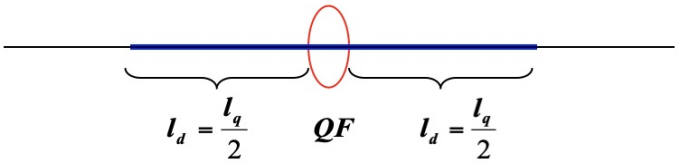

Fig. I.3.81: Schematic description of a long quadrupole in thin lens approximation.

So we write

$$M_{\text{foc}} = \begin{pmatrix} 1+\frac{l_q}{2}\cdot kl_q & l_q/2\cdot(2+k\cdot l_q\cdot\frac{l_q}{2}) \\ k\cdot l_q & 1+kl_q \end{pmatrix} \quad .$$

With the parameters given in the example,

$$\frac{l_q}{2} = 2.75\,\text{m}, \tag{I.3.85}$$

$$k\cdot l_q = \frac{-1}{f} = \frac{-1}{18.2\,\text{m}} = -0.0549\,\text{m}^{-1} \tag{I.3.86}$$

we get the numerical values for the thin lens description

$$M_{\text{thinlens}} = \begin{pmatrix} 0.848 & 5.084 \\ -0.055 & 0.848 \end{pmatrix}$$

which is pretty close to the exact values for this $5.5\,\text{m}$ *long super conducting beast.*

Exercise 5

In our case we know already that

$$L_{\text{cell}} = 0.5\,\text{m} + 2.5\,\text{m} + 0.5\,\text{m} + 2.5\,\text{m} = 6\,\text{m}$$

and so

$$\frac{L_{\text{cell}}}{4} = 1.5\,\text{m} \qquad .$$

The focal length is obtained via

$$1/f = k \cdot l_q = 0.5\,\text{m} \cdot 0.54\,\text{m}^{-2} = 0.27\,\text{m}^{-1} \rightarrow f = 3.7\,\text{m} \qquad .$$

And so we are stable.

Exercise 6

Calculate the shift in momentum that has been applied during the measurement.

Momentum change and horizontal orbit are connected via the dispersion function

$$\Delta x = D \cdot \frac{\Delta p}{p_0} \qquad .$$

The orbit shift measured in the horizontal plane is about $\Delta x \approx 3\,\text{mm}$ and—referring to Fig. I.3.51—we use a dispersion of $D_x = 2\,\text{m}$. So we conclude that the momentum shift applied was

$$\frac{\Delta p}{p_0} = 1.5 \cdot 10^{-3} \qquad .$$

Was the beam momentum shifted to lower or higher values?

Usually in a typical synchrotron type accelerator, the dispersion is a positive number. As the orbit observed shows a shift to negative values, i.e. to a smaller bending radius of the machine, the momentum change applied was negative.

In Fig. I.3.51 we realise in addition to the expected orbit change in the horizontal plane a small change in the vertical orbit. Can you explain where this might come from?

As there are no dipoles in the vertical plane, there is no dispersion in this plane and no orbit effect should be observed in the vertical direction. However the strong solenoids of the experiments represent a large source of coupling between the transverse planes. And if not compensated perfectly with local skew quadrupoles, any shift in the horizontal orbit might lead—to a certain extend—to vertical orbit effects. The location of the particle detectors is visible by the fact that at these two positions (IPs) the dispersion must vanish. And so we are not surprised to obtain a vertical orbit effect between these to locations, marked as red arrows in the figure.

In fact the orbit measurement shown can act as tool for a precise decoupling procedure of the machine.

References

[1] E.D. Courand and H.S. Snyder,Theory of the alternating-gradient synchrotron, *Ann. Phys.* **3** (1958) 1–48, doi:10.1016/0003-4916(58)90012-5.

[2] V.K. Zworykin, *et al.*, *Electron optics and the electron microscope* (John Wiley & Sons, New York, 1945), Internet Archive.

[3] E. Jaeschke *et al.*, The Heidelberg Test Storage ring for Heavy Ions TSR in Proc. First European Particle Accelerator Conf.(EPAC), Rome, 7–11 Jun. 1988, pp. 365–367, JACoW.

[4] H. Goldstein, C. Poole and J. Safko, *Classical mechanics* 3rd ed. (Addison-Wesley, San Francisco, 2002), Internet Archive.

[5] K. Wille, *The physics of particle accelerators*, (Oxford Univ. Press, Oxford, 2001), doi:10.1093/oso/9780198505501.001.0001.

[6] Gaius Julius Caesar, priv. com. . . . ok, . . . ok, also see https://en.wikipedia.org/wiki/Veni,_vidi,_vici.

[7] G. W. Hill, On the part of the motion of the lunar perigee which is a function of the mean motions of the sun and moon, *Acta Math.* **8** (1886) 1–36, doi:10.1007/BF02417081.

[8] P.J. Bryant, Insertions, Proc. CERN Accelerator School: 5th General Accelerator Physics Course, University of Jyväskylä, Finland, 7–18 Sep. 1994, Ed. S. Turner, CERN-94-01 (CERN, Geneva, 1994), pp.159–190, doi:10.5170/CERN-1994-001.159.

[9] K.D.J. André, Lattice design and beam optics for the energy recovery linac of the Large Hadron-Electron Collider, PhD Thesis, Univ. Liverpool, 2023, doi:10.17638/03161486.

[10] M. Sands, The physics of electron storage rings, SLAC-121, UC-28 (ACC) (Stanford Linear Accelerator Center, Menlo Park, CA, 1969), Inspire.

[11] B.A. Mecking, The ELSA Stretcher Ring at the Bonn Physics Institute, in Proc. 2nd Workshop on Perspectives in Nuclear Physics at Intermediate Energies, Trieste, Italy, 25–29 Mar 1985, Eds. S. Boffi, C. Ciofi degli Atti and M.M. Giannini (World Scientific, Singapore, 1985), pp. 195–203.

[12] H. Frauenfelder and E.M. Henley, *Nuclear and particle physics* (Benjamin, Reading, MA, 1975).

[13] W. Herr, B. Muratori, Concept of luminosity, in Proc. CERN Accelerator School: Advanced Accelerator Physics Course, Zeuthen, Germany, 15–26 Sep. 2003, Ed. D. Brandt, CERN-2006-002 (CERN, Geneva, 2006) pp.361–378, doi:10.5170/CERN-2006-002.